Improved Expanded Bed Adsorption Chromatography Systems

Arpanaei, Ayyoob; Hobley, Timothy John; Thomas, Owen R. T.

Publication date:
2007

Document Version
Publisher's PDF, also known as Version of record

Improved Expanded Bed Adsorption Chromatography Systems

Ayyoob Arpanaei

Ph.D. Thesis
July 2008

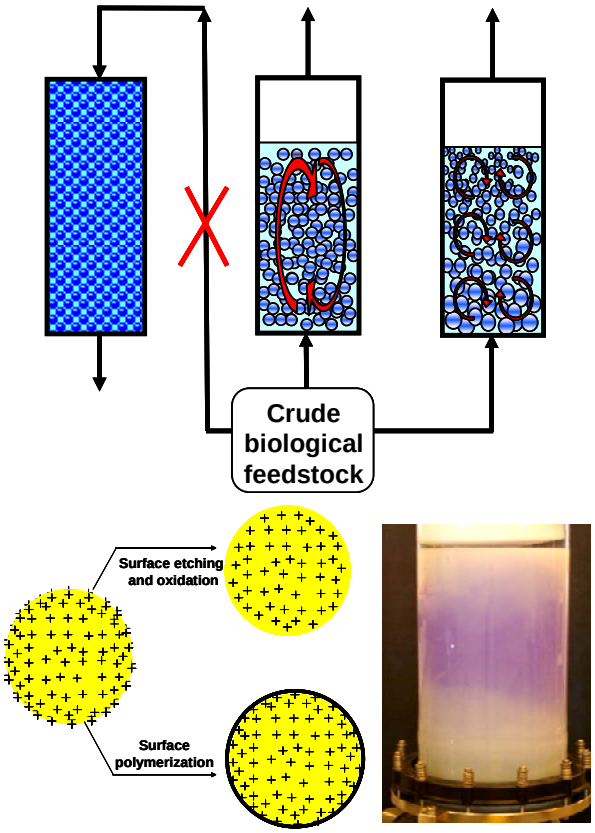

BioCentrum-DTU
Technical University of Denmark

Improved Expanded Bed Adsorption Chromatography Systems

Ayyoob Arpanaei

Ph.D. Thesis
July 2008

BioCentrum-DTU
Technical University of Denmark

Thesis summary

Expanded bed adsorption (EBA) is a type of stabilized fluidized bed chromatography that was originally conceived as a first capture step compatible with crude bio-feedstocks containing a mixture of insoluble and soluble biological molecules e.g. proteins, genomic DNA fragments, RNA molecules and cell debris. Despite commercialization of the technology, it was quickly found that for the vast majority of process streams the hydrodynamic properties of EBA were fatally compromised by crude substances or particulates, which caused blockage of the column inlet fluid distributor, as well as cross-linking of the fluidised adsorbent beads. The broad aims of this thesis were to develop a better understanding of how the hydrodynamics in an EBA column are affected by fluid distribution, to understand the mechanisms behind EBA bed cross-linking and thus to find new solutions for better adsorbent design and EBA operation.

The effects of fluid distribution on hydrodynamics were examined by evaluating and comparing the performance of rotating and oscillating distributors in EBA columns of 30 cm and 150 cm diameter, with systems based on local stirring in EBA columns with 60 cm or 150 cm diameters. Residence time distribution analysis of tracer, and dye band profiling methods were used. In general, it was found that under similar operational conditions, a rotating fluid distributor (RFD) gave superior hydrodynamic characteristics in the 30 cm and 150 cm diameter columns than using the local stirrer (LS) in both the 60 cm and 150 cm diameter columns. The shortcomings of the local stirring distributor at large scale were apparent: dead zones were present which could not be removed by increasing rotation rates or flow rates, and such changes led to deterioration of the hydrodynamic properties. In contrast, fluid introduction through a rotating distributor was found to be suitable for feed application to

large EBA columns. Residence time distribution studies showed that under the conditions studied, oscillatory movement of the RFD fluid distributor led to increased mixing and poorer performance than rotary movement.

EBA bed cross-linking was studied by examining the interaction between homogenized calf thymus DNA molecules, employed as a model for macromolecules and big particulates in crude biological feedstocks, and the strong anion exchange EBA adsorbent Q HyperZ. The effects of raising ionic strength by increasing the concentration of NaCl in the loading buffer on two prototypes of Q HyperZ having different ionic capacities (0.122 and 0.147 mmol $Cl^-.ml^{-1}$), i.e. ligand density, on cross-linking and aggregation was investigated. It was found that these adsorbents had high DNA binding capacities (4.4 and 12.4 $mg.mL^{-1}$) the value of which was determined by the ligand density. However, conditioning of the feed by adding moderate concentrations of NaCl (up to 0.35 M) in simple 50 mM Tris-HCl pH 8 buffers resulted in large increases in DNA binding (up to 9.7 and 18.9 $mg.mL^{-1}$), rather than decreases, with little effect on bed cross-linking and contraction until the salt concentration exceeded 0.35 M. These effects could be partially explained by considering the 'Slab' model as well as other models from the literature on how salt affects the DNA molecule itself, i.e. causing compaction, and effects on interaction with solid phases, i.e. permitting rearrangements, and closer packing via charge neutralisation. However, the effects of salt on weakening bead cross-linking, reducing channelling, and thus improving bed hydrodynamics were found to be responsible for the unexpected behaviour of NaCl on dynamic binding capacity. Feedstock conditioning by salt addition may therefore lead to unexpected and undesirable effects on EBA performance and new types of EBA bead are required.

Low temperature plasma was studied as a means of preparing EBA beads with reduced-surface binding of large molecules such as DNA, whilst still maintaining high

capacities for protein binding inside the adsorbent. Q HyperZ adsorbents were employed and two strategies were examined for creating nano-scale changes to the surface, namely shaving off exposed ligands via etching and oxidation mediated by plasma, and secondly covering surface ligands via polymerization mediated by plasma. Analysis of the adsorbents prepared by light microscopy, electron scanning microscopy and X-ray photoelectron spectroscopy, showed that plasma treatment did not have any destructive effect on the surface morphology or the structure of the beads. Batch binding tests with bovine serum albumin and homogenized calf thymus DNA showed that the beads obtained by plasma etching and oxidation of the surface, or by coating with vinyl acetate had the best performance. Furthermore, EBA tests showed that the dynamic binding capacity of plasma-treated adsorbent beads for big molecules like homogenized calf thymus DNA or plasmid DNA (pUG6) was reduced significantly, but was not changed considerably for the test protein bovine serum albumin, as compared to the untreated beads. Furthermore, aggregation of the beads and bed compression in the EBA column was reduced markedly for plasma-treated adsorbents compared to untreated ones. In general, plasma-treated adsorbents obtained through etching and oxidation showed better performance than for the surface-coated ones.

Dansk resumé

Expanded bed adsorption (EBA) er en chromatografisk enhedsoperation kendetegnet ved at kolonne materialet fluidiseres, hvilket giver mulighed for at oprense protein-produkter fra uforarbejdede uklarede biologiske fødestrømme, som eksempelvis fermenteringsvæske og celle lysater med videre. På trods af kommercial udnyttelse blev det tidligt erkendt at teknikken ikke levede op til det forventede, og at de fleste biologiske fødestrømme i udstrækt grad kompromitterede EBA systemets hydrodynamiske egenskaber gennem tilstopning af kolonnens væskefordelingssystemer eller ved promovering af aggregation af kolonne materialet.

Det primære formål med denne afhandling har været at undersøge væskefordelingsindflydelse på EBA søjlens hydrodynamiske egenskaber samt at opnå en forståelse af de bagved liggende mekanismer, der forårsager kolonne materialet aggregering. Derudover har det været målet at benytte den nye viden som udgangspunkt for udviklingen af nye gel baserede EBA partikler med mere hensigtsmæssige egenskaber under behandling af ’beskidte” fødestrømme.

Væskefordelings indflydelse på EBA kolonne hydrodynamiske egenskaber blev undersøgt og evalueret i roterende og oscillerende fordeler-systemer i EBA søjler med diametre på henholdsvis 30 cm og 150 cm, og sammenlignet med søjler på 60 cm og 150 cm med lokale omrøringsfordelingssystem. Undersøgelsen blev foretaget ved at sammenligne retentiontider for farvestoffer og acetone. Resultaterne viste at de hydrodynamiske egenskaber for søjlerne med roterende væskefordeler tydeligt var forbedret sammenlignet med tilsvarende søjler udstyret med lokale fordeler systemer. For de søjler der brugte lokale omrøringsvæskefordeling var der områder hvortil distribution af farve udeblev, og trods øget omrørings- og væske gennemstrømningshastighed kunne dette problem ikke løses. Den øgede

bevægelse af væsken resulterede tværtimod i forringelse af de hydrodynamiske egenskaber. Det blev således konkluderet, at introduktion af væske i EBA søjler gennem anvendelse af roterende fordelere var den bedste løsning, og lokale omrøringsystemer i den forbindelse ikke synes egnet. Det blev desuden påvist en roterende bevægelse sammenlignet med oscillerende gav anledning til bedre retentionstider og mindre turbulence.

Undersøgelsen af EBA partikel aggregering blev udført gennem studier af interaktionen mellem den stærke EBA anionbytter gel Q HyperZ og et model system bestående af homogeniseret DNA fra kalve skjoldsbugkirtler. To prototyper af Q HyperZ med forskellig ligand densitet, og derigennem forskellig ion kapacitet (0.122 og 0.147 mmol Cl^- $\cdot ml^{-1}$), blev anvendt og undersøgt under forskellige NaCl koncentrationer. Resulaterne viste at DNA bindingskapacitet var relativt høje (henholdsvis 4.4 mg/ml og 12.4 mg/ml) og afhængige af ligand densiteten, og at adsorptants kapacitet yderligere kunne forøges ved anvendelse af en simple buffer (50 mM Tris-HCl, pH 8) indeholde 0.35 M NaCl (op til 9.7 mg/ml og 18.9 mg/ml). Dette resultat var overraskende, da det var forventet at kapacitet ville falde, og der blev kun obsereveret en mindre forøgelse af aggregering af adsorbanten (sammentrækning af kolonnematerialet) ved NaCl koncentration op til 0.35 M. En mulig forklaring på den forøgede kapacitet kan tilskrives 'Slab' modellen samt andre modeller, der beskriver hvorledes salt påvirker DNA. Under øget ionstyrke sammentrækkes DNA molekylet, og bliver derved mere kompakt, hvilket muligører en bedre pakning gennem ladningsneutralisering samt en ændret mere dynamisk interaktion med faste overflader ligeledes forårsaget af en dæmpning af de elektrostatiske kræfter.

Den reducerede gel aggrerering samt den observerede reduktion af kanaldannelse i EBA kolonnen, og der i gennem forbedrede hydrodynamiske egenskaber, blev konkluderet som værende hovedårsag til den uventede effekt af salt på bindingskapacietet af det

undersøgte EBA gel. Tilsætning af salt til ubehandlede biologiske fødestrømme med det formål at reducere binding af DNA samt mindsket gel aggerering kan føre til uønskede og uforventede hydrodynamiske egenskaber af det anvendte EBA system.

Anvendelsen af lav temperatur plasma til fremstilling af EBA adsorbanter blev undersøgt med det formål, at frembring et kolonne materiale med bevaret høj indre bindingskapacitet samt stærkt reduceret overflade binding af store molekyler, som foreksempel DNA. Som udgangspunkt for udviklingen af en sådanne adsorbant blev anvendt Q HyperZ, og to forskellige strategier blev anvendt baseret på henholdsvis oxidering og ætsning med kold plasma samt indkapsling af overfladen gennem plasma induceret polymerisering. De fremstillede geler blev studeret med lys mikroskopi, elektronskanning samt røntgen fotoelektron mikroskopi, og det blev konkluderet at adsorbanternes overflade strukture ikke var blevet beskadiget.

Bindingsstudier af Bovine Serum Albumin (BSA) samt homogeniseret DNA fra kalve skjoldsbugkirtler viste, at behanding med induceret overflade ætsning/oxidation samt plasma induceret overflade polymerisering af vinyl acetat resulterede i gel-materialer med de bedste egenskaber. Yderligere blev den dynamiske binding kapacitet af homogeniseret DNA fra kalve skjoldsbugkirtler samt plasmid DNA (pUG6) undersøgt for de plasma behandlede adsorbanter, og det blev konkluderet at denne var stærkt reduceret samtidig med at bindingskapacitet af BSA stortset forblev uændret. Derudover blev der observeret en mærkbar reduktion af sammentrækning i kolonne højden samt af gel aggrerering. Den afsluttende konklusion baseret på de indsamlede data blev således, at de generelt bedste egenskaber vedrørende reduktion af geler materialets aggregering/binding til DNA uden samtidig tab af protein bindingskapacitet kunne opnås gennem plasma induceret ætsning/oxidering sammenlignet med plasma inducerede overflade polymerisering.

Acknowledgements

This report is my thesis for a PhD degree, carried out at the Center for Microbial Biotechnology (CMB), BioCentrum-DTU, Technical University of Denmark from April 2002 to July 2006. This project was supported by the Iranian Ministry of Science, Research and Technology by granting a full PhD scholarship to me, which is gratefully acknowledged.

I wish to thank my supervisor, Dr. Timothy Hobley, who is not only a great supervisor, but also a reliable, patient and kind friend.

I also would like to express my gratitude to my former supervisor, Prof. Owen Thomas who accepted me as a PhD student and gave me this great opportunity to come to Denmark to pursue my studies.

Part of the work done in chapter 2, was in collaboration with Anders Heebøll-Nielsen, also part of the work reported in chapter 3 was conducted with some help from Niels Mathiasen. I wish to thank both of these people for their collaboration.

I also acknowledge the administrative staff, technicians and workshop men at CMB who have an important role in creating a place in which work is truly facilitated.

During my PhD program, I was very lucky to have very nice and kind office mates at different times. Mohammad, Claudia, Manny, Anders, Fanny, Henrik, Wai, Thomas, Ana, Cleo and Roberto have made the office a very warm and friendly environment. I had very many great times with these people, and I have already missed all of them. I also would like to thank my colleagues at the Bioseparation group, in particular Kim and Trine for their kind hospitality. Usually I had a lot of problems to understand Danish letters that I was receiving. Kianoush as well as Kim and Trine helped me a lot with translation of those letters which is truly appreciated.

I am also grateful to my parents who always encouraged and supported me during different steps of my life and education.

I dedicate this work to my wife, Mehrnoosh, who has dedicated herself to our life and our wonderful children.

List of Contents

Chapter 3: Study of DNA binding during expanded bed adsorption and factors affecting adsorbent aggregation

Chapter 4: Surface plasma modification: a means of preparing expanded bed adsorption beads with reduced surface binding

1 Expanded bed adsorption: Principles and applications

Introduction

Downstream processing of biological materials usually involves different unit operations including centrifugation, filtration, chromatography, crystallization, and precipitation (Figure 1). Depending on the product, these unit operations may be used more than once in the different sections of downstream processing. A significant part of the production costs of biological products, and in particular for biopharmaceuticals, is due to the downstream processing. Therefore, decreasing the number of unit operations in downstream processing can potentially lead to a striking reduction in production costs. Reducing the number of unit operations results in lower capital and operation costs, decreased overall process time and increased overall yield. To achieve that, the integration of several unit operations in one step is one of the approaches that can be taken. Expanded bed adsorption (EBA) chromatography was developed in the early 1990s as a multifunctional integrated unit operation (Figure 1). By using this technique, solid-liquid separation (clarification), concentration and initial purification of a biological compound, e.g. a protein, can be integrated in one unit operation. Despite initial success (Noda et al., 1996), EBA has been faced with significant limitations on its application due to two crucial problems: i) fouling of the fluid distributor by suspended materials in crude bio-feedstocks and fermentation broths; and ii) adsorbent bead cross-linking by macromolecules and crude materials.

This chapter is a general review on work published on the principles of EBA, important parameters affecting EBA system performance and some recently published applications. Limitations and related solutions will be examined in detail in chapters 2-4.

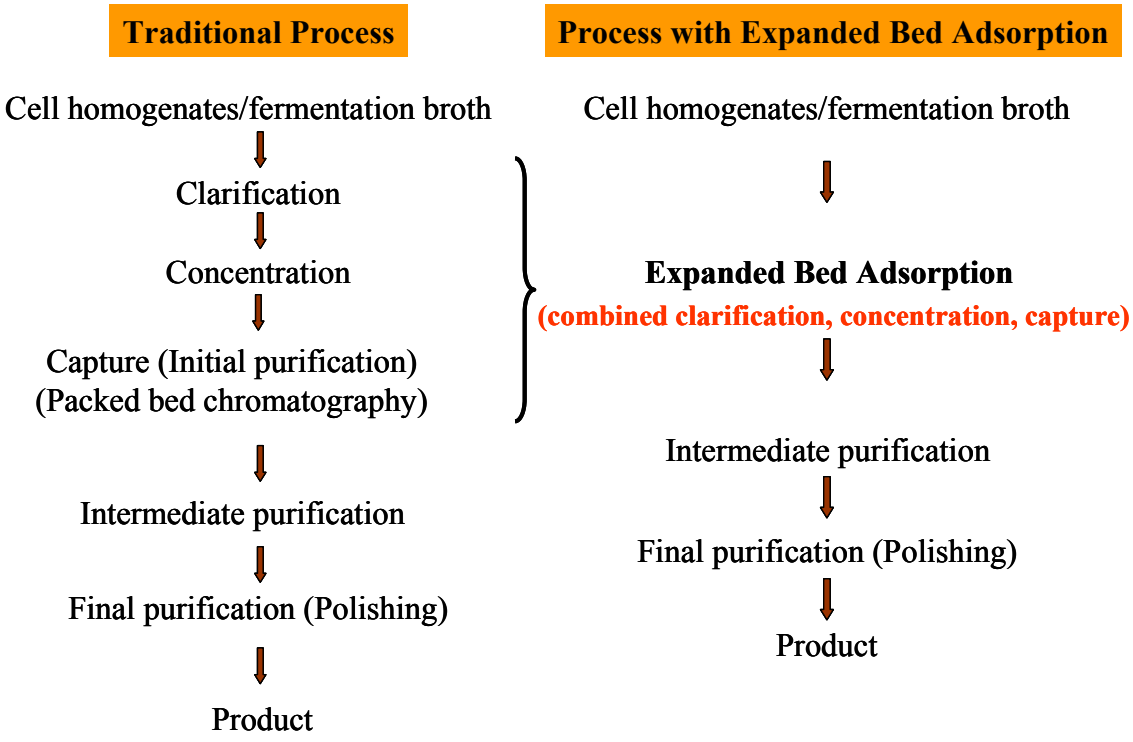

Figure 1: **Comparison between traditional downstream processing and one with EBA.**

Principles

EBA is based on similar principles to those governing conventional adsorptive chromatography techniques. Namely, a flow containing a target compound as well as contaminants is introduced into a column filled with functionalized solid matrices or adsorbents. Under the conditions employed, an attractive interaction between the target molecules (or rarely the contaminants) and the solid matrix material is exploited to promote adsorption and to allow contaminants to pass through without binding. Then, by changing the conditions, the adsorbed target molecule is eluted from the bed. However, in contrast to

conventional chromatography systems which are fed from the top, in EBA the bed is allowed to fluidize by introducing flow from the bottom of the column and allowing space for the bed to expand (Figure 2). This expansion gives an increased voidage within the bed. Under such a condition, solid materials, colloids and very large molecules existing in crude biological feedstocks can pass through the expanded bed. In theory this enables the application of crude biological feedstocks without any need for clarification (solid-liquid separation) (Chase, 1994 and Hjorth, 1997). If the product has been bound to the matrix, it can be concentrated using EBA by applying an appropriate elution step. Application of a crude feedstock to a conventional packed bed chromatography system is generally not possible due to fouling with insoluble materials, which leads to blocking, high back pressure and the need to stop column loading.

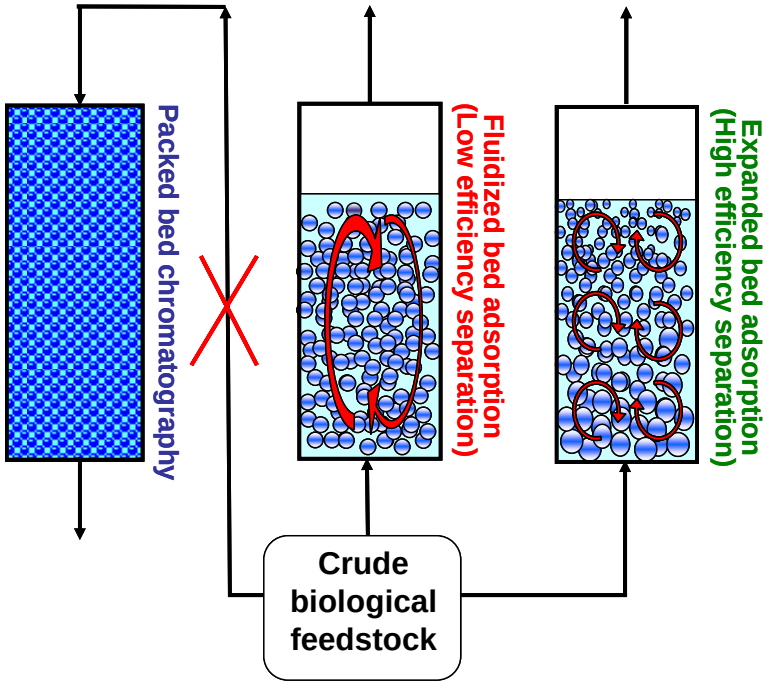

***Figure 2*: EBA system compared to packed bed and fluidized bed systems. Fluid application is shown by the thin arrows. The large arrows depict differences in the extent of axial mixing in the columns.**

Operation

The steps involved in operation of an EBA system are depicted in Figure 3. A flow of an equilibration buffer which is usually the loading buffer is introduced into the column in the first step. After expansion to a desired extent (*ca.* 2-3 fold) and stabilisation of the bed occurs after approximately 30 minutes the feedstock is pumped in at a constant flow velocity, e.g. 200-600 $cm.h^{-1}$ to maintain bed expansion at 2-3 folds. The column adaptor (outlet) is kept at a distance of 5-10 cm above the expanded bed surface. It must be considered that biological feeds usually have different characteristics (e.g. higher viscosity) than the equilibrium buffer, which causes different expansion characteristics. Therefore, the position of the top adaptor must be adjusted in such a way that over-expansion of the bed by the biological feedstock does not affect performance adversely (Barnfield-Frej et al., 1994), or the flow rate must be adjusted. High viscosity or density of biological feedstocks leads to the need to use lower flow velocities during loading to maintain a certain expansion (Draeger and Chase, 1991a), which will result in lower productivities. After loading a washing solution is pumped in and weakly bound or entrained materials are flushed out by applying a flow velocity similar to that for feed application. In this step, the adaptor is kept very close to the bed surface to minimize buffer consumption.

Elution of the target compound is performed after washing and can be done with the bed expanded. The elution buffer may have a similar composition to the washing buffer except typically the pH or ionic strength is changed by adding acid or base or salts. The viscosity of the liquid can increase while elution is taking place due to the high concentration of biological materials (e.g. protein) being released. This leads to over expansion of the bed and either the flow rate must be decreased or the top adaptor must be pulled up. Reduction of flow rate is usually preferred since it generally leads to reduced axial mixing, reduced bed

volume and thus lower elution volume and consequently better concentration factors (Chang and Chase, 1996). Elution can also be performed in a packed bed mode for the columns equipped with perforated plates and mesh as their bottom fluid distribution system (Figure 3). Following elution, the bed must be cleaned appropriately. For different adsorbents and feedstocks different protocols for cleaning are advised by the column and adsorbent manufacturers.

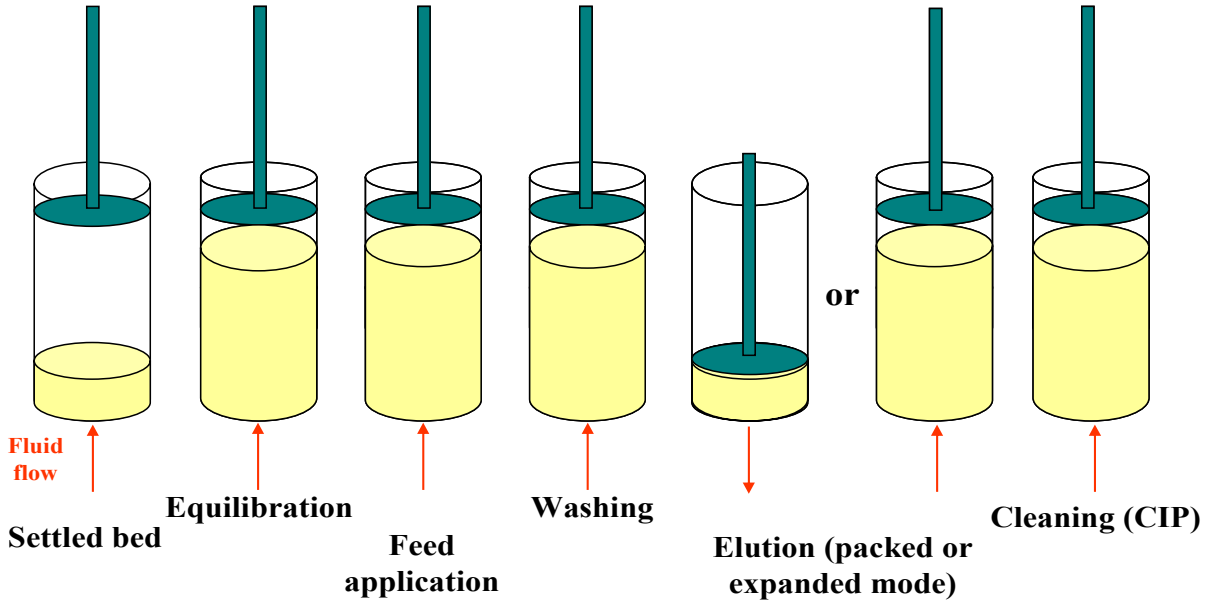

Figure 3: **Operational stages for an EBA system. Arrows show the flow direction (redrawn and modified from Thömmes, 1997).**

Adsorbents

All adsorbent beads commercially available for EBA consist of two phases: (i) a polymer gel or composite part which is functionalized and carries ligands; and (ii) a single solid core or dispersed solid material imbedded in the polymer gel or composite. Thus densified beads result which permit their use with the high flow velocities usually applied in EBA columns. Many types of EBA adsorbents have been prepared based on this fundamental

design and are reported in the literature, however broadly speaking, these can be broken down into four major categories with particular relevance. In the first design, porous gel materials such as agarose have been densified by encapsulating solid particles such as quartz (e.g. Streamline beads, from GE Healthcare) and then coupling ligands for product binding. In the second type of EBA bead, a single solid core made from glass, stainless steel or tungsten carbide (e.g. UpFront Chromatography A/S; Streamline Direct, GE Healthcare) is coated by porous gel materials such as agarose and derivatized with ligands. In some cases this design is modified by coupling tentacles of high molecular weight polymers such as dextran to the densified gel material followed by functionalization with suitable ligands. This enhances ligand accessibility and thus protein binding capacity (Thömmes, 1999). A suffix of 'XL' is added to the name of these beads (e.g. Streamline Q XL). A third adsorbent type is manufactured by BioSepra (now part of PALL) called HyperD or HyperZ which consists of a porous silica or zirconia ceramic core filled and coated with non-porous polymer composites containing ligands for binding. The fourth design for EBA beads consists of a porous solid core activated and functionalized only on the surface, i.e. no polymer fillings or coatings are applied. For this last type of bead, adsorption is limited to the outer surface or within the pores of the solid which leads to a low capacity (Zhang et al., 2001) since a highly derivatized porous polymer has not been used. This design has not been used for the commercial production of EBA beads.

EBA beads with different binding functionalities including anion exchange (e.g. quaternary amine or tertiary amine groups), cation exchange (e.g. sulphonic acid and carboxymethyl groups), hydrophobic (e.g. phenyl group) and affinity (e.g. immobilized metal and rProtein A) have been prepared and are commercially available. The method scouting and process optimization is very strongly dependent on the bead type, functionality and surface

architecture (Zhang et al., 2001 and Theodossiou and Thomas, 2002). In general the greatest capacity is achieved with ion exchange types and given that they are also the cheapest to produce and are resilient to harsh cleaning, they are generally perceived to be desirable as a generic EBA workhorse.

Hydrodynamics

The term 'expanded bed' as coined by Chase and Draeger (1992) and used for marketing by Pharmacia (now GE HealthCare) rather than fluidized bed is a critical detail worth noting. In a traditional fluidized bed adsorption system (Somers et al., 1989), the chromatography beads have no significant difference in size or density relative to each other. A high degree of axial mixing in a fluidized bed is thus inevitable, which leads to a small number of equilibrium stages within the bed and consequently low purification efficiency (Figure 2). However, in EBA systems, adsorbent beads usually have different sizes. By using beads with a size ratio of 2-3 between the biggest and smallest, classification of the bed within the EBA column takes place during application of the flow and bed expansion (Draeger and Chase, 1991b; Thömmes, 1997 and Hjorth et al., 1998). The location of an individual bead depends on its size and density which determines the terminal settling velocity according to Stoke's law (equation 1) (Thelen and Ramirez, 1997):

$$U_t = \frac{(\rho_b - \rho_l) d_b^2 g}{18\eta} \qquad (1)$$

Where, U_t is terminal velocity, ρ_b and ρ_l are densities of beads and liquid, d_b is the bead diameter, g is acceleration due to gravity and η is the viscosity of liquid. This equation is valid for infinitely dilute solutions where the bead is far from the vessel wall and for conditions

under which the Reynolds number for the bead (Re_b) is less than 0.2 (Hjorth et al., 1998). The latter can be calculated from equation 2.

$$\mathrm{Re}_b = \frac{\rho_l U_i d_b}{\eta} \qquad (2)$$

Here, U_i is the interstitial velocity and is calculated by dividing superficial velocity (U_s) by the bed voidage (ε). In order to estimate an average value for the terminal velocity or Re_b of beads in an EBA column, average values of ρ_b and d_b must be used.

During fluidization, large beads have the highest settling velocity (equation 1) and move to the bottom, becoming localized there. Their exact placement is dictated by the interplay between the local voidage in different parts of the bed, which dictates the local interstitial fluid velocity. If too many beads try to occupy the same local space, voidage decreases, fluid velocity increases and the beads with lower settling velocities are pushed up out of the area to a place where their settling velocity is balanced by the local fluid velocity. This classification of the beads leads to lower axial mixing within the column and to a flow regime which becomes close to plug flow (Figure 2).

Classification of the beads in an expanded bed has been experimentally demonstrated by a number of workers, for example Tong and Sun (2002) showed that beads with different sizes were present at different heights in a 2.6 cm Ø EBA column containing Streamline quartz base matrix beads (size distribution 80-500 μm). They conducted this study by sampling from the column at different heights during expansion. They showed that the average size of the beads situated in the bottom part of the column was larger than in the upper parts. A linear relation between the average size of the beads and their height in the system studied was found (Tong and Sun, 2002). Interestingly, for the beads studied there was no difference between the densities of the beads found at different heights in the column, emphasising the large impact that diameter has on the settling velocity (see equation 1).

Evidence for voidage changes in different parts of EBA beds has also been found by a number of workers (Bruce and Chase, 2001; Tong and Sun, 2002 and Yun et al., 2004). Based on these studies it has been confirmed that voidage is less in the bottom part of an expanded bed than in the top, and is consistent with the size distribution of beads in expanded beds at different heights as explained above (Tong and Sun, 2002 and Yun et al., 2004). Kaczmarski and Bellot (2004 and 2005) studied the effect of taking into account axial variation of bed porosity (i.e. voidage) and particle size distribution in a general rate model compared to when an average value was used in modelling of adsorption process of proteins by an EBA system. They showed that using average values does not cause a significant deviation compared to when axial distributions of size and voidage are used for the modelling (Kaczmarski and Bellot, 2004 and 2005). Interestingly, there are so far no direct measurements on the actual movement of EBA beads in a column during processing, due to the difficulty in tracking individual beads in a bed. However, the method of positron emission particle tracking pioneered at the University of Birmingham (Parker et al., 1997) may be one way to quantify the effects on bead movement of different processing conditions.

The characterization of fluidization in EBA columns generally starts with a study of the bed expansion profile at different flow velocities and a linear relation is to be expected. EBA beads with larger size and/or higher densities need higher flow velocities to achieve a certain expansion. Usually however, there is considerable deviation from the fluidization velocity predicted from the Stokes equation, since although wall effects can usually be ignored ($d_b/d_c > 0.01$) the beads are not infinitely diluted and thus hindered settling as well as swarming may be expected, Richardson and Zaki developed an empirical correlation to describe the effects of hindered settling for large glass mono-sized beads (equation 3) and this

is often used when describing EBA bed expansion (Thömmes, 1997), even though the assumptions in the correlation are not met.

$$U_s = U_t \varepsilon^n \tag{3}$$

In this equation, n is the constant of Richardson and Zaki's equation. This equation is valid for the very small bead to column diameters (d_c), namely ratios (d_b/d_c)>0.01, where the wall effect is negligible. Under this condition, Richardson and Zaki showed n is constant (4.65), when Re_p<0.2 (Thömmes, 1997; Theodossiou et al., 2002). The average voidage for an expanded bed (ε) can be calculated from the bed expansion profile at different flow velocities by using equation 4:

$$\varepsilon = 1 - \frac{H_0}{H}(1 - \varepsilon_0) \tag{4}$$

Here, H_0 is settled bed height, H is expanded bed height and ε_0 is the voidage of the settled bed, which is generally assumed to be 0.4 (see Theodossiou et al., 2002). According to equations 3 and 4, n and U_t can be calculated by curve fitting of experimental data for ε and U_s obtained from bed expansion profiles at different flow velocities by using the correlation between lnU_s and lnε (modified form of equation 3), in which the slope and y-intercept are therefore n and U_t, respectively. The value of n obtained with curve fitting can be compared with its theoretical value of 4.65 as determined by Richardson and Zaki. Furthermore, U_t obtained from curve fitting can also be compared with its theoretical value calculated by equation 1 (Thömmes, 1997 and Theodossiou et al., 2002). In practice, values of n other than 4.65 are found in expanded beds (see for example Theodossiou et al., 2002) since the ideal conditions used by Richardson and Zaki are not employed, and the EBA beads have a wide distribution of sizes and densities rather than being large mono dispersed glass spheres.

As was indicated above, to achieve a high efficiency separation, axial mixing within the expanded bed must be minimized to allow an approach to plug flow. The factors affecting that include design parameters, e.g. the flow distribution system and column diameter, and operational parameters such as flow velocity, bed height and fluid viscosity, which will be discussed in the later parts of this chapter. For the evaluation of the flow regime within the column a residence time distribution (RTD) study is usually conducted and data are analyzed with two models, i.e. the dispersion and the tanks in series models (Levenspiel, 1999). For that, a pulse of an inert tracer is introduced into the column at time zero. The broadening of the tracer band within the column is evaluated by monitoring concentration of the tracer at the outlet (Figure 4).

The variance of the dimensionless exit age distribution curve of tracer (σ_θ^2) is proportional to the extent of mixing and axial dispersion within the column (dispersion model). For small extents of dispersion (Levenspiel, 1999):

$$\sigma_\theta^2 = 2\left(\frac{D_{ax}}{U_i H}\right) \tag{5}$$

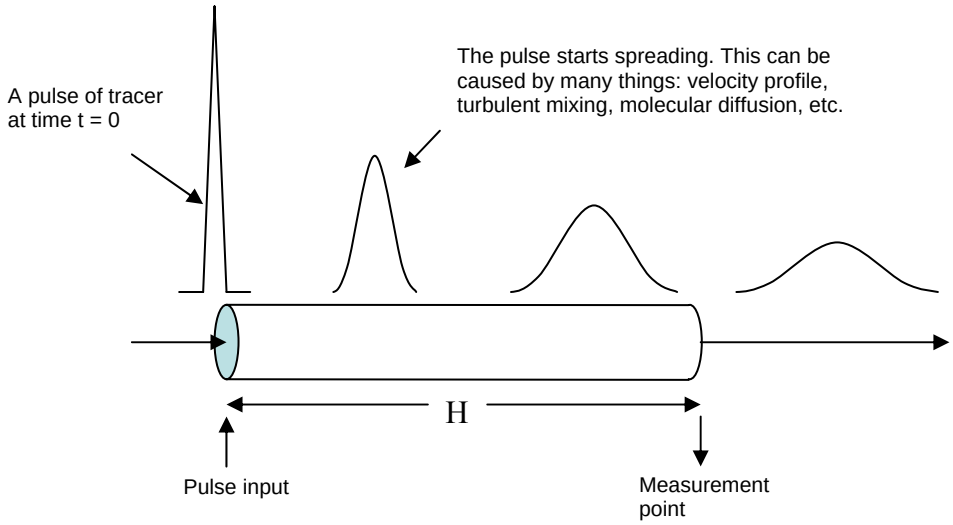

Figure 4. The spreading of tracer according to the dispersion model (redrawn from Levenspiel, 1999).

D_{ax} is the axial dispersion coefficient and the term D_{ax}/U_iH is called the vessel dispersion number. Error for this model is less than 5% if $D_{ax}/U_iH < 0.01$. However, for the higher values of dispersion, when there are larger deviations from plug flow, the σ_θ^2 is correlated to the vessel dispersion number by (Levenspiel, 1999):

$$\sigma_\theta^2 = 2(\frac{D_{ax}}{U_i H}) - 2(\frac{D_{ax}}{U_i H})^2 \left[1 - e^{-(\frac{U_i H}{D_{ax}})} \right] \quad (6)$$

The reciprocal of vessel dispersion number (U_iH/D_{ax}) is called Peclet number (*Pe*). Therefore, the higher *Pe* indicates lower mixing and less axial dispersion for the whole column.

In the tanks in series model, the σ_θ^2 is correlated to the so-called number of theoretical plates (*N*) representing the number of equilibrium stages within a vessel or column by:

$$\sigma_\theta^2 = \frac{1}{N} \quad (7)$$

Better chromatography performance is expected when higher *N* is attained. The height equivalent to a theoretical plate (*HETP*) can be calculated by:

$$HETP = \frac{H}{N} \quad (8)$$

HETP is a parameter comparable with D_{ax}, namely both are 'internal' parameters describing the quality of the flow within a column. However, *Pe* and *N* and (D_{ax}/U_iH) are 'system' parameters and are dependent on the characteristics of the whole system setup, namely the dimensions of the column, in particular the height, and quantitatively indicate the extent of mixing within the whole column. The above models are idealised and do not account for channelling due to adsorbent cross-linking or problems with the system setup (e.g. not having a vertical column) and thus considerable care needs to be exercised when evaluating RTDs

and the parameters yielded by the two models. For example, it can be envisaged that a very badly cross-linked or poorly expanded EBA column with a few large channels may give an almost perfect RTD pulse response at the outlet, and consequently apparently high values for N, Pe etc. Examination of the actual time taken for the tracer to be observed at the outlet and a crude calculation of the time expected may thus be needed to qualify the data, as well as visual observations of the bed, for example using dyes.

Operational parameters and their impacts on EBA performance

Liquid dispersion, adsorbent dispersion, kinetics of adsorption, film mass transfer and intraparticle mass transfer are important parameters affecting EBA performance (Thömmes, 1997 and Clemmitt and Chase, 2003). A complex interplay exists between these parameters and operational characteristics such as flow velocity, fluid viscosity, buffer composition and ionic strength, and target molecule concentration and these will be discussed briefly in the following.

Hjorth et al. (1995) showed that increasing settled bed height of Streamline SP (i.e. the amount of the adsorbents) from 5 to 30 cm in a Streamline 50 column (5 cm diameter) results in an increase in the dynamic binding capacity for lysozyme during EBA from ~15 to ~70 $mg.mL^{-1}$ adsorbent at a flow rate of 300 $cm.h^{-1}$ The difference between the dynamic binding capacities of the system after changing the settled bed heights from 20 to 30 cm was much less (from 65 to 70 $mg.mL^{-1}$, respectively) than when it was increased from 5 cm. Such results could be due to a number of effects including poor fluid distribution and significant axial mixing which leads to low capacity when short bed heights are used, but which becomes less problematic as bed height is raised and the bottom parts of the bed assist fluid distribution. However, the data could also indicate that intraparticle and film mass transfer is poor for the

feedstock and adsorbent used and longer residence times in the column (by using a higher bed height) improve capacity. The authors also showed that increasing the flow velocity from 100 to 200, 300, 400 and 500 $cm.h^{-1}$ led to a continuous decrease in dynamic binding capacities of Streamline DEAE and Streamline SP for BSA and lysozyme, respectively (Hjorth et al., 1995). Such effects could possibly be attributed to increased axial mixing, shorter residence time or increased voidage (affecting film mass transfer). The authors themselves did not interpret these data.

Karau et al. (1997) also found that the effect of flow velocity on dynamic binding capacity was dependent on the settled bed height. When a low settled bed height (14 cm) of Streamline DEAE was fluidized at 420 $cm.h^{-1}$, the dynamic binding capacity of BSA decreased by more than 7 times as compared to when 90 $cm.h^{-1}$ was employed. However, in contrast to the results of Hjorth et al. (1995), the binding capacity did not decrease significantly when higher settled bed heights (33 and 51 cm) were used and flow velocity changed over the same range. These authors attributed the findings to improved mass transfer capability as well as less axial mixing at higher settled bed heights compared to those at lower ones (Karau et al., 1997).

Similar results to those of Hjorth et al. (1995) were reported by Finette et al. (1998), Wright and Glasser (2001) and Clemmitt and Chase (2003). Finette et al. (1998) studied the effect of flow velocity in a 1.6 cm × 26 cm EBA column on human serum albumin (HSA) and lyzosyme adsorption to the triazine dye biomimetic adsorbent Cibacron Blue F3G-A, which had been immobilized on Fractosil 1000 (63-100 μm diameter beads). Their results showed that binding capacity decreased for both proteins when the flow velocity was increased from 38.4 $cm.h^{-1}$ to 76.8, 153 and to 229.2 $cm.h^{-1}$. The settled bed height was only 3 cm in their experiments which is low in comparison to what most other workers use (> 5 cm and often

~15 cm), and thus such a system can be expected to be very susceptible to the quality of the fluid distribution and problems with jet streams in the column leading to rapid breakthrough and low capacity. Furthermore, the use of a dye ligand may lead to a greater contribution from the kinetics of protein binding to the ligand in the system examined and potentially a higher dissociation constant as compared to the long-range and strong electrostatic interactions of the ion exchangers used by Hjorth et al (1995) or Karau et al. (1997) above.

Clemmitt and Chase (2003) studied the effect of flow velocity in the range of 53.5-153 $cm.h^{-1}$ for adsorption of *Saccharomyces cerevisiae* to Concanavalin A derivitized perfluorocarbon beads in a 1 cm Ø EBA column. They revealed that dynamic binding capacity decreased by a factor of 50% due to this change in flow velocity. They also showed that increasing the settled bed height from 5 to 20 cm increased the dynamic binding capacity by a factor of ~50%. In that system, the cells bind only to the outside of the adsorbents, thus there are no contributions from intraparticle pore diffusion limitations, highlighting that other effects such as film mass transfer and mixing are important. Results obtained by Wright and Glasser (2001) also confirm the adverse effect of increased flow velocity on dynamic binding capacity of lysozyme to either of the cation exchange adsorbents HyperD LS or Streamline SP.

The interplay of mixing, mass transfer, adsorption/desorption kinetics and system variables is not confined only to the loading phase. Hjorth et al. (1995) showed that carrying out elution in an expanded mode leads to higher eluted volumes (by a factor of ~35%) leading to lower concentrations of final product compared to that for a downward elution in packed bed mode. However, it was emphasized by Lihme et al. (1999) that EBA processes will be simplified and more robust by conducting elution in expanded bed mode. Subsequently, Hjorth (1999) showed that the elution volume could be decreased by using lower flow

velocities which decrease mixing within the column and thus leads to greater elution efficiency (Hjorth, 1999).

Chang and Chase (1996) examined the effects of viscosity on EBA performance in a Streamline 50 column containing Streamline SP at a constant flow velocity (300 $cm.h^{-1}$). These authors found that increasing the liquid viscosity by adding glycerol (e.g. 0%, 25% and 32% v/v glycerol in 100 mM sodium acetate buffer, pH 5.0) led to a significant increase in liquid mixing within the column as well as a considerable decrease in binding capacity (by ~50%) as compared to processing with solutions not containing added glycerol. However, when processing was conducted in the solutions with increased viscosity together with a decrease in the flow velocity to give an unchanged expanded bed height (i.e. for all values of viscosity tested), the increased viscosity *per se* did not lead to any significant change in liquid dispersion or dynamic binding capacity. These results imply that liquid dispersion and mass transfer changes were responsible for the observations and highlights the complex interplay between these different factors, and how they can to some extent be controlled by changing viscosity and flow velocity. Nevertheless, a number of different studies have shown that in EBA columns in which mixing is low, the limiting factors for protein adsorption are usually intraparticle and film mass transfer rather than solid and liquid dispersion (Draeger and Chase, 1991; Change and Chase, 1996; Barnfield–Frej et al., 1997; Wright et al. 1999 and Wright and Glasser, 2001). A brief consideration of film and intraparticle mass transfer is made below.

The hydrodynamic condition within the EBA column affects film mass transfer due to different factors such as flow velocity and viscosity and their effects on film mass transfer (K_f) can be described by an equation developed by Fan et al. (1960):

$$K_f = \frac{D_m}{d_b}\left\{2 + \left[1.5\left((1-\varepsilon)\,\mathrm{Re}_b\right)^{1/2} Sc^{1/3}\right]\right\} \qquad (9)$$

Re_b is calculated by using equation 2. The Schmidt number (Sc) in equation 9 can be calculated from equation 10 and quantifies the ratio between viscous forces to buoyancy forces in a fluidized bed. D_m ($cm^2.s^{-1}$) is the molecular diffusion coefficient and can be obtained from equation 11 (Young et al. 1980).

$$Sc = \frac{\eta}{\rho D_m} \tag{10}$$

$$D_m = 8.34 \times 10^{-15} \frac{T}{\eta (M_A)^{1/3}} \tag{11}$$

In this equation, T is absolute temperature (K) and M_A is the relative molecular mass of the adsorbate (eg. protein) in $g.mole^{-1}$. η is viscosity in cP.

Recently, He and Niemeyer (2003) developed another correlation for the protein diffusion coefficient based on molecular weight and radius of gyration (R_G) of the adsorbent:

$$D_m = \frac{6.85 \times 10^{-15} T}{\eta \cdot \sqrt{M^{1/3} \cdot R_G}} \tag{12}$$

In this equation, D_m is in $m^2.s^{-1}$, R_G is in Å, T is in K, η is in Pa.s and M is in $kg.kmole^{-1}$.

Based on equations 9, 11 and 12, increasing viscosity results in decreasing film mass transfer. Exploring the effect of flow velocity on film mass transfer is more complicated due to the multiple and opposing effects on voidage and Re_p. In fixed beds, increasing the flow rate can be expected to reduce the thickness of the stagnant layer around the beads and thus increase the film mass transfer rate, however in EBA beds, increased flow rate also leads to increased voidage, which leads to reduced film mass transfer rates (see Eq 9). This has been experimentally proven by Karau et al. (1997) who examined breakthrough curves for different EBA bead size populations at different flow rates and used the slopes at the start and middle of the breakthrough curves for their analysis. They showed that film mass transfer for bovine serum albumin (BSA) during adsorption to Streamline DEAE beads with a size distribution of

120-160 μm decreased by 58% when the flow velocity was increased from 180 to 420 cm.h^{-1}. However, for the same bead types with a size distribution of 250-300 μm, the film mass transfer rate increased by approximately 11% when the same change in the flow velocity was made. The result of this is that at low flow rates (180 cm h^{-1}) film mass transfer rate is higher for the small 120-160 μm beads than the larger 250-300 μm diameter beads, but as flow rate is increased (to 420 cm h^{-1}) the relationship is reversed. For large beads with high terminal settling velocities, increasing the flow rate has less effect on voidage than for small beads. Thus, large beads can be expected to experience less adverse effects on film mass transfer rates as flow rate is increased than will be experienced by small beads (see equation 9).

Karau et al. (1997) also showed that pore diffusion is strongly dependent on the bead size. They found that for smaller beads (120-160 μm) pore diffusion is 3-4 times faster than that for larger ones (250-300 μm) at different flow velocities (180, 300 and 420 cm.h^{-1}) due to the smaller diffusional path lengths.

The structure of the gel material (part of adsorbent bead carrying the ligands) has a great impact on the mechanism and extent of intraparticle and film mass transfer (Wright et al. 1998 and 1999). In porous gels (such as Streamline EBA beads) protein molecules move and diffuse within the liquid phase trapped in the pores. However, in solid gels (such as HyperD and HyperZ), the molecules move between the ligands during diffusion into the solid material. The charge density of the gel and the charge on the molecule have an important impact on this movement. Wright et al. (1998 and 1999) showed that intraparticle mass transfer (pore diffusion) in a porous gel (Streamline SP beads) was reduced by increasing the viscosity of the buffer during adsorption of lysozyme. However, intraparticle mass transfer did not change significantly when the viscosity was increased and the solid gel bead S HyperD LS was used.

Film mass transfer rate decreased for both types of beads by increasing viscosity (Wright et al. 1998 and 1999),

Wright et al. (1998) also showed that increasing the protein concentration decreased the dynamic binding capacity of Cibacron Blue F3G-A-immobilized Fractosil 1000 beads (63-100 μm) for both HSA (concentration range of 0.1-1.0 $mg.mL^{-1}$) and lysozyme (concentration range of 0.1-0.50 $mg.mL^{-1}$). Very similar results were obtained by Thömmes (1999) for adsorption of human polyclonal IgG by Streamline Q XL in a 0.5 cm Ø EBA column with a settled bed height of 53 cm and a flow velocity of ~150 $cm.h^{-1}$. He showed that increasing the concentration in the range of 1,0-4.8 $mg.mL^{-1}$ IgG decreased the dynamic binding capacity of the EBA system by ~ 28%. Thömmes attributed that to the structure of agarose-dextran composite media used in Streamline Q XL adsorbent beads and concluded that such a media can be regarded as comparable to a homogenous gel phase. Based on his explanation, it has been shown that under solid-diffusion-limited conditions, solute (protein) concentration of the bulk affects dynamic binding capacity of chromatography systems (Thömmes, 1999).

Hydrodynamics within an EBA system are significantly affected by fluid distribution system type and design. This topic will be discussed completely in chapter 2.

Applications

A number of review papers have been published between 1994-1999, in which the applications of EBA for processing different biological materials have been reported as well as on the EBA system itself and the problems faced, such as blockage of the fluid distribution system and interactions between adsorbent beads and cells, cell debris and macromolecules

(e.g. genomic DNA) (Hubbuch et al., 2005). Nevertheless, a number of new applications at lab and pilot scale have been reported since 1999 which show the potential for this unit operation, thus a brief review on new applications is given below.

Pyo et al. (2001) used EBA for purification of the recombinant Histone H1.5. A 10 cm Ø EBA column containing 900 mL of the strong cation exchanger Streamline SP adsorbent was successfully used for capture of the product directly from an *Escherichia coli* cell lysate. It was showed that by applying EBA clarification, concentration and an initial purification of recombinant Histon H1.5 could be integrated in one unit operation (Pyo et al., 2001).

In an interesting study, Ohashi et al. (2002) developed the *in situ* capture of immunoglobulin G subclass 2a (IgG_{2a}) from a 2.2-L stirred tank reactor containing a fermentation culture of mouse-mouse hybridoma cells by using a 2.5 cm Ø EBA column containing Streamline rProtein A adsorbent beads. A repeated-batch fermentation process was performed for 11 days and during that time product was purified semi-continuously using a multi-cycle approach with high recovery (95%) and product purity (95%). The productivity was reported to be 58 IgG $mg.cycle^{-1}$ (day^{-1}) for this process, whereas it was only 17 IgG $mg.day^{-1}$ for a simple batch.

Choe et al. 2002 reported applying EBA for capture of the recombinant L1 protein (the major capsid protein of human papilloma virus type 16) from harvested *E. coli* cells following extraction of inclusion bodies of the product directly from the cells using urea. They used Streamline metal immobilized affinity adsorbents in a 1 cm Ø EBA column and obtained a purity factor of 10 and a yield of 60% under unoptimized conditions.

EBA also has been used for purification of biological products from microalgae biomass. For example, Bermejo et al. (2003) purified B-phycoerythrin pigment from a red microalgae called *Porphyridium cruentum* by applying 4 steps including: osmotic shock of

biomass, centrifugation, EBA and conventional chromatography with a column of DEAE-cellulose. A 5 cm Ø EBA column containing Streamline DEAE adsorbent beads was used in this research. Under optimal conditions a total yield of 66% was obtained. Recovery of product by the EBA column was 80%.

Process development for isolation of the insulin precursor MI3 was described by Brixius et al. (2005). They successfully used EBA as a primary recovery step in this process. A home-made 2 cm Ø EBA column and a commercial Streamline 25 (2.5 cm Ø) column were used in method development, and a Streamline 200 (20 cm Ø) column for the scaled up process. Streamline SP, Streamline SP XL and Zirconia S adsorbent beads were used. They observed no interaction between *Saccharomyces cerevisiae* cells and adsorbent beads during loading of a feedstock containing 15% biomass. A yield of 88% was obtained for the capture step by EBA and scalability was proven by scaling up that process from 26 L to 1600 L feed application.

Chang et al. (2006) used immobilized metal expanded bed affinity chromatography for capture of clotting factor IX from unclarified human plasma by using immobilized metal expanded bed affinity chromatography. Different metal ions including Cu(II), Ni(II), Zn(II) and Co(II), were trialled and Cu(II) was found to be the most suitable chelating ligand for capture of the aforementioned protein in a 2.5 cm Ø EBA column containing 50 mL adsorbent beads. A very high purification factor of 83 was obtained in a single step purification using EBA, however the yield was very low (16%).

A comparison between performance of two EBA adsorbent beads; Streamline SP (a cation exchanger with sulphonyl groups) and Streamline Direct HST 1 (a multi-modal so-called mixed-mode adsorbent bead) introduced by Amersham Biosciences (GE HealthCare) was conducted by Charoenrat et al. (2006). They used a 2.5 cm Ø EBA column containing

almost 100 mL of adsorbent for recovery of recombinant β-glucosidase from *Pichia pastoris* high-cell-density culture broth. They showed this recovery could be conducted by using Streamline Direct HST 1 much more effectively than by Streamline SP. Streamline Direct HST 1 successfully captured the enzyme from a feedstock containing 24.8% biomass and with a conductivity of 15 $mS.cm^{-1}$. The only drawback for multi-modal ligand adsorbents could be the unspecific adsorption and elongated elutions due to complexity of interaction by these ligands (Li et al., 2005).

General remarks

A very broad range of applications of EBA have recently been shown through successful studies on the primary recovery of bioproducts. Furthermore, considerable information on the operational parameters and their effects on EBA performance also exists, nevertheless few truly large scale applications seem to exist. Solving the problems in EBA especially those related to either the fluid distribution system (chapter 2 in this thesis) or unwanted interaction between adsorbents and cells, cell debris and macromolecules (chapters 3 and 4 in this thesis), as well as growing advances in developing new affinity ligands and smart polymers (Nicolov and Woodard, 2004) give hope that EBA can develop into a truly widespread, robust and efficient technique for the downstream processing of bioproducts.

References

1. Barnfield Frej, A.K.; Johansson, H.J.; Johansson, S. and Leijon, P.; 1997; **Expanded bed adsorption at production scale: Scale-up verification, process example and sanitization of column and adsorbent**; *Bioprocess Engineering*, 16, 57-64.
2. Barnfield-Frej, A.N.; Hjorth, R. and Hammarström, Å.; 1994; **Pilot scale recovery of recombinant Annexin V from unclarified Escherichia coli homogenate using expanded bed adsorption**; *Biotechnology and Bioengineering*, 1994, 44, 922-929.
3. Bermejo, R.; Acien, F.G.; Ibanez, M.J.; Fernandez, J.M.; Molina, E. and Alvarez-Pez, J.M.; 2003; **Preparative purification of B-phycoerythrin from the microalgae Porphyridium cruentum by expanded bed adsorption chromatography**; *Journal of Chromatography B*, 790, 317-325.
4. Brixius, P.; Mollerup, I.; Jensen, O.E.; Halfar, M.; Thömmes, J. and Kula, M.R.; 2005; **Expanded bed adsorption as a primary recovery step for the isolation of the insulin precursor MI3 process development and scale up**; *Biotechnology and Bioengineering*, 91(3), 14-20.
5. Bruce, L.J. and Chase, H.A.; 2001; **Hydrodynamics and adsorption behaviour within an expanded bed adsorption column studied using in-bed sampling**; *Chemical Engineering Science*, 56, 3149-3162.
6. Chang, Y.K. and Chase, H.A.; 1996; **Development of operating conditions for protein purification using expanded bed techniques: the effect of the degree of bed expansion on adsorption performance**; *Biotechnology and Bioengineering*, 1996, 49, 512-526.
7. Chang, Y.K.; Horng, J.T.; Haung, R.Z. and Lin, S.Y.; 2006; **Direct capture of factor IX from unclarified human plasma by IMEBAC**; *Biochemical Engineering Journal*, 29, 12-22.
8. Charoenrat, T.; Ketudat-Carins, Mariena; Jahic, M.; Enforce, S.O. and Veide, A; 2006; **Recovery of recombinant β-glucosidase by expanded bed adsorption from *Pichia pastoris* high-cell-density culture broth**; *Journal of Biotechnology*, 122, 86-98.
9. Chase, H.A. and Draeger, N.M.; 1992; **Expanded bed adsorption of proteins using ion-exchangers**; *Separation Science and Technology*, 27(14), 2021-2039.

10. Chase, H.A.; 1994; Purification of proteins by adsorption chromatography in expanded beds; *Trends in Biotechnology*, 12, 296-303.
11. Choe, W.S.; Clemmitt, R.H.; Chase, H.A. and Middelberg, A.P.J.; 2002; **Coupling of chemical extraction and expanded bed adsorption for simplified inclusion body processing: Optimization using surface plasmon resonance**; *Biotechnology and Bioengineering*, 81(2), 221-232.
12. Clemmitt, R.H. and Chase, H.A.; 2003; **Impact of operating variables on the expanded bed adsorption of *Saccharomyces cerevisiae* cells using a concanavalin A derivatized perfluorocarbon**; *Biotechnology and Bioengineering*, 82(5), 506-516.
13. Draeger, N.M. and Chase, H.A.; 1991a; **Liquid fluidized beds for protein purification**; *Transactions of IChemE*, 69, 45-58.
14. Draeger, N.M. and Chase, H.A.; 1991b; **Liquid fluidized bed adsorption of protein in the presence of cells**; *Bioseparation, 2*, 67-80.
15. Fan, L.T.; Yang, Y.C. and Wen, C.Y.; 1960; **Mass transfer in semifluidized beds for solid-liquid system**; *AIChE journal*, 6(3), 482-487.
16. Finette, G.M.S.; Mao, Q.M. and Hearn, M.T.W.; 1998; **Examination of protein adsorption in fluidized bed and packed bed columns at different temperatures using frontal chromatographic methods**; *Biotechnology and Bioengineering*, 58(1), 35-46.
17. He, L. and Niemeyer, B.; 2003; **A novel correlation for protein diffusion coefficients based on molecular weight and radius of gyration**; *Biotechnology progress*, 19, 544-548.
18. Hjorth, R.; 1999; Expanded bed adsorption: elution in expanded bed mode; *Bioseparation*, 8, 1-9.
19. Hjorth, R.; Kampe, S. and Carlsson, M.; 1995; **Analysis of some operating parameters of novel adsorbents for recovery of proteins in expanded beds**; *Bioseparation*, 5, 217-223.
20. Hjorth, R.; Leijon, P; Barnfield Frej, A.K. and Jagersten, C.; 1998; **Expanded Bed Adsorption Chromatography**; In: Subramanian, G. (ed.), *Bioseparation and Bioprocessing*, Vol. 8, Wiley-VCH Verlag GmbH, Weinheim, Germany, Pages: 199-226.
21. Hjorth, R; 1997; **Expanded bed adsorption in industrial bioprocessing: recent developments**; *TIBTECH*, 15, 230-235.

22. Hubbuch, J.; Thömmes, J. and Kula, M.R.; 2005; **Biochemical engineering aspects of expanded bed adsorption**; *Advances in Biochemical Engineering/Biotechnology*, 92, 101-123.
23. Kaczmarski, K. and Bellot, J.C.; 2004; **Theoretical investigation of axial and local particle size distribution on expanded bed adsorption process**; *Biotechnology Progress,* 20, 786-792.
24. Kaczmarski, K. and Bellot, J.C.; 2005; **Influence of particle diameter distribution on protein recovery in the expanded bed adsorption process**; *Journal of Chromatography A*, 1069, 91-97.
25. Karau, A.; Benken, J; Thömmes, J. and Kula, M.R.; 1997; **The influence of particle size distribution and operating conditions on the adsorption performance in fluidized beds**; *Biotechnology and Bioengineering*, 55(1), 54-64.
26. Levenspiel, O.; 1999; ***Chemical reaction engineering***; 3rd ed. New York, John Wiley and Sons, Inc.
27. Li, P.; Xiu, G. and Rodrigues, A.E.; 2005; **Experimental and modeling study of protein adsorption in expanded bed**; *AIChE Journal*, 51(11), 2965-2977.
28. Lihme, A.; Zafirakos, E.; Hansen, M. and Olander, M.; 1999; **Simplified and more robust EBA processes by elution in expanded bed mode**; *Bioseparation*, 8, 93-97.
29. Nicolov, Z.L. and Woodard, S.L.; 2004; **Downstream processing of recombinant proteins from transgenic feedstock**; *Current Opinion in Biotechnology*, 15, 479-486.
30. Noda, M.; Sumi, A.; Ohmura, T. and Yokoyama, K.; 1996; **Process for purifying recombinant human serum albumin**; *European patent*, EP0699687.
31. Ohashi, R.; Otero, J.M.; Chwistek, A.; Yamato, I.; Hamel, J.F.; 2002; **On-line purification of monoclonal antibodies using an integrated stirred-tank reactor/expanded-bed adsorption system**; *Biotechnology Progress*, 18(6), 1292-300.
32. Pyo, S.H.; Lee, J.H.; Park, H.B.; Hong, S.S. and Kim, J.H.; 2001; **A large scale purification of recombinant Histone H1.5 from *Escherichia coli***; *Protein Expression and Purification*, 23, 38-44.
33. Somers, W.; Van'T Reit, K.; Rozie, H.; Rombouts, F.M. and Visser, J.; 1989; **Isolation and purification of endo-polygalacturonase by affinity chromatography in fluidized bed reactor**; *The Chemical Engineering Journal*, 7-19.

34. Thelen, T.V. and Ramirez, W.F.; 1997; **Bed-height dynamics of expanded beds;** *Chemical Engineering Science*, 52, 3333-3344.
35. Theodossiou, I. and Thomas, O.R.T.; 2002; **DNA-induced inter-particle cross-linking during expanded bed adsorption chromatography: impact on future support design**; *Journal of Chromatography A*, 971, 73-86.
36. Thömmes, J.; 1997; **Fluidized bed adsorption as a primary recovery step in protein purification**; *Advances in Biochemical Engineering /Biotechnology*, 58, 185-230.
37. Thömmes, J.; 1999; **Investigations on protein adsorption to agarose-dextran composite media**; *Biotechnology and Bioengineering*, 62(3), 358-362.
38. Tong, X.D. and Sun, Y.; 2002; **Particle size and density distributions of two dense matrices in an expanded bed system;** *Journal of Chromatography A*, 977(2), 173-182.
39. Wright, P.R. and Glasser, B.J.; 2001; Modeling mass transfer and hydrodynamics in fluidized bed adsorption of proteins; *AIChE Journal*, 47(2), 474-488.
40. Wright, P.R.; Muzzio, F.J. and Glasser, B.J.; 1998; **Batch uptake of lyzosyme: effect of solution viscosity and mass transfer on adsorption**; *Biotechnology progress*, 14, 913-921.
41. Wright, P.R.; Muzzio, F.J. and Glasser, B.J.; 1999; **Effect of resin characteristics on fluidized bed adsorption of proteins**; *Biotechnology progress*, 15, 932-940.
42. Young, M.E.; Carroad, P.A. and Bell, R.L.; 1980; **Estimation of diffusion coefficients of proteins**; *Biotechnology and Bioengineering*, 22, 947-955.
43. Yun, J.; Yao, S.J.; Lin, D.Q.; Lu, M.H. and Zhao, W.T.; 2004; **Modeling axial distributions of adsorbent particle size and local voidage in expanded bed**; *Chemical Engineering Science*, 59, 449-457.
44. Zhang, Z.; Burton, S.; Williams, S.; Thwaites, E. and Lyddiatt, A.; 2001; **Design and assembly of solid-phases for the effective recovery of nanoparticulate bioproducts in fluidized bed contactors**; *Bioseparation*, 10, 113-132.

2 Critical evaluation and comparison of fluid distribution systems for Expanded Bed Adsorption

Arpanaei, Ayyoob[1]; Heebøll-Nielsen, Anders[1,3]; Thomas, Owen R.T.[1,2], *Hobley, Timothy J.[1]

[1]Center for Microbial Biotechnology, Building 223, BioCentrum-DTU, Technical University of Denmark, 2800-Kgs. Lyngby, Denmark

[2]Current address: Department of Chemical Engineering, University of Birmingham, Edgbaston, B15 2TT, UK

[3]Current address: Danish Technological Institute, Centre for Microtechnology and Surface Analysis, Gregersensvej, DK-2630, Taastrup, Denmark

*Author for correspondence: Timothy J. Hobley, Center for Microbial Biotechnology, BioCentrum-DTU, Technical University of Denmark, Building 223, Søltofts Plads, DK-2800-Kgs. Lyngby, Denmark (Tel: +45 4525 2706, Fax: +45 4588 4148; E-mail: th@biocentrum.dtu.dk)

Abstract

The hydrodynamic properties of an expanded bed contactor with 30 cm or 150 cm internal diameter, which employs a rotating or oscillating fluid distributor, were compared to prototype columns of 60 cm or 150 cm diameter employing local stirring for fluid distribution. When compared at the same flow rates and with similar heights of settled bed, fluid introduction *through* a rotating fluid distributor (RFD) gave superior hydrodynamic characteristics in the 30 cm and 150 cm diameter column than using the local stirrer (LS) in both the 60 cm and 150 cm diameter columns. The shortcomings of the local stirring distributor at large scale were apparent: dead zones were present which could not be removed by increasing rotation rates or flow rates, and such changes lead to deterioration in hydrodynamic properties. In contrast fluid introduction through a rotating distributor was found to be suitable for feed application to large EBA columns: no dead zones were observed, and residence time distribution tests showed that plate numbers remained constant or increased slightly as flow rate was raised from 200 – 470 $cm.h^{-1}$. However at very low rotation rates combined with low flow rates (e.g. 200 $cm.h^{-1}$) performance of the RFD dropped. Residence time distribution studies showed that under the conditions studied oscillatory movement of the RFD fluid distributor led to increased mixing and poorer performance than rotary movement. The results suggest that the best column performance relies on an interplay between: (i) fluid distribution resulting from the jets leaving the RFD distributor; (ii) rate of fluid application over the column base; and (iii) turbulence created by the distributor.

Keywords: EBA, Hydrodynamics, Fluid distributor, Rotating, Oscillating, Chromatography.

Introduction

Expanded bed adsorption (EBA) has the potential to markedly simplify existing downstream processing purification trains by fusing three classical steps – clarification, concentration and initial purification – into one unit operation (Hansson et al., 1994; Johansson et al., 1996; Pierce et al., 1999; Anspach et al., 1999 and Gonzalez et al., 2003). In EBA, adsorbent particles with a defined size and density distribution are fluidized by a mobile phase directed upwards to form a stable 'classified' fluidized bed, which is commonly termed an expanded bed (Draeger and Chase, 1991; Chase, 1994; Thömmes, 1997; Hjorth et al., 1998 and Anspach et al., 1999). Central to the performance of the EBA system is that axial mixing is low and that the void fraction is increased which allows the application of crude bioprocess liquors such as culture broths or cell homogenates without the risk of blocking the chromatographic bed (Chase, 1994; Thömmes, 1997; Hjorth, 1997; Draeger and Chase, 1991; Hjorth et al., 1998 and Anspach et al., 1999). Under ideal conditions the adsorbent beads move little relative to each other and fluid moves through the bed in a laminar flow type way, giving rise to a number of theoretical plates in the column and chromatographic behavior that is analogous to that of a packed bed (Chase, 1994; Thömmes, 1997 and Hjorth, 1997). In order to maximize plate numbers, dead zones and channeling should be avoided and the amount of axial dispersion minimized. The quality of the flow introduced within the column has a large impact on bed stability, mixing and ultimately system performance. The type of distributor employed within a fluidized bed column can have very significant effects on the resulting chromatographic performance of the system given that the latter is inextricably linked to the prevailing mixing conditions (Hjorth, 1997; Thömmes, 1997 and Anspach et al., 1999). Perforated plate distributors give suitable hydrodynamic properties in columns up to 60 cm in diameter (Bjarnfield Frej et al., 1997 and Hjorth et al., 1998) and larger (Noda et al.,

1996), however are prone to severe fouling and consequent cleaning in place difficulties (Anspach et al., 1999; Brobjer, 1999 and Feuser et al., 1999).

In view of these constraints on EBA, new types of fluid distributors have been sought with perhaps the most plausible being the recent invention of a rotating fluid distributor (RFD) prototype, which was successfully demonstrated in expanded bed columns of up to 150 cm internal diameter (Hubbuch et al., 2001 and 2002 and Hobley et al., 2003). In the only reported studies with such a large column, Hubbuch et al. (2001 and 2002) studied hydrodynamic performance under different operational conditions and showed by applying a rotating fluid distributor that a parabolic flow pattern suitable for EBA processing was obtained and up to 29 theoretical plates were measured. Those authors also showed that the hydrodynamic conditions within the column are very susceptible to small changes in rotation rate of the distributor. The optimal condition needed for the lowest value of axial dispersion was obtained at a rotation rate of 2.5 rpm. Since the report of Hubbuch et al. (2001), Feuser et al. (2002) and Nilsson (2004) both studied the performance of EBA columns (Streamline Direct) with diameters of 2.4-60 cm equipped with a fluid distribution system capable only of oscillating through ca. 180^{o} (i.e. not rotating) and concluded that a robust scale up could be achieved as well as suitable cleaning in place (CIP).

Despite the above successes, alternative fluid distribution systems have also been studied. Clemmitt and Chase (2003) reported stable expansion was obtained by applying a stirred distribution system in a 1 cm column and compared the performance to that for a sintered distribution system. They showed that shear within the column created by the stirred distribution system was sufficient to prevent the formation of aggregates and bed collapse, whereas applying a sintered distribution system led to formation of aggregates and a large drop in *Saccharomyces cerevisiae* binding capacity (~ 85%) when a prototype resin made of

perfluorocarbon coated by polyvinyl alcohol and functionalized by concanavalin A was used. Menkhaus and Glatz (2004) compared the performance of different inlet designs for processing of corn endosperm extract by expanded bed adsorption. They showed that applying a localized mixing and stirring style of distributor allowed corn solids up to 550 µm to enter the column (FastLine 20 column, UpFront Chromatography A/S) without clogging. Applying a 50-µm or 80-µm pore sized mesh type of distributor within the column (Streamline 25 column, Amersham BioSciences) led to clogging of the inlet at all flow velocities used (up to 570 $cm.h^{-1}$) (Menkhaus and Glatz, 2004). However, Anspach et al. (1999) as well as others (Diehl, 1998 and Hubbuch et al., 2002) proposed that the performance of a distributor based on local stirring for columns larger than those evaluated by Zafirakos and Lihme (1999) (i.e. >40 cm diameter) is questionable due to the prediction of excessive mixed zones for columns of larger diameters. In the locally stirred design, flow is introduced into the column through one or more inlets located around the column wall (Zafirakos and Lihme, 1999). Those authors showed that stable bed expansion above the mixed zone created by the stirrer leads to efficient adsorption of *Lens culinaris* agglutinin by UFC MIMO (mixed mode ligand) beads from an extract of crushed red split lentils under the tested conditions. They also showed that increasing the column diameter from 2 cm to 40 cm increased the ratio of the mixed zone height to expanded bed height from 12.5% to 20%, which in turn led to lower numbers of theoretical plates (Zafirakos and Lihme, 1999). To date, no examinations of the hydrodynamic properties, of EBA columns above 40 cm in diameter employing localised stirring appear to have been reported and no concrete data has been presented to support the contention that they cannot be scaled up.

In this paper, we conduct a systematic investigation of the hydrodynamic properties of large scale columns (30 cm and 150 cm diameter) employing a rotating fluid distributor and

under the same conditions, directly compare the performance with 60 cm and 150 cm diameter columns employing localized stirring fluid distribution. Using dye and acetone tracers, the effects of rotation rate and flow rate in the columns on dead zones, turbulent and mixing zones and on hydrodynamic parameters are examined. In contrast to previous studies, the effect of distributor oscillation period is also examined in the 30 cm diameter commercial column from UpFront Chromatography A/S.

Materials and methods

Materials

Underivatized EBA chromatography matrix consisting of 1-4 silica beads surrounded by cross-linked agarose (density 1.3 – 1.5 $kg.L^{-1}$ and size distribution 100 – 300 μm) was donated by UpFront Chromatography A/S (Copenhagen, Denmark). Bromophenol blue and acetone were supplied by Sigma Chemical Co. (St. Louis, Mo). Tap water was used to fluidize the supports in all experiments.

Columns employing a rotating fluid distributor

A FastLine 300 EBA column (30 cm diameter) from UpFront Chromatography A/S (Copenhagen, Denmark) was used (designated here as RFD30). The glass column was equipped with a controllable rotating or oscillating fluid distribution system fixed to a stainless steel bottom. The drive shaft for the distributor was a tube and passed through the base plate and ended in a boss that screwed into the central distribution chamber, from which was connected 8 cylindrical arms ~ 2 cm above the base plate, and with 2 holes (facing down) in each. Water was pumped by a peristaltic pump (624U, Watson-Marlow Bredel Pumps,

Cornwall, England) through a tube that was split in two parts: one connected to the drive shaft tube and another one to a space underneath the base surrounding the drive shaft. Thus the flow was introduced to the column through both the drive shaft tube (and the arms connected to that) and in the middle of the column around the drive shaft (Figure 1). In total, eight holes were located in the tips of the distributor arms and 8 more holes were located either 3 or 7 cm from the distributor center (Figure 1). Liquid was removed from the column via a floating adaptor and peristaltic pump.

The 150 cm diameter column equipped with a rotating fluid distributor (RFD150) is shown schematically in Figure 1 and has been described previously (Hubbuch et al., 2002). Briefly, a 150 cm diameter, 71 cm high PVC column was bolted to a stainless steel base plate, underneath which motor and gear box were mounted. The shaft of the gear box passed through the base and the distributor was attached by means of a central bolt. The influent passed through a pipe next to the drive shaft and into the rotating distributor from which it was distributed through 12 tubular pipes, each carrying 4 fluid outlet holes (for more details see Hubbuch et al., 2002). At the other end of the influent feed pipe was placed, in order, a non-return valve, flow meter (Type SK 30, Georg Fischer, Schaffhausen, Switzerland), sample loop (200 ml or 600 ml) and a centrifugal feed pump. The top of the column contained a floating collector manifold which was connected to a centrifugal pump for fluid removal (as described in Hubbuch et al., 2002).

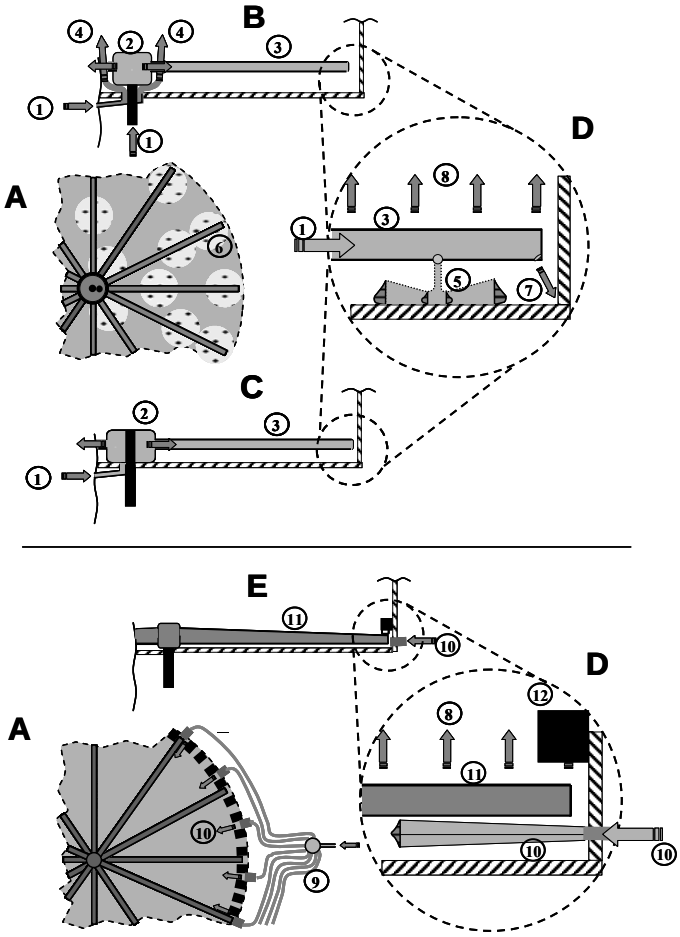

***Figure 1*: Schematic of the fluid distribution systems examined. Upper panel: RFD 30 and RFD150. Lower panel: LS60 and LS150. (A) top view of the bottom of the columns, (B) Side view of the RFD30, (C) side view of the RFD150, (D) expanded side view of the distributor tips and column walls, (E) side view of the LS60 and LS150 columns. Legend: 1, fluid entry into the distributor; 2, distributor central chamber; 3, hollow distributor arm; 4, liquid flow around the RFD30 central chamber; 5, liquid jet leaving the distributor blade and impacting column base; 6, zones from fluid jets impacting floor of the RFD150 column; 7, fluid jet from end of distributor; 8, fluid rising up through the column; 9, manifold on LS150 column; 10, fluid jet entering the LS columns; 11, stirrer; 12, baffle.**

Columns employing localized stirring distributors

The 150 cm diameter column using localized stirring (LS150) was as described above for the RFD150 except that the central fluid inlet tube was blocked off and instead fluid

entered the from the column walls (Figure 1). The pump and flow meter as described above were used, then the feed was split into two manifold systems each comprising 8 pipes to feed in total 16 ports (3 mm ID) placed evenly around the column wall. The ports were ~3 cm above the column base. Forty eight baffles were placed evenly around the column wall above the ports, and 5 cm from the column base. The stirrer was rotated by the motor and gearbox described above for the RFD150 and was constructed of 12 stainless steel blades which extended to within 2 cm of the column wall and which had a flat frontal profile ~2 cm high at the wall and ~7 cm high in the centre. Liquid was removed from the column via the self adjusting floating top adaptor and a centrifugal pump as described above for the RFD150.

The 60 cm diameter locally stirred column (LS60) was constructed on the same principles (Figure 1) as that for the 150 cm diameter system with the following differences. The PVC column was 60 cm in diameter and 150 cm high. Fluid was fed via 8 radial ports (3 mm ID) placed 3.5 cm above the base and 16 baffles (7 cm high) were placed 8 cm above the base. The bottom of the stirrer was 1 cm above the column base and was a scaled down version of that used in the 150 cm diameter column. The stirrer diameter was 56 cm and consisted of 8 blades with a flat front edge of ~2 cm at the column wall and ~5 cm in the middle and was rotated by a motor and gearbox placed under the base plate. Fluid was removed from the column via a floating adaptor and a pump as described above for the LS150.

Operation of the columns

For all columns, chromatography matrix was added to give the desired settled bed height (~25 cm for the RFD30 and ~30 cm for the other column types) then tap water (approx. 10^{o}C) was pumped at a superficial velocity of 283 cm. h^{-1} to the column until the bed had

expanded approx. 1.3 – 1.4 times. Rotation of the stirrer or distributor at the desired speed was then initiated and subsequently, the flow rate changed to that required. The head-space between the top of the bed and the top of the fluid level was maintained at approx. 7 cm (ca. 3 cm for the RFD30) by manual adjustment of the outflow pump. After stabilisation of the complete system for at least 30 minutes the expanded height (H) of the bed was recorded. The settled bed height (H_o) was then determined after allowing the bed to settle. A spirit level was used to ensure the column was vertical.

Bed expansion characteristics

Expansion of the matrix inside the columns was examined by measuring the bed height at different flow rates and distributor rotation rates. The voidage of the expanded bed (ε) was calculated by applying equation 1 (McCabe et al., 1985):

$$\frac{H}{H_0} = \frac{(1-\varepsilon_0)}{(1-\varepsilon)} \qquad (1)$$

For the settled bed voidage (ε_0) the standard assumption that ε_0=0.4 was used (Di Felice, 1995; Thelen and Ramirez, 1997 and Theodossiou et al., 2002).

Determination of turbulent and dead zones, flow patterns and interstitial velocities

Freshly prepared bromophenol blue solution in 1 M NaOH (20 mL, 20 $g.L^{-1}$ for the 30 cm column, or 20 mL of 10 $g.L^{-1}$ for the 60 cm column, or 200 ml of 10 $g.L^{-1}$ for the 150 cm diameter columns) was added after the feed pump to study dye band dispersion at the fluid velocities, rotation rates and oscillation periods mentioned in the text. The dye band broadening in the RFD30 was investigated by measuring the height of the leading and trailing

edges of the dye band at the column wall at various times. The rate of dye band movement and thus the interstitial fluid velocity at the column wall were determined by plotting the rate of movement of the leading edge of the dye and comparing to that expected theoretically from a knowledge of the superficial flow velocity and average bed voidage. The interstitial flow velocity in the center was determined by measuring the height of the expanded bed and observing the time taken for the first trace of a pulse of dye to be visible at the surface of the bed (Hubbuch et al., 2002). For the RFD150 and LS150, photographs were taken of the dye band with a digital camera (Optio330, PENTAX Digital Camera, Asahai Opt.Co.Ltd., assembled in Philippins) and the images processed with Quantity one version 4 software (BioRad Laboratories, Hercules, CA) using the suppliers instructions in a similar way to quantification of *coomasie* blue stained protein bands on polyacrylamide gels.

Residence time distribution study

The residence time distribution (RTD) of tracer was studied by injection of freshly prepared acetone solution (50% v/v) to the expanded bed at different flow velocities and distributor rotation rates. Tracer injection with a syringe (20 mL, or 50 mL respectively) was used for the 30 cm and 60 cm diameter columns and via a sample loop (600 mL) for the 150 cm diameter columns. The UV absorbance of the outlet stream was measured by a UV-1 detector (Amersham Biosciences, Upsala, Sweden) fitted with an industrial flow cell and a 280 nm filter after splitting a small stream from the column outflow tube. The output signal from the detector was captured every second using Baseline 810, version 3.30, data acquisition software (Dynamic Solutions Division, Millipore, Bedford, MA).

RTD curves were prepared based on dimensionless exit age distribution of tracer (E_θ) versus dimensionless time (θ) at superficial flow velocities, distributor rotation rates and

oscillation periods as mentioned in the text. The RTD data obtained were evaluated by the dispersion and tanks in series models (Levenspiel, 1999) assuming a large deviation from plug flow as described previously (Hubbuch et al., 2002; Theodossiou et al., 2002). The dimensionless variance of the RTD curves was used to determine the axial dispersion coefficient, D_{ax}, the column Peclet number, Pe, the number of theoretical plates, N and height equivalent to a theoretical plate, HETP (calculated based on expanded bed height) (Levenspiel, 1999).

Results and discussion

Bed expansion characteristics

The expansion profile of the supports in a column is typically used to determine the range of operating flow rates that may be used and can also provide qualitative information about fluid distribution. Bed expansion for the different columns examined here increased linearly as flow rate was raised, except for the LS60 column which had a convex shape (Figure 2). This may result from channeling of the jets of fluid entering the column, leading to under expansion of the bed (Figure 2). This contention is supported by the observation that bed expansion in the LS60 column increased when rotation rate was increased from 5 to 10 rpm and fluid distribution in the bottom was improved. For all of the other columns, bed expansion was found to remain almost constant when the distributors were rotated at different rates (data not shown). Oscillation of the distributor (periods of 10, 20, 30 and 40 seconds) in the RFD30 column had no obvious effect on bed expansion. Nevertheless, when the distributor rotation rate in the RFD30 was increased to 60 rpm the bed surface was rotating vigorously and obvious fluctuations in the surface were observed.

For all columns, bed expansion was lower when there was no rotation (i.e. 0 rpm). In the RFD30 the expansion factor was lower when not rotated, but increased with the same slope as the flow velocity was raised as compared to that for rotation rates between 2-60 rpm (Figure 2). The Y-intercept value (i.e. corresponding to zero flow rate) in Figure 2 for the RFD30 is 1.06 (i.e. above 1), most likely due to high voidage in the turbulent zone at the bottom of this column, as hypothesized by Theodossiou et al. (2002) to account for observations in 1 cm diameter columns. The Y-intercept for the LS60 column is considerably below 1 (0.88), which is further indication that poor fluid distribution was present, leading to channeling and under expansion. For the LS150 and RFD150, the Y-intercept values at zero flow rate were 0.98 and 0.99, respectively.

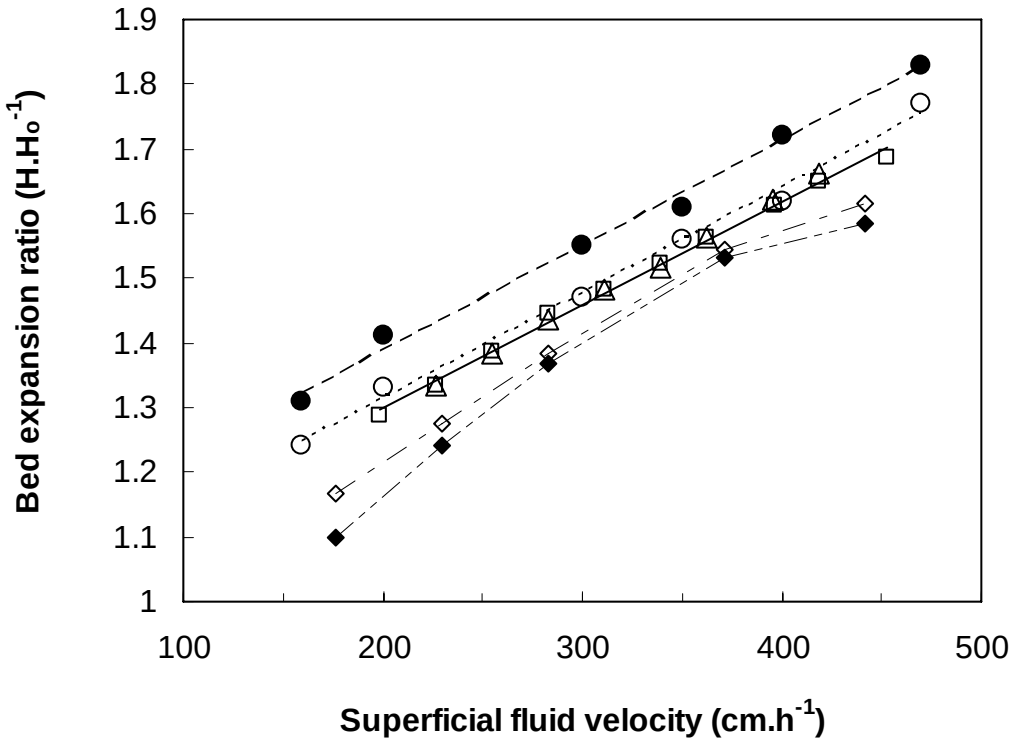

***Figure 2*: Bed expansion of the different columns studied at different flow velocities. (--●--) RFD30, 20 rpm; (…○…) RFD30 not rotating; (—□—) RFD150, 2.5 rpm; (-·-◆-·-) LS60, 5 rpm; (-···-◇-···-) LS 60, 10 rpm; (△) LS 150, 7.5 rpm. Linear regression through the data is shown for: RFD30, 20 rpm; RFD30 not rotating; RFD150, 2.5rpm.**

Visual observations of flow in the columns

The results above suggested that bed expansion was affected by rotation rate, especially for the LS60 column, but also that in general for all columns proper bed expansion did not occur if the distributor was not rotated. It therefore seems reasonable to assume that under some conditions, channeling and formation of dead zones may be occurring. Dead zones should not be present in an EBA column, since in these areas matrix capacity will not be fully utilized, and cleaning in place and sanitization are also hampered.

Addition of dye tracer showed that for all columns rotation of the distributor was necessary, otherwise dead zones existed. As an example, dye spots remained within the RFD30 column in the spaces between the distributor arms for at least 120 s after injection, if no rotation was used (Figure 3).

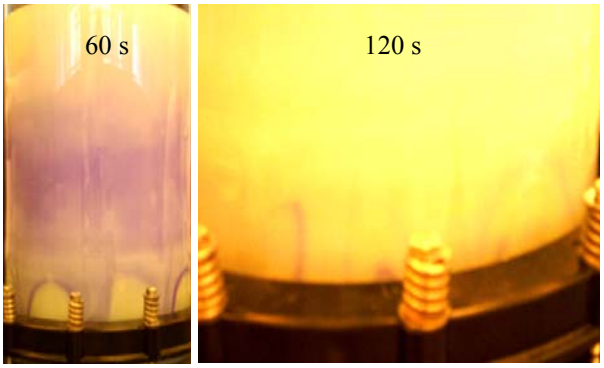

***Figure 3*: Channeling occurring in the RFD30 when the distributor was not rotated, shown at different times after dye tracer injection. Flow velocity=300 cm.h^{-1}, H.H$_o^{-1}$=1.55.**

When the distributor in the RFD30 was rotated at 20 rpm, the dye band rose up as a discrete band (Figure 4) and similar results were seen in all other columns. In all columns, increasing the distributor rotation rate led to a larger mixed or turbulent zone in the bottom (Figure 5). For the RFD30 with a distributor rotation rate of 60 rpm, the mixed zone occupied more than 70% of the expanded bed. The dye dispersed within this zone a few seconds after injection,

with the result that the dye slowly rose up the column as a much wider band than when 10 and 20 rpm were used. In general the greater the mixed zone the wider the dye band which resulted (see Figure 6).

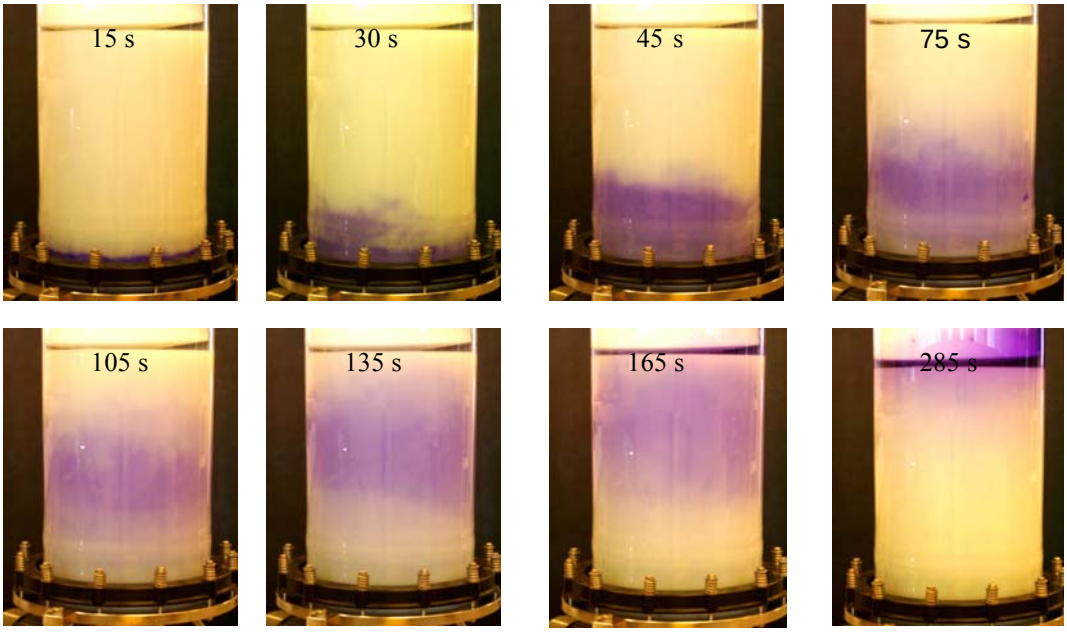

***Figure 4*: Movement of a dye band through the RFD30 shown at different times after injection of tracer. Flow velocity: 470 cm.h^{-1}, H.H$_o^{-1}$ = 1.95, rotation rate = 20 rpm (no oscillation).**

For the LS60 and LS150 columns with local stirring, a dead zone could be seen under the distributor which was not removed when rotation rate was increased from 5 to 20 rpm or 3.75 to 7.5 rpm for the 60 or 150 cm columns, respectively (Figure 5). Increases in rotation rate to 20 rpm in the LS60 column not only could reduce the dead zone under the distributor, but also led to a dramatic increase in the mixing zone height (Figure 5). The same effect was observed at all of the flow rates studied. However, more serious was the observation at low flow velocities (174 cm.h^{-1}) and low rotation rates (5 rpm), of dye in the region between the baffles in the LS60 column after the dye front had exited the bed. In both the LS columns the height of the mixing zone could not be reduced below a minimum value (~13 cm and ~14 cm for the LS60 and LS150, respectively) due to the presence of the baffles. In contrast no dead

zones were present in either column using the RFD and the size of the turbulent zone could be minimized by reducing the rotation rate (Figure 5). As stated earlier (Hubbuch et al., 2002), a factor contributing to the height of the turbulent zone in RFD columns is the distance between the distributor blades and the bottom of the column as well as turbulence caused by the moving blades. Thus the minimum mixed zone heights for the RFD 150 prototype and the RFD30 examined here were ~ 10.7 cm, and ~11 cm (see Figures 5A and 6B). For the RFD30, the lowest mixed zone was obtained when the flow velocity was 470 $cm.h^{-1}$ and rotation rate 20 rpm.

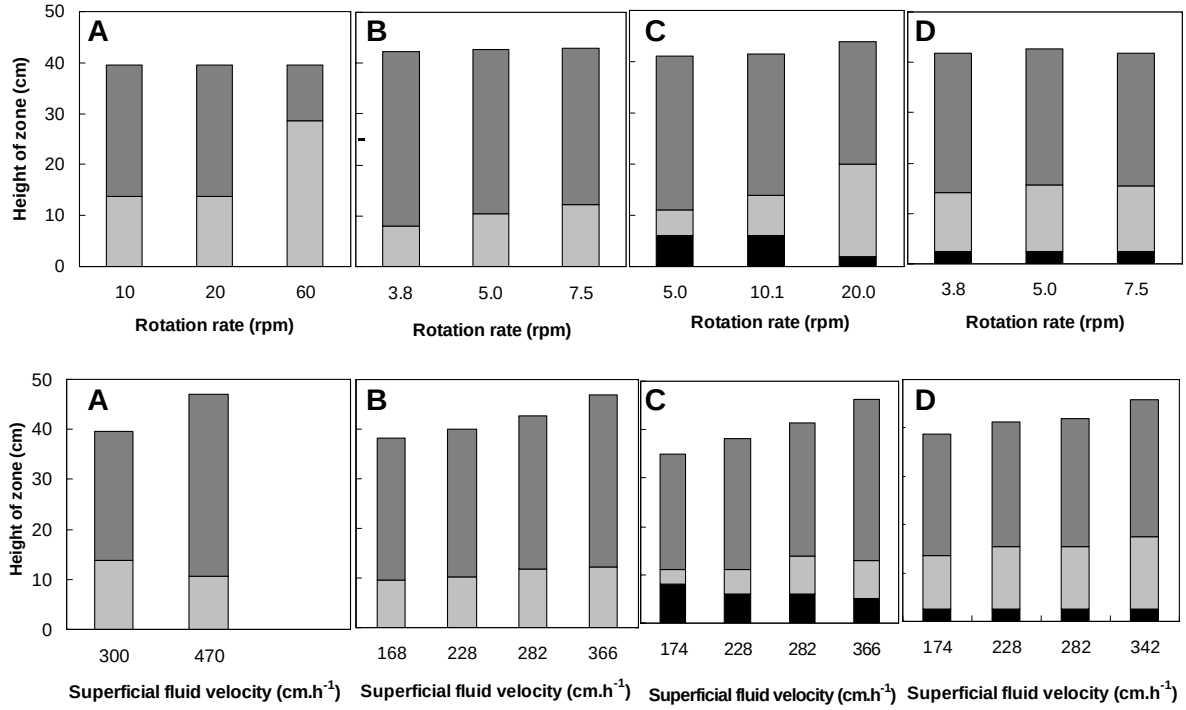

***Figure 5*: Comparison of dead zones under the distributor (■), turbulent zone (■) and total expanded bed height (■) in (A) the RFD30, (B) RFD150, (C) LS60, (D) LS150. Upper panels show the effects of varying rotation rate whilst holding superficial fluid velocity constant at 300 $cm.h^{-1}$ for the RFD30 or 282 $cm.h^{-1}$ for the other columns. The bottom panels show the effect of changing fluid velocity whilst holding rotation rate constant at 20, 7.5, 10 and 7.5 rpm for the RFD30, RFD150, LS60 and LS150, respectively.**

Progression of dye bands up the columns was followed in order to determine the rate of fluid travel and to examine band broadening. Figures 6A and 6B show the effect of rotation

rate (no oscillation) on dye band movement in the RFD30 at flow velocities of 300 and 470 $cm.h^{-1}$, respectively. It was observed that in both cases, the leading edge of the dye band moves at a higher rate than the trailing edge, leading to band broadening. The dye band broadening rate gives an indication of the extent of dispersion within the column overall, which is a combination of dispersion in the mixed zone and in the area above it. The results show that dye band broadening was greatest when the rotation rate was 60 rpm or when the distributor was stationary (Figures 6A, 6B). However at 0 rpm, channeling rather than increased dispersion is likely to be responsible for these observations (Figure 3). At 60 rpm, no distinct trailing edge was observed during the measurement period for both rotary and oscillatory movements of the distributor (Figures 6A, 6C). Interestingly, band broadening was much reduced using a rotation rate of 20 rpm, compared to 10 rpm, when high flow rates were used (Figure 6B) than at lower flow rates (Figure 6A), which may be due to the observation that the mixed zone decreased for all rotation rates when the flow velocity was raised from 300 to 470 $cm.h^{-1}$ (Figure 5). However, even under this condition, the dye band broadened to a width of 30 cm just before exiting the RFD30 column. Oscillation of the distributor in the RFD30 led to no benefit with respect to band broadening. For example, using a period of 20 seconds at a flow velocity of 470 $cm.h^{-1}$ and rotation rate of 20 rpm, led to an increased band width as compared to the same condition without oscillation (cf. Figures 6D and 6B). Analysis of dye band broadening for the RFD150 has been presented earlier (Hubbuch et al., 2002) and thus in the current work a new analysis method was employed to examine movement of the dye band peak in the RFD150 and LS150. A comparison of band movement for the RFD150 and LS150 at a superficial fluid velocity of 283 $cm.h^{-1}$ and rotation rates of 3.75 rpm is shown in Figure 7. Photographs were taken every 10s and then spliced together. The rate of movement of the dye and of peak broadening appears similar in both columns,

although considerable variation in the bed height of the LS150 is evident (Figure 7). The dye bands in each photo strip were analysed with BioRad software allowing identification of the dye band peak. A summary of the data for rate of dye band movement and the corresponding interstitial fluid velocities calculated is presented in Figure 8 and Table 1.

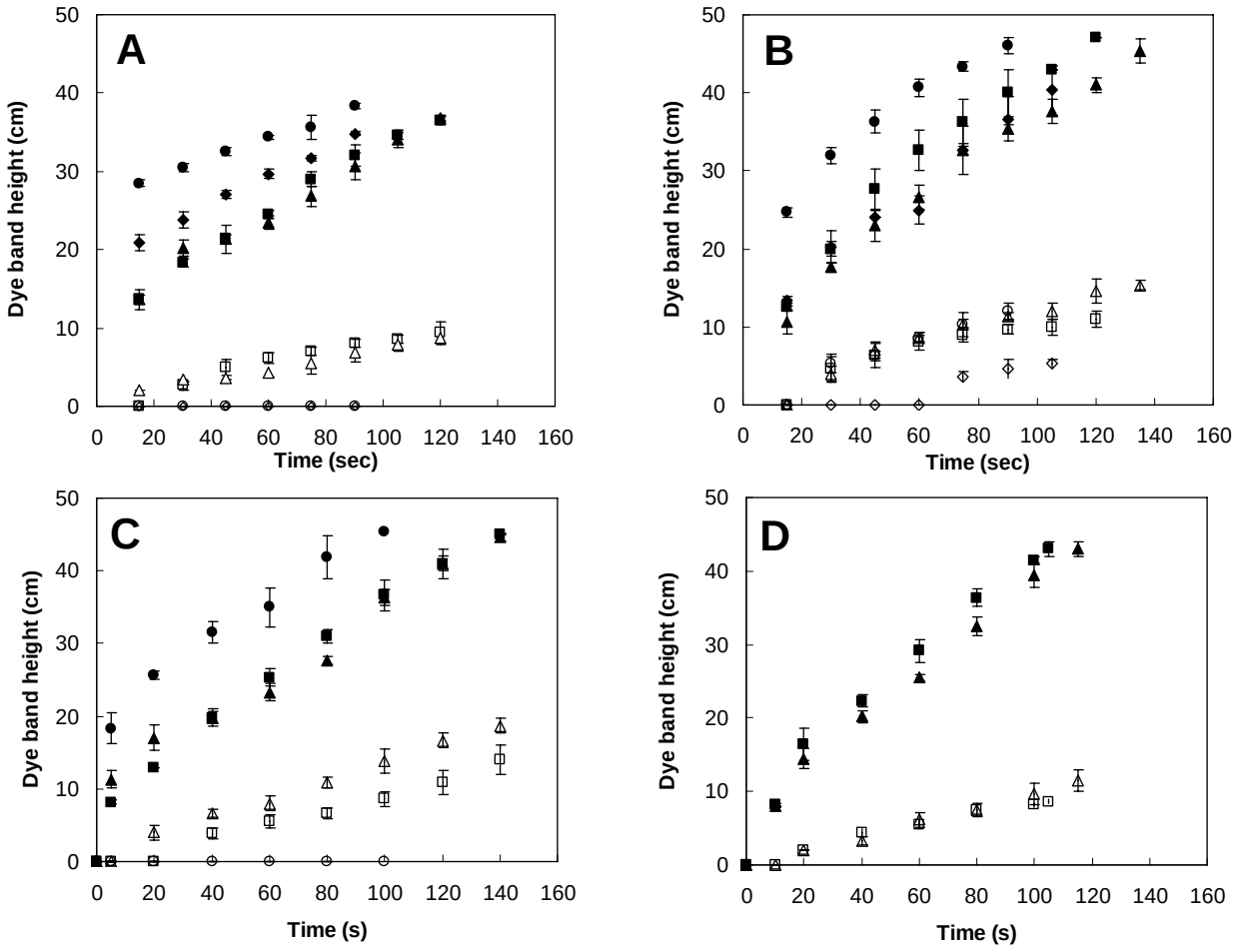

***Figure 6*: Effect of RFD30 distributor rotation rate on dye band movement measured at the column wall for rotary movement of the distributor at flow velocities of: (A) 300 cm.h^{-1} (1.55-fold expansion), (B) 470 cm. h^{-1} (1.95 fold expansion), or (C) oscillation of the distributor with a period 10 seconds and flow velocity 470 cm. h^{-1} and (D) oscillation of the distributor with a period of 20 s and flow velocity 470 cm.h^{-1}. Legend for (A) and (B): rotation rates of (◆,◇) 0 rpm, (■,□) 10 rpm, (▲,△) 20 rpm, (●,○) 60 rpm; closed symbols: top of band and open symbols: bottom of band. Legend for (C) and (D): rotation rates: (■,□) 5 rpm, (▲,△) 20 rpm, (●,○) 60 rpm; closed symbols: top of band and open symbols: bottom of band. Note: rotation rate of 60 rpm was not studied in figure 6D.**

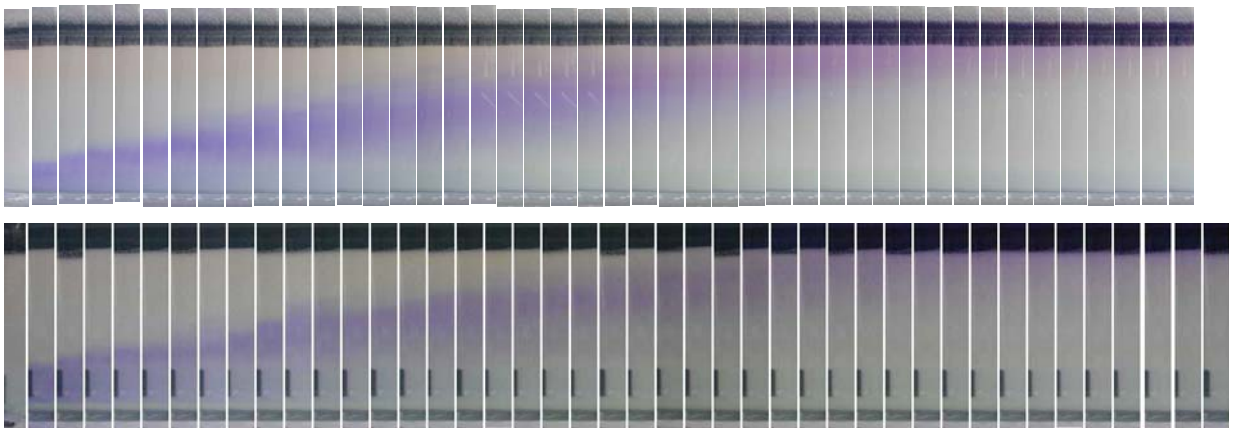

***Figure 7*: Comparison of dye band movement in RFD150 (top panel) and LS150 (bottom panel) at 282 cm.h^{-1} and distributor rotation rate of 3.75 rpm. Each photo is taken 10 s apart from 0 - 440 s after injection of dye tracer (no photo at 370 s for RFD 150).**

The method did not prove sensitive enough to accurately identify the leading or trailing edge of the dye band. Thus only data for the peak (i.e. the part of the band with the most intensity) is given. The data suggests that the band peak travels more rapidly through the RFD150 than the LS150, however in the former the interstitial fluid velocity was higher (479 cm.h^{-1} compared to 397 cm.h^{-1}).

In order to better understand the flow properties in the columns, movement of the dye tracer at the column wall was used to calculate liquid velocities. The time taken for the dye band to reach the bed surface and the expanded bed height were used to determine the average interstitial fluid velocities of the dye band at the wall (U_{iw}) and center (U_{ic}). The average theoretical interstitial fluid velocity (U_i) was determined by dividing superficial flow velocity by bed voidage. Furthermore since the mixed zone in the bottom of the columns was very significant at high rotation rates, a further term was calculated for the interstitial fluid velocity at the wall above the mixed zone, (i.e. only considering the rate of band movement above the mixed zone) and was denoted U_{iw}^*. Under all conditions for the RFD30, U_{iw} was lower than U_{ic} and U_{iw}^* was very much lower than U_{iw}; the latter observation highlights the detrimental effect of a large mixed zone in the columns (Table 1). Reducing the rotation rate of the RFD30

brought U_{iw} closer to U_{iw}*, since the height of the mixed zone was lowered and the length of the classified expanded bed was thus longer. Interestingly, at a superficial flow rate of 300 cm. h^{-1}, high rotation rates led to the lowest value of U_{iw}^{*}, suggesting that at these very high rotation rates, the liquid was distributed best and that axial dispersion in the rest of the column was not increased significantly. Nevertheless, the excessive height of the mixed zone under such conditions resulted in a very short stabilized expanded bed region.

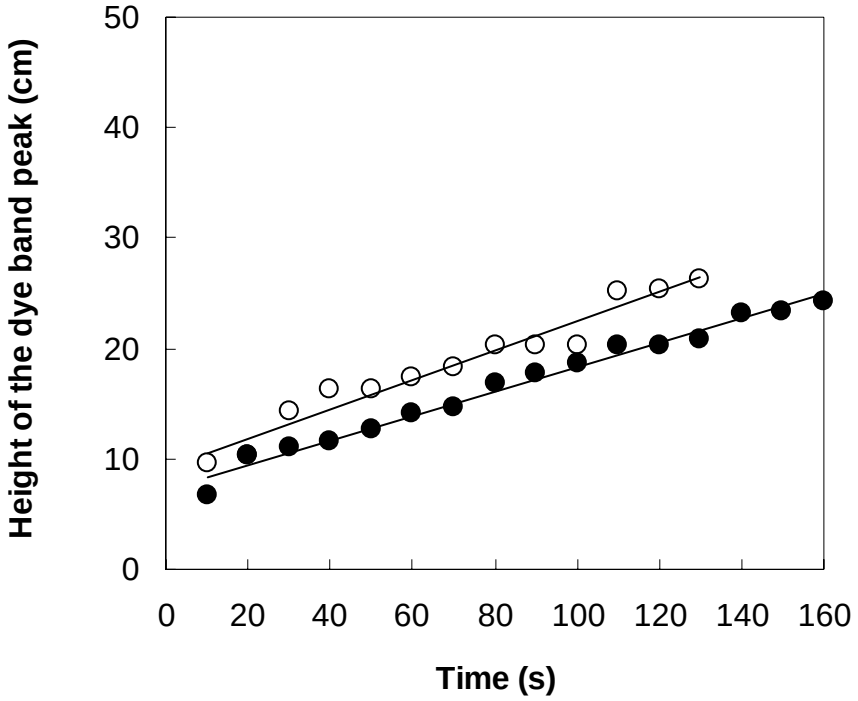

***Figure 8*: Movement of the peak of the dye band in the RFD150 (○) and LS150 (●) determined using the photos in Figure 7 and analysis by Biorad software (see materials and methods). The lines show a linear regression through the data. Superficial linear fluid velocity used during expansion and rotation rates were in all cases 283 cm. h^{-1} and 3.75 rpm respectively. Expanded bed heights were 42.2 cm and 46.5 cm for the RFD150 and LS150 respectively. Settled bed heights were 29.7 and 31.2 cm, for the RFD150 and LS150 respectively.**

***Table 1*: Comparison of interstitial fluid velocities at the column center and wall when different superficial fluid velocities, distributor rotation rates and oscillation periods were used for movement of the distributors in the different columns. For the RFD30: H_0= 25 cm; for the LS60, LS150 and RFD150: H_o = ~30 cm.**

Column	[A]Oscillation period (s)	Rotation rate (rpm)	U_s ($cm.h^{-1}$)	[B]U_i ($cm.h^{-1}$)	H (cm)	ε	U_{iw} ($cm.h^{-1}$)	U_{iw}^* ($cm.h^{-1}$)	U_{ic} ($cm.h^{-1}$)
RFD30	0	0	300	500	37.5	0.60	1132±74	575±49	1392±29
	0	10		484	39.5	0.62	1011±11	740±42	1103±39
	0	20		484	39.5	0.62	961± 13	699±19	1097±4
	0	60		484	39.5	0.62	1488±40	489±30	1635±51
RFD30	0	0	470	701	45.5	0.67	1200±49	953±44	1446±39
	0	10		690	47.0	0.68	1179±44	966±31	1455±40
	0	20		690	47.0	0.68	1013±16	861±50	1229±22
	0	60		690	47.0	0.68	1627±32	904±43	1840±40
RFD30	10	5	470	690	47.0	0.68	1157±0	973±0	1462±39
	10	20		690	47.0	0.68	1107±74	862±39	1361±38
	10	60		690	47.0	0.68	1659±83	895±70	1953±115
	20	5		690	47.0	0.68	1442±66	1292±57	1698±54
	20	20		690	47.0	0.68	1321±55	1180±54	1639±39
LS150	0	3.75	283	474	46.5	0.58	647	386	ND
RFD150	0	3.75	283	490	42.2	0.6	750	540	ND
[C]RFD150	0	3.75	283	488	45	0.58	ND	465±9	572±60

A. Oscillation period of 0 indicates rotation only was employed.
B. U_i was determined by dividing superficial flow velocity by bed voidage
C. Data from Hubbuch et al. (2002)
ND: Not determined

When considering the whole RFD30 EBA system, the lowest values of U_{iw} and U_{ic} for rotary movement of the distributor (961and 1097 $cm.h^{-1}$, respectively) at a superficial flow velocity of 300 $cm.h^{-1}$ and at a superficial flow velocity of 470 $cm.h^{-1}$, (1013 and 1229 $cm.h^{-1}$, respectively) were obtained at a rotation rate of 20 rpm (Table 1). The later condition gave the lowest difference between interstitial velocities at the wall and the center and the lowest value of the mixed zone height as well. The slower movement of the fluid at the wall compared to in the middle of the columns suggests a parabolic flow profile in the RFD30 and is consistent with what was observed previously for the RFD150 (Hubbuch et al., 2002). The average interstitial flow velocities calculated from dye movement for rotation of the distributor were in general lower than those for oscillatory movement under the same conditions (Table 1). Since bed expansion was not significantly affected by oscillation, this effect is most likely due to increased axial dispersion. The lowest values of U_{iw} and U_{ic} (1107±74 and 1361±38 $cm.h^{-1}$, respectively) in the RFD30 were obtained at superficial flow velocity of 470 $cm.h^{-1}$ and oscillation period of 10 seconds with rotation rate of 20 rpm, whereas the lowest value for the mixed zone height was found at a rotation rate of 5 rpm under the same conditions.

The results suggest that the dye band peak observed at the wall moved marginally faster in the RFD 150 (479 cm. h^{-1}) than the LS150 (397 cm. h^{-1}), however the theoretical interstitial fluid velocities in these columns (i.e. based on superficial fluid velocity and voidage) were 490 cm. h^{-1} and 474 cm. h^{-1} for the RFD 150 and LS150, respectively. For comparison, it was reported earlier (Hubbuch et al, 2002) that under the same conditions, but taking manual measurements of the height of the leading edge of the dye band (i.e. as was done here for the RFD30), that the rate in the RFD150 was 553 cm. h^{-1} at a theoretical interstitial fluid velocity of 488 cm. h^{-1}. Nevertheless, in the present work the dye band took longer to break through the RFD150 than the LS150 column due to the lower turbulent zone

in the bottom of the former column. Furthermore, when fluid breakthrough was observed with the top of the columns removed, it was seen that dye broke through the surface of the LS150 column in a thin (20 cm wide) ring at the column wall (data are not shown). This breakthrough pattern suggests channeling at the wall due to insufficient penetration of the fluid jets into the column and poor fluid distribution. In contrast, the RFD150 had dye breakthrough in a large ~100 cm diameter ring. Dye breakthrough of the 60 cm column diameter was essentially even over the surface of the bed.

Residence time distribution studies

The above results suggest that high distributor rotation rates are required for adequate fluid distribution in the LS columns in order to minimise dead zones under the distributor. However, the dye studies suggested that there is a trade off between turbulence leading to unwanted mixing in the whole column and good fluid distribution. Furthermore, the dye results show that high rotation rates (e.g. 60 rpm in the RFD30) drastically increase the average interstitial fluid velocity in the whole column leading to a short residence time. Residence time distribution studies using pulses of acetone tracer were undertaken to quantitatively assess how the hydrodynamic properties of the RFD30 were affected by increased rotation rates and comparisons with the LS60 and RFD150 are also made. It was shown previously that for the RFD150 system, increases in rotation rate led to a reduction in plate numbers (Hubbuch et al., 2002) and that study is extended here to examine the effects of flow rate on the RFD30 and prototype LS columns. In all cases, the RTD traces were analysed using the tanks in series model or the dispersion model and almost the same results were obtained.

Rotary movement of the distributor

Examples of normalised RTD traces using acetone are shown for the RFD30 column at different flow rates with and without oscillation in Figure 9. The results show that for rotary movement of the distributor in this 30 cm diameter column the most symmetrical curves were observed at rotation rates of 20 rpm, which also gave the highest numbers of theoretical plates (Figure 10A), the highest column Peclet number and lowest height equivalent to a theoretical plate (HETP) (Table 2, 3). Excessive tailing and early breakthrough of the RTD curves occurred when high rotation rates, i.e. 40 and 60 rpm were applied at both low and high fluid velocities (300 and 470 $cm.h^{-1}$) (Figures 9A and 9B) and indicates that axial mixing was increased. Thus the numbers of theoretical plates and column Peclet number were reduced drastically and HETP increased (Tables 2 and 3). When low superficial fluid velocity (300 $cm.h^{-1}$) was used and rotation rate of the distributor was reduced to below 20 rpm, early breakthrough of tracer resulted and the curves became broader, particularly when there was no rotation (Figure. 9A), due to poor fluid distribution (as shown in the dye studies above). However, there was little effect on plate numbers in the RFD30 caused by using low rotation rates (Table 2). Interestingly, increasing the flow velocity to 470 cm. h^{-1} which consequently raised the expanded bed height, resulted in sharper and almost gaussian shaped RTD curves at rotation rates lower than 20 rpm, and even when the distributor was stationary (Figure 9B). Evidence of better hydrodynamic properties was also seen in the dye experiments (above) under these conditions, and may indicate that the high velocity of the fluid jets exiting the bottom of the distributor and impacting the column base plate leads to improved fluid distribution by creating turbulence and a large zone of rising liquid, rather than a thin stream (see (5) and (6) in Figure 1). This flow rate (i.e. 470 cm. h^{-1}) led to the highest numbers of

theoretical plates (27) (Figure 10A) and value of Pe (~53) (Table 3) measured for the RFD30 column.

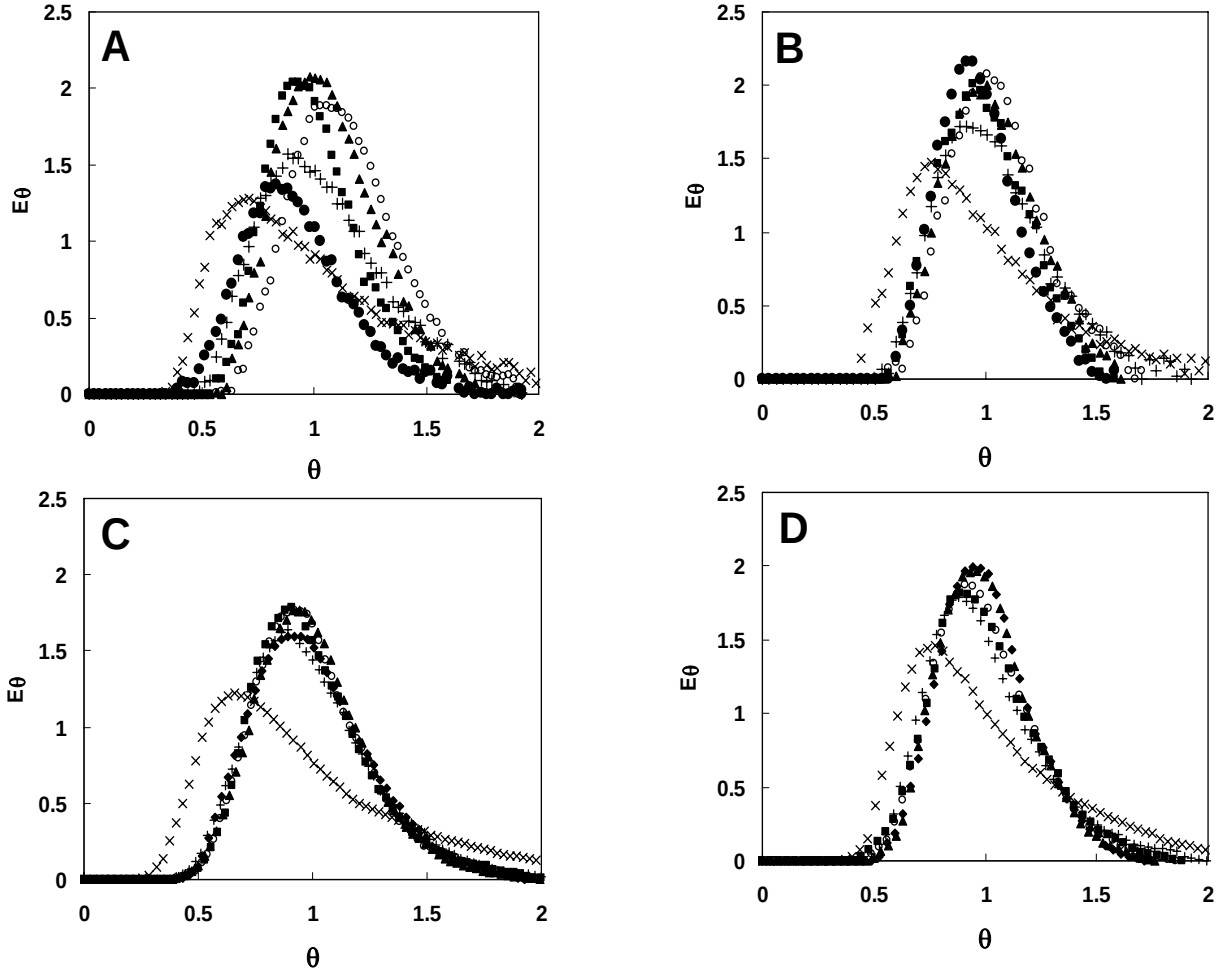

***Figure 9*: Effect of distributor rotation rate on the dimensionless residence time (θ) of an acetone tracer pulse for: (A) rotary movement of distributor with a fluid velocity of 300 cm.h^{-1}; (B) rotary movement of the distributor and a flow velocity of 470 cm.h^{-1} ; (C) oscillatory movement of the distributor with a period of 20 s and a liquid flow velocity of 300 cm.h^{-1}; (D) oscillatory movement of the distributor with a period of 20 s and a flow velocity of 470 cm.h^{-1}. Legend for (A) and (B) rotation rates: (●) 0rpm, (■) 2 rpm, (▲) 10 rpm, (○) 20 rpm, (+) 40 rpm and (×) 60 rpm; legend for (C) and (D) rotation rates: (■) 2 rpm, (♦) 5 rpm, (▲) 10 rpm, (○) 20 rpm, (+) 40 rpm and (×) 60 rpm. Note: for the analysis, the whole RTD curve was used, however to aid visual interpretation of the data, the curves have been cut at θ = 2.**

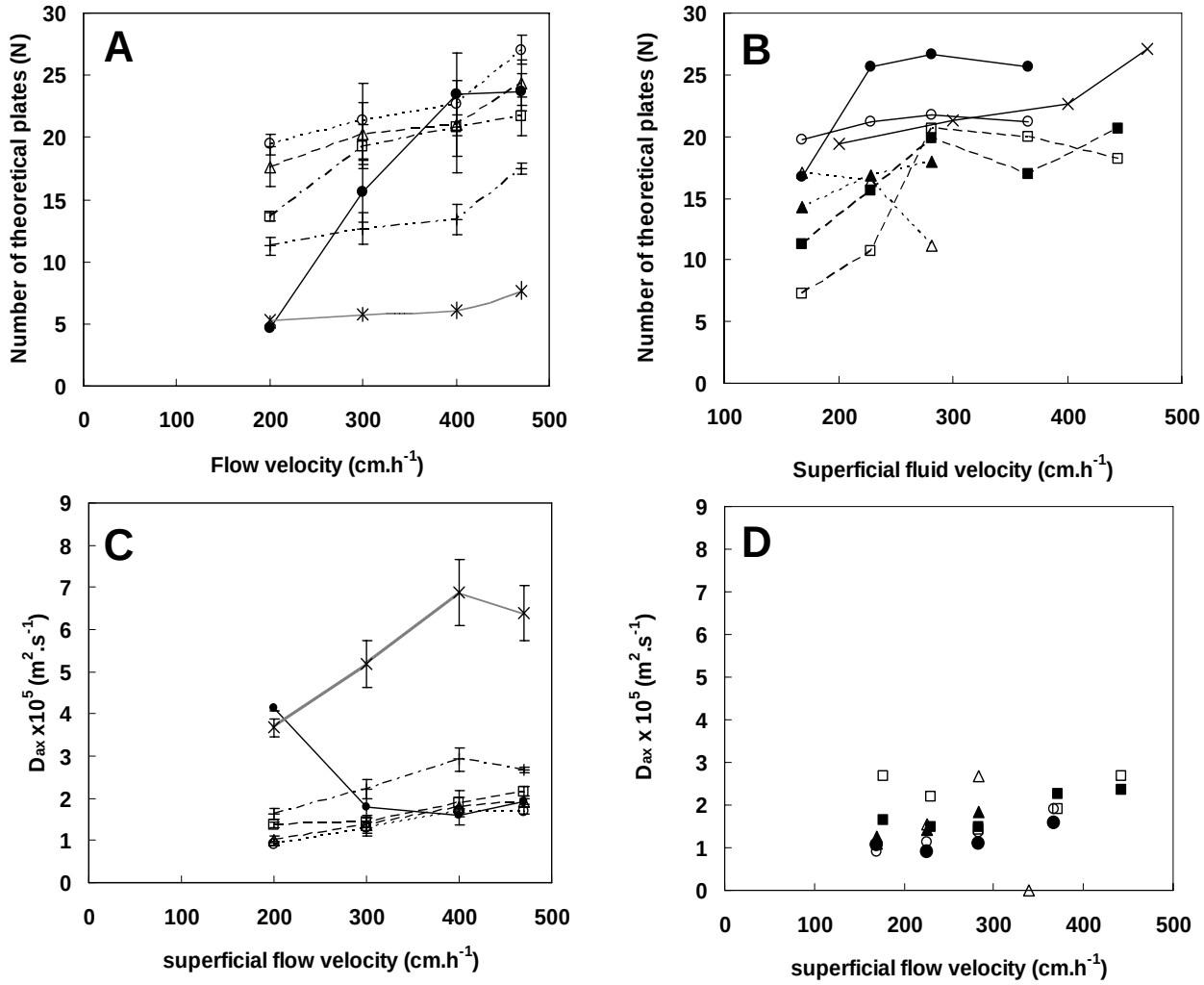

***Figure 10*: Effect of flow velocity on number of theoretical plates (N) and axial dispersion coefficient (D_{ax}) for rotary movement of the different distributors. (A) and (C) RFD30 at rotation rates of: (●) 0rpm, (□) 2 rpm, (△) 10 rpm, (○) 20 rpm, (+) 40 rpm and (×) 60 rpm. (B) and (D) Comparison of the different distributors: (×) RFD30, 20 rpm; (●) RFD150, 3.75rpm; (○) RFD 150, 7.5 rpm; (▲) LS150, 5 rpm; (△) LS150, 7.5 rpm; (□) LS60, 4.8 rpm; (■) LS60, 10 rpm.**

Since the values of the column Peclet number and numbers of theoretical plates take the expanded bed height into account, the true effects of rotation rate and fluid velocity on mixing can be masked. The values for the axial dispersion coefficient indicate for the RFD30 column that at all rotation rates, increasing the fluid velocity resulted in increased D_{ax}, the only exception being if the distributor was not rotated (Figure 10C). For all superficial fluid

velocities, increasing the rotation rate up to 20 rpm led to no significant effect on $D_{ax,}$ which then increased as rotation rate was raised to 60 rpm (Figure 10C). The lowest value of D_{ax} (9.18×10^{-6} $m^2.s^{-1}$) was obtained when a rotation rate of 20 rpm and fluid velocity 200 $cm.h^{-1}$ were applied (Figure 10C), which did not correspond to the greatest number of theoretical plates (found at 470 $cm.h^{-1}$, 20 rpm).

When rotation rate of both of the LS columns was increased above 5 rpm, plate numbers dropped (Table 2, Figure 10B) and there was a consequent increase in axial dispersion as shown by the values for the HETP and D_{ax} (Table 2). For the LS60 column, a distributor rotation rate of 20 rpm resulted in the highest HETP, the value of which was largely independent of flow rate, suggesting that here turbulence from the distributor is the predominating influence.

The results show that fluid distribution in the LS60 and LS150 columns could not be improved by increasing stirring. One way to improve fluid distribution in the LS columns may be to increase fluid flow rates since the jets from the column walls would be expected to penetrate deeper into the column. The results of the dye studies (i.e. the observation of a thin dye ring when viewed from above) with the column suggested that fluid did not penetrate adequately into the centre of the LS150 column. Figure 10B shows that increases in flow rate did appear to improve fluid distribution for the LS60 column as demonstrated by the increase in theoretical plate number, however expanded bed height also increases and measurements showed the lowest HETP and D_{ax} using 282 $cm.h^{-1}$ for the LS distributor which increased as flow rate was raised (Table 3, Figure 10D).

***Table 2*: Comparison of the hydrodynamic properties of EBA columns employing local stirring (LS) of fluid introduced through radial ports on the column wall, or of fluid introduced through a rotating fluid distributor (RFD). Superficial fluid velocities of 300 cm.h^{-1} in the RFD30 and 283 cm. h^{-1} were used and in the LS60, LS150 and RFD150.**

Column	[A]Rotation rate (rpm)	N	HETP (cm)	D_{ax} ($\times 10^{-5}$ m^2.s^{-1})	Pe	Mixed zone height (cm)	Dead zone height (cm)
RFD30	2	19.2	2.1	1.45	37.2	ND	0
	10	20.3	2.0	1.37	39.2	13.7	0
	20	21.3	1.9	1.31	41.0	13.7	0
	40	12.6	3.2	2.24	24.0	ND	0
	60	5.8	6.9	5.20	10.3	28.5	0
LS60	5	20.6	2.0	1.43	40.0	11.0	6
	10	19.9	2.1	1.50	38.5	14.0	6
	20	10.0	4.3	3.10	18.9	20.0	2
LS150	3.75	16.0	2.6	1.80	31.3	14.2	2.5
	5	18.0	2.6	1.80	34.5	15.6	2.5
	7.5	11.1	3.7	2.70	21.3	15.5	2.5
[B]RFD150	2.5	29.4	1.5	1.00	58.8	8.0	0
	3.75	26.6	1.6	1.10	52.6	8.0	0
	5	23.2	1.8	1.30	45.5	10.5	0
	7.5	21.7	2.0	1.40	41.7	12.2	0

[A.] Rotation rate of the distributor. All data obtained using a settled bed height of 29-30 cm of matrix and at a superficial linear flow velocity of 282 cm.h^{-1} giving an expanded bed height of between 41 and 44 cm in all cases.

[B.] For the RFD150, data for the N and HETP are taken from Hubbuch et al. (2002)

ND: not determined.

***Table 3*: Effect of superficial fluid velocity on numbers column Peclet number and HETP at different rotation rates for the distributors studied.**

Column	[A]Rotation rate (rpm)	Flow velocity ($cm.h^{-1}$)							
		200	300	400	470	200	300	400	470
		Pe				HETP (cm)			
RFD30	0	8.3	30.3	46.0	46.3	6.0	2.4	1.8	1.9
	2	25.6	37.4	40.7	42.4	2.7	2.1	2.2	2.2
	10	34.3	39.5	41.2	47.5	2.1	2.0	2.1	1.9
	20	37.9	41.7	44.3	53.1	1.9	1.9	1.9	1.7
	40	21.4	24.2	25.7	33.9	3.3	3.2	3.3	2.7
	60	9.5	10.4	11	14.3	6.9	6.9	7.3	6.1
		Flow velocity ($cm.h^{-1}$)							
		168	228	282	366	444	168	228	282	366	444
		Pe					HETP (cm)				
LS60	4.8	13.3	20.3	40.2	38.6	35.2	4.6	3.4	2.0	2.1	2.6
	10.4	21.5	29.9	38.4	32.9	40.2	3.1	2.4	2.1	2.5	2.4
LS150	5	27.5	32.5	35.0	ND	ND	2.7	2.4	2.6	ND	ND
	7.5	33.0	31.5	21.1	ND	ND	2.4	2.7	3.7	ND	ND
RFD150	3.75	32.3	50.2	52.0	49.8	ND	2.2	1.5	1.6	1.9	ND
	7.5	37.9	41.4	42.0	41.4	ND	1.8	1.9	2.0	2.2	ND

[A.] Height equivalent to a theoretical plate calculated based on expanded bed height and numbers of theoretical plates.

ND: Not determined.

For the LS150 column, raising fluid velocity led to a small increase in the numbers of theoretical plates at 5 rpm, but led to a reduction in plate number when a rotation rate of 7.5 rpm was used (Figure 10B). The number of theoretical plates for the RFD150 system

remained approximately constant as flow rate was increased at a rotation rate of 7.5 rpm (Figure 10B). However at low rotation rates (i.e. 3.75 rpm), which in general deliver higher plate numbers (Hubbuch et al., 2002), it was observed (Figure 10B) that for this column the performance dropped markedly at low flow rates (i.e. 170 cm. h^{-1}).

Oscillation movement of the distributor

When the RFD30 distributor was oscillated, a marked difference was seen in the family of RTD curves that resulted (Figures 9C and 9D), as compared to when rotation only was employed (Figures 9A and 9B). The differences between the curves as rotation rate was increased were reduced drastically at low flow rates (300 cm. h^{-1}) by oscillation of the distributor. However, oscillation reduced the numbers of theoretical plates as compared to rotation only, for example a reduction from 27 at 470 cm. $h^{-1}$and 20 rpm rotation, to 21 at 20 rpm with an oscillation of a 10s period (Figure 11). Furthermore, applying oscillation led to higher values of D_{ax} compared to that for rotary movement for all corresponding flow velocities and rotation rates (Table 4). Increasing the oscillation period from 10 s to 40 s led to no significant effect on plate numbers (Figure 11). There was no significant effect on D_{ax} by increasing the oscillation period from 10 to 40 s when the rotation rate was 5 rpm or 20 rpm. The lowest value of D_{ax} for oscillatory movement of the distributor was 1.77×10^{-5} $m^2.s^{-1}$ at the highest flow velocity studied (i.e. 470 $cm.h^{-1}$), rotation rate of 5 rpm and oscillation period of 40 seconds (Table 4). The results in this work suggest that oscillation offered only a marginal benefit when the distributor was rotated slowly (i.e. at 5 rpm), but even better performance could be obtained simply by rotating the distributor (without oscillation) at 20 rpm.

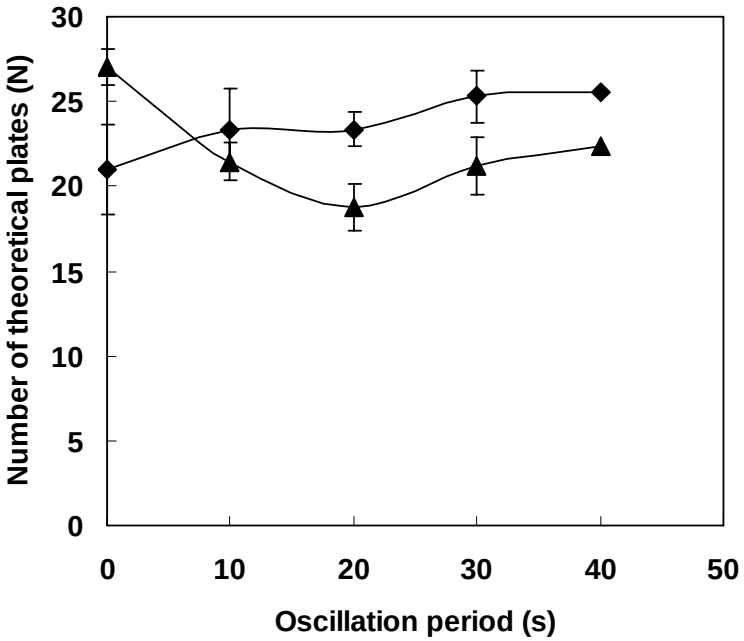

***Figure 11*: Effect of oscillation period on number of theoretical plates (N) for oscillatory movement of distributor at flow velocity 470 cm.h^{-1} and rotation rates: (♦) 5 rpm and (▲) 20 rpm. Oscillation period of 0 indicates rotation only was employed.**

***Table 4*: Effect of distributor oscillation period on axial dispersion coefficient (D_{ax}) and height equivalent to a theoretical plate (HETP) at rotation rates 5 and 20 rpm for oscillatory movement of distributor. Superficial flow velocity was 470 cm. h^{-1}.**

Oscillation period (s)	Rotation rate (rpm)	D_{ax} $\times 10^{-5}$ ($m^2.s^{-1}$)	HETP (cm)
10	5	1.96±0.24	2.03±0.24
20	5	1.95±0.21	2.03±0.22
30	5	1.79±0.72	1.86±0.07
40	5	1.77±0.11	1.84±0.11
10	20	2.12±0.11	2.20±0.12
20	20	2.34±0.15	2.51±0.15
30	20	2.15±0.14	2.23±0.14
40	20	2.03±0.17	2.11±0.17

General discussion

The results presented here clearly show that in general large columns using local stirring have inferior hydrodynamic performance as compared to the rotating fluid distributors studied, but also possess properties making them unsuitable for bioprocessing – in particular the presence of dead zones and channeling under the distributor and between the baffles. Thus rotating fluid distributors appear to be the mechanism of choice for large EBA column design. However, the results found here also imply that in contrast to the earlier report of Hubbuch et al. (2002), where it was suggested that turbulence caused by rotation of the distributor should be minimized as far as possible, that there may be a role for turbulence in ensuring proper fluid distribution.

Results with the RFD30 showed that the best performance was not obtained under conditions in which turbulence would be expected to be minimized. In fact, the best performance for the RFD30 was obtained at the highest flow rate studied (470 cm. h^{-1}) and at an intermediate rotation rate of 20 rpm (Reynolds number at the tip ≈ 3000), conditions which would be expected to impart a significant amount of turbulence. However, under those conditions 27 theoretical plates were measured, HETP was lowest, and Pe highest (Table 3), whilst D_{ax} was not significantly different compared to other conditions (Figure 10C). Furthermore, the lowest turbulent zone in the column (and thus longest stabilized expanded bed) was also observed with dye tracer (Figure 5A) under this condition. Change of the rotation and fluidization conditions away from the optimum led to reduced performance as observed by the measurements of all variables studied. This generalization also holds for the use of oscillation, which did not have better performance found with rotary movement (Figure 11, Table 4). Excessive speed of rotation of the distributor (i.e. 60 rpm) (Figure. 10A) led to dramatic reductions in performance. However this seems to be due to the formation of a large

but localized turbulent zone and thus reduction in the length of the stable EBA bed above (see Figure 5A), rather than as a result of high axial dispersion in the whole column. The slowest rate of movement of the dye band (and consequently slowest interstitial velocity in this region) was found above the zone created by rotating the RFD30 at 60 rpm (Table 1).

When the evidence is considered for the RFD150 a more uncertain picture arises as to the benefits or problems caused by turbulence on efficient fluid distribution and column performance. The RFD150 yielded a similar number of theoretical plates as the RFD30 (Figure 10C), in the range of flow rates studied (228-366 $cm.h^{-1}$) when rotation rate was low (3.75 rpm). Furthermore, HETP and D_{ax} were low and Pe high under these conditions (Table 3). Reducing the rotation rate further to 2.5 rpm improved the numbers of theoretical plates to 29 (see Hubbuch et al., 2002). However, reducing fluidizing velocity to 168 $cm.h^{-1}$ led to a large drop in theoretical plate numbers to 17 (Figure 10B), suggesting that distribution was not sufficient. On the other hand, creating more turbulence by increasing the rotation rate (to 7.5 rpm) at a fluid velocity of 168 $cm.h^{-1}$ improved performance to a level (N = 20) essentially equivalent to that seen for the other flow rates at this rotation rate (i.e. N = 21-22) (Figure 10B).

The turbulence created by moderate rotation rates thus appears to remove channeling and aid fluid distribution in both RFD columns studied, but further increases led to a detrimental increase in mixing. The above results have important implications for the future operation and design of RFD equipped systems. It may be expected that flow rates as low as 120 $cm.\ h^{-1}$ may be used with commercial media such as STREAMLINE (GE Healthcare) or CM Hyper Z (Pall) which have considerably lower densities and diameters, respectively, than the media used in this work, leading to lower fluidization velocities. Furthermore, elution in expanded bed mode is the method of choice in RFD equipped EBA columns and flow rates

are often reduced during this phase in order to maximize concentration of the product and improve resolution. Modulation of rotation rate during different stages of an EBA process may thus be required in view of the above results.

In general, it can be seen that as the RFD column is scaled up from 30 cm to 150 cm diameter, the rotation rate must be lowered considerably, from 20 rpm to 2.5-3.75 rpm, respectively to yield the best performance. This is most likely due to differences in the amount of turbulence created by the distributors. Furthermore, Hubbuch et al. (2002) showed that RFD150 column performance is susceptible to small increases in distributor rotation rate, with the number of theoretical plates dropping by 21% as rotation rate was increased from 2.5 to 5 rpm. This susceptibility to small changes in distributor rotation rate was not observed for the RFD30 (Table 2). Sensitivity to turbulence in the column and being able to control it to yield the best performance is more difficult with the RFD150 than the RFD30, most likely due to the difference in diameter and the effect this has on the variation in linear velocity of the blades. For example a change in rotation rate from 2.5 and 10 rpm in the RFD150 leads to a large increase in tip velocity and thus an increase in Reynolds number (Re) from 4000 to 15000 (Hubbuch et al., 2002), whereas for the RFD30 column studied here the same change in rotation rate leads to Re numbers increasing from 350 to 1400 at the tips. For the optimal conditions for the RFD30 and RFD150 (i.e. 20 rpm or 2.5 rpm, respectively) the tip velocities are 27 and 19 $cm.s^{-1}$ corresponding to Re of 2800 and 4000, respectively. Furthermore, the velocity changes and thus Re values are much greater from the distributor centre to the tip for the RFD150 than the RFD30 (e.g. at 10 rpm from 2400 to 15000 for the RFD150 and 200 to 1400 for the RFD30). At $60<Re<5000$ a von Karman vortex street will be formed (Blevins, 1984 and Granger, 1985), and at $Re>5000$ the wake behind the cylinder can no longer sustain the laminar shed vortices and consequently the region behind the moving cylindrical pipes is

completely turbulent (Granger, 1985). In the RFD30, at rotation rates ≥40 rpm for rotary movement a completely turbulent region is formed around the tip of the blades, due to the high values of Re (≥6000) and which explains the very large mixed zone with resulting poor performance. Therefore, the value of Re can be used as a criterion for estimation of maximum rotation rate to achieve an acceptable hydrodynamic condition within the column. However, the minimum rotation rate needed to achieve an acceptable hydrodynamic condition within the column is also dependent on other factors affecting the introduction of flow, in particular design parameters such as the outlet hole distribution pattern. It is believed that introducing the flow more evenly will allow the use of a lower value for the minimum rotation rate.

The above evidence points to the conclusion that rotation rate should be optimized for different distributor sizes and fluidizing velocities to obtain an optimal value for turbulence, which also depends on other operational parameters such as the flow velocity and the effects of the jets leaving the distributor, as well as the rate of fluid application over the column base. In general the turbulent zone should be reduced as much as possible, since it reduces the length of the stabilized expanded bed. Thus, blade design should aim to reduce turbulence in order to increase plate numbers (e.g. via use of streamlined rather than tubular shaped blades), however care must be taken in the minimization of turbulence which may reduce the efficiency of the distributor under conditions of high flow rate as well as low flow rates. One means of overcoming this conundrum may be to apply improved outlet hole patterning which improves the performance of the distributor at all flow rates and negates the need for any type of turbulence.

Surprisingly, the RFD30 did not lead to better performance than the RFD150. Workers using other types of EBA systems have shown that performance declines as scale is increased up to 60 cm diameter (Barnfield-Frej et al., 1997). Reasons for the similar performance of the

two columns studied here could be due to a slightly lower settled bed height used with the RFD30 (i.e. ~25 cm c.f. ~29 cm with the RFD150), but most likely are related to using distributors with differences in design and geometry. For example, the ratios of distributor diameter and blade thickness, chamber diameter and distributor blade outlet hole area: to column base area were different, as well as other design parameters such as the number of distributor blades, numbers of outlet holes and position of the outlet holes were quite different between the two RFD columns. In particular a much greater number of holes (51) with a 2 mm diameter and a carefully designed distribution pattern were used in RFD150 (Hubbuch et al., 2002), which can be expected to lead to more even distribution of flow into the column, than for the RFD30 column. Asif et al. (1991) showed to avoid the presence of dead zones a distributor with a hole density as large as possible should be used.

Implicit in the above conclusion that turbulence is needed, is that the fluid distribution is not good enough in the current EBA column designs. Thus we believe that there is considerable scope for improving the design and optimising the use of large RFD distributors for EBA columns such that an even flow is introduced under conditions in which low rotation rates are necessary, and thus the height of the turbulent zone is minimized. The design, construction and evaluation of such distribution systems requires a more directed approach than the mostly empirical approach which has apparently been used until now, and should involve the adaptation of techniques used in other branches of equipment design, such as computational fluid dynamics and positron emission imaging.

Conclusions

The rotating fluid distributor systems provide acceptable performance (theoretical plate numbers of 27 – 29 at flow rates up to 470 $cm.h^{-1}$) for columns between 30 cm and 150

cm in diameter, due to the ability to apply liquid evenly over the base of the column. In contrast the local stirring principal cannot be scaled up successfully to columns greater than 60 cm in diameter.

The current crop of rotating fluid distributors relies partly on turbulence to achieve satisfactory fluid distribution. Nevertheless, low distributor rotation rates must be used in an effort to keep the degree of mixing to a minimum. Changing distributor movement from rotation to oscillation led to no benefits for performance and caused a ~14% decrease in numbers of theoretical plates. Increasing the oscillation period from 10 s to 40 s led to no significant change in performance. Further improvement in distributor design is needed and careful attention should be given to the trade off between turbulence and adequate fluid distribution.

Acknowledgments

The authors are grateful to UpFront Chromatography A/S for the loan of the matrix and columns used in this study. The authors would also like to thank Rene Thrane for technical assistance. The authors are grateful to the workshop at BioCentrum-DTU and JPJ Engineering, Denmark for construction of the RFD150. The Iranian ministry of science, research and technology is thanked for supporting this work by granting a PhD scholarship to Ayyoob Arpanaei.

References

1. Anspach, F.B.; Curbelo, D.; Hartmann, R.; Grake, G. and Deckwer, W.; 1999; **Expanded-bed chromatography in primary protein purification**; *Journal of Chromatography A*, 865, 129-144.
2. Asif, M.; Kalogerakis, N. and Behie, L.A.; 1991; **Distributor effects in liquid fluidized beds of low-density particles**; *AIChE Journal*, 37, 1825-1832.
3. Barnfield Frej, A.K.; Johansson, H.J.; Johansson, S. and Leijon, P.; 1997; **Expanded bed adsorption at production scale: Scale-up verification, process example and sanitization of column and adsorbent**; Bioprocess Engineering, 16, 57-64.
4. Blevins, R.D.; 1984; ***Applied fluid dynamics handbook***; New York, Van Nostrand Reinhold, Pages: 7-319.
5. Brobjer, M.; 1999; **Development and scale up of a capture step (expanded bed chromatography) for a fusion protein expressed intracellularly in *Escherichia coli***; *Bioseparation*, 8, 219-228.
6. Chase, H.A.; 1994; **Purification of proteins by adsorption chromatography in expanded beds**; *Trends in Biotechnology*, 12, 296-303.
7. Clemmitt, R.H. and Chase, H.A.; 2003; **Impact of operating variables on the expanded bed adsorption of Saccharomyces cerevisiae cells using a concanavalin A derivatized perfluorocarbon**; *Biotechnology and Bioengineering*, 82, 506-516.
8. De Luca, L.; Hellenbroich, D.; Titchener-Hooker, N.J. and Chase, H.A.; 1994; **A study of the expansion characteristics and transient behaviour of expanded beds of adsorbent particles suitable for bioseparations**; *Bioseparation*, 4, 311-318.
9. Diehl, P.; 1998; **Expanded-bed adsorption for biomanufacturing**; *Genetic Engineering News*, October, 14-43.
10. Di Felice, R.; 1995; **Hydrodynamics of liquid fluidization**; *Chemical Engineering Science*, 50, 1213-1245.
11. Draeger, N.M. and Chase, H.A.; 1991; **Liquid fluidized beds for protein purification**; *Transactions of IChemE*, 69, 45-58.
12. Feuser, J.; Dietl, B.; Buchholz, A.; Barnfield Frej, A.K.; Lundkuist, M. and Walter, J.K.; 2002; **The effect of fluid inlet design on mammalian cell culture integrity**; *Poster, 4th international conference on expanded bed adsorption*, Florida, USA Sept 8-11.

13. Feuser, J.; Halfar, M.; Lutkemeyer, D.; Ameskamp, N.; Kula, M. and Thömmes, J.; 1999; **Interaction of mammalian cell culture broth with adsorbents in expanded bed adsorption of monoclonal antibodies**; *Process Biochemistry*, 34, 159-165.
14. Gonzalez, Y.; Ibarra, N.; Gomez, H.; Gonzalez, M.; Dorta, L.; Padilla, S. and Valdes, R.; 2003; **Expanded bed adsorption processing of mammalian cell culture fluid, comparison with packed bed affinity chromatography**; *Journal of Chromatography B*, 784, 183-187.
15. Granger, R.A.; 1985; ***Fluid mechanics***; New York, Holt, Rineheart and Winston, Pages: 483-791.
16. Hansson, M.; Ståhl, S.; Hjorth, R.; Uhlen, M. and Moks, T.; 1994; **Single-step recovery of a secreted recombinant protein by expanded bed adsorption**; *Bio/Technology*, 12, 285-288.
17. Hjorth, R.; Leijon, P.; Barnfield Frej, A.K. and Jagersten, C.; 1998; **Expanded bed adsorption chromatography**. In: Subramanian, G., editors; *Bioseparation and Bioprocessing*; Weinheim, Germany, Wiley VCH, Pages: 199-226.
18. Hjorth, R; 1997; **Expanded bed adsorption in industrial bioprocessing: recent developments**; *TIBTECH*, 15, 230-235.
19. Hobley, T.J.; Hubbuch J.J.; Heebøll-Nielsen, A. and Thomas, O.R.T.; 2003; **Scale flexible fluid distribution system for expanded bed adsorption**; *Downstream, EBA'02 special edition*, Amersham Biosciences AB.
20. Hubbuch, J.J.; Heebøll-Nielsen, A.; Hobley, T.J. and Thomas, O.R.T.; 2002; **A new fluid distribution system for scale-flexible expanded bed adsorption**; *Biotechnology and Bioengineering*, 78, 35-43.
21. Hubbuch, J.J.; Hobley, T.J.; Thomas, O.R.T.; Lihme, A; Hansen, M.B. and Olander M.A.; 2001; **A bed adsorption system**. *International patent application*, publication number WO01/85329.
22. Johansson, H.J.; Jagersten, C. and Shiloach, J.; 1996; **Large scale recovery and purification of periplasmic recombinant protein from E.coli using expanded bed adsorption chromatography followed by new ion exchange media**; *Journal of Biotechnology*, 48, 9-14.
23. Levenspiel, O.; 1999; ***Chemical reaction engineering***; 3rd ed. New York, John Wiley and Sons, Inc.

24. McCabe, W.L.; Smith, J.C. and Harriott, P.; 1993; ***Unit operations of chemical engineering***; 5th ed. New York, McGraw-Hill, Inc., Pages: 143-180.
25. Menkhaus, T.J. and Glatz, C.E; 2004; **Compatibility of column inlet and adsorbent designs for processing of corn endosperm extract by expanded bed adsorption**; *Biotechnology and Bioengineering*, 87, 324-336.
26. Nilsson, I.; 2004; **STREAMLINE Direct; new adsorbent and columns for expanded bed adsorption**. Poster, *5th European symposium on biochemical engineering science*, Stuttgart, Germany Sept 8-11.
27. Noda, M.; Sumi, A.; Ohmura, T. and Yokoyama, K.; 1996; **Process for purifying recombinant human serum albumin**; *European patent*, EP0699687.
28. Pierce, J.J.; Fischer, E.J.; Smith, M.P.; Turner, C.; Keshavarz-Moore, E. and Dunnill, P.; 1999; **Purification of a periplasmic enzyme by a stirred adsorbent, and by expanded and packed beds**; *Bioprocess Engineering*, 20, 449-457.
29. Thelen, T.V. and Ramirez, W.F.; 1997; **Bed-height dynamics of expanded beds**; *Chemical Engineering Science*, 52, 3333-3344.
30. Theodossiou, I.; Elsner, H.D.; Thomas, O.R.T. and Hobley T.J.; 2002; **Fluidisation and dispersion behaviour of small high density pellicular expanded bed adsorbents**; Journal of Chromatography A, 964, 77-89.
31. Thömmes, J.; 1997; **Fluidized bed adsorption as a primary recovery step in protein purification**; Advances in Biochemical Engineering/Biotechnology; 58, 185-230.
32. Zafirakos, E. and Lihme, A.; 1999; **EBA columns with a distribution system based on local stirring**; *Bioseparation*, 8, 85-91.

3 Study of DNA binding during expanded bed adsorption and factors affecting adsorbent aggregation

Arpanaei, Ayyoob[1]; Mathiasen, Niels[1]; *Hobley, Timothy J.[1]; Thomas, Owen R.T.[1,2]

[1]Center for Microbial Biotechnology, Building 223, BioCentrum-DTU, Technical University of Denmark, 2800-Kgs. Lyngby, Denmark;
[2]Current address: Department of Chemical Engineering, University of Birmingham, Edgbaston, B15 2TT, UK

*Author for correspondence: Timothy J. Hobley, Center for Microbial Biotechnology, BioCentrum-DTU, Technical University of Denmark, Building 223, Søltofts Plads, DK-2800-Kgs. Lyngby, Denmark (Tel: +45 4525 2706, Fax: +45 4588 4148; E-mail: th@biocentrum.dtu.dk)

Abstract

The DNA induced aggregation and contraction of expanded bed adsorption chromatography beds has been examined using the strong anion exchanger Q HyperZ and calf thymus DNA in buffers containing added NaCl. Two batches of adsorbent with different ionic capacities (0.122 and 0.147 mmol Cl^-.mL^{-1} gel) were used allowing the effects of different ligand densities to be examined, and very high dynamic binding capacities at 10% breakthrough ($Q_{10\%}$) were found in the absence of added salt (4.43 and 12.44 mg DNA applied.mL^{-1} gel, respectively). However the highest binding capacities (9.71 and 18.94 mg DNA applied.mL^{-1} gel) were found in buffers containing added salt at concentrations of either 0.25 M or 0.35 M, for the low and high ligand density adsorbents, respectively. Bed contraction was observed, but did not correlate with $Q_{10\%}$ or with the amount of DNA loaded. No differences in bed contraction were seen by varying the concentration of DNA loaded in the range of 20-80 μg.ml^{-1} even though the dynamic binding capacity was reduced as DNA concentration was increased. The extent of bed contraction during DNA loading was found to be a function of added salt concentration and ligand density of adsorbent. The mechanisms underlying the observations are discussed with reference to models from the literature and it is concluded that adding salt to increase the ionic strength leads to a combination of effects: electrostatic interactions between the adsorbent and DNA are modulated, however the DNA becomes more compact, and bed hydrodynamics are affected due to changes in aggregation of the adsorbents. The results imply that ligand density significantly affects the salt tolerance of anion exchangers when binding DNA. However more importantly, that with the adsorbents examined here, attempts to reduce bed aggregation by feedstock conditioning with added salt may lead to a reduction in EBA performance compromising protein capture in real feedstocks.

Keywords: EBA, Q HyperZ, Cross-linking, Aggregation of beads, Dynamic binding capacity, Ligand density, Ionic strength.

Introduction

The interaction of large molecules such as DNA, RNA, cell walls and whole cells as well as other debris in crude feedstocks with adsorbents continues to plague the application of expanded bed adsorption chromatography. The expanded bed (Draeger and Chase, 1991; Hansson et al., 1994; Thömmes, 1997; Hjorth et al., 1998; Anspach et al., 1999 and Rito-Palomares, 2004) contains fluidized adsorbents, which are susceptible to aggregation, leading to breakdown of the hydrodynamic conditions necessary for successful capture of the product (Feuser et al., 1999a and 1999b; Lin et al., 2001, 2003a and 2004, Theodossiou and Thomas, 2002). Subsequently low capacities result and difficulties in cleaning and adsorbent reuse arise. Different strategies have been employed to develop improved EBA adsorbent types with minimized propensity for aggregation (Dainiak et al., 2002a and 2002b, Viloria-Cols et al., 2004 and Senthuran et al., 2004), however without broad application or commercialization to date. Alternatively, feedstock conditioning strategies have been employed (Lin et al., 2001, 2003a and 2003b). Feedstock conditioning by changing pH or ionic strength through salt addition has been the primary focus, since anion exchange adsorbents are often the preferred choice for first capture. Such adsorbents have high capacity and low cost, but suffer the most from aggregation problems since many of the contaminants causing aggregation are negatively charged, e.g. RNA and genomic DNA, cell debris and intact cells.

It is generally accepted that adsorption of large molecules, such as plasmid DNA molecules, is limited to the outer layer of adsorbent beads (Ljunglof et al., 1999). Thus it may be tempting to assume that a simple mechanism similar to colloidal flocculation occurs inside the EBA bed in the presence of DNA (Theodossiou and Thomas, 2002). Theodossiou et al. (2000, 2001 and 2002) and Theodossiou and Thomas (2002) studied the use of prototype

EBA adsorbents considerably smaller (ca. 40 μm diameter) than conventional EBA beads (ca. 100-300 μm) with the objective of having large surface areas and thus high capacities for purifying plasmid DNA. They observed a reversible aggregation and cross-linking of the beads during loading of a feedstock containing homogenized calf thymus DNA, as a model molecule as well as E. *coli* cell homogenate containing plasmid DNA. In their studies, aggregation of beads by DNA molecules was monitored through bed expansion profiling. Aggregation of beads led to contraction of the expanded bed. By using different adsorbent beads, they found that aggregation of the beads by DNA molecules and consequently bed compression was dependent on parameters such as buffer composition, ionic strength, bead size and surface configuration (Theodossiou and Thomas, 2002). They attributed aggregation of the small adsorbent beads by DNA to a mechanism similar to flocculation in colloid systems (Theodossiou and Thomas, 2002). Nevertheless, the effects of most of the parameters studied on the aggregation were not examined independently due to the fact that the systematic variation of one parameter at a time was not possible. Nevertheless, it was clear that ionic strength had a marked effect on bed aggregation, and led also to a reduction in DNA binding capacity (Theodossiou et al., 2001).

The effects of ionic strength of a solution on DNA binding are likely to be complex. Not only are the surface characteristics of the both adsorbent and DNA likely to be affected by ionic strength, but the ligand density of the adsorbent is likely to play a role. Furthermore, when the adsorbing species is a polyelectrolyte macromolecule such as DNA its characteristics in solution and on the surface of the adsorbent beads is also likely to be influenced. It has been shown by many researchers that increasing salt concentration leads to a change in the configuration of DNA molecules, making them more compact (Stigter, 1977; Manning, 1978; Stigter and Dill, 1993; Schlick, 1994; Ma and Bloomfield 1995; Hunt and

Hearst, 1995; Rybenkov et al., 1997a and 1997b; Bloomfield, 1998 and Cherny and Jovin, 2001). At zero or low salt concentrations, electrostatic repulsion between the negatively charged phosphate groups of the DNA makes the strands repel each other and expand giving a loose and open structure to the molecule. By increasing the salt concentration and shielding negatively charged groups with counter ions, repulsive forces between and within DNA strands are overcome and the molecule starts compacting leading to a decrease in the length and thickness of the DNA molecule. Very similar changes in the structure and configuration of linear DNA molecules compared to supercoiled and circular forms have been showed by Ma and Bloomfield (1995) in different salt concentrations. Those authors concluded that counter ions bind in the same manner to both forms. A very similar result was observed by Schlick et al. (1994).

Feedstock conditioning by changing ionic strength is likely to have complex effects on DNA binding to EBA adsorbents, due to the interacting effects on the DNA, the adsorbent and the column hydrodynamics. In this work we examine the effects of NaCl additions on DNA binding and EBA bed aggregation with two different batches of the strong anion exchange adsorbent Q HyperZ, which have different ligand densities. The adsorbent is approximately twice the size of that used by Theodossiou et al. (2001) and Theodossiou and Thomas (2002) and consists of a different base matrix and ligand type. Models from the literature explaining the effect of salt on the DNA structure and electrostatic interactions are employed to gain a better understanding of the mechanisms governing aggregation and cross-linking of EBA beads by DNA molecules.

Theory

The relation between the effect of salt or counter ion valence and concentration on the configuration of DNA molecules and consequently their electrophoretic mobility was described by Ma and Bloomfield (1995). In the first step, equations (1) and (2), taken from Manning (1978) were used for this purpose. The fractional charge neutralization of DNA molecules (r) and the salt valence (Z) are correlated by:

$$r = 1 - \frac{1}{Z\xi} \tag{1}$$

where, ξ (a dimensionless structural parameter) is given by:

$$\xi = \frac{q^2}{\varepsilon k_B T b} \tag{2}$$

Here, q is the protonic charge, ε the bulk dielectric constant of solvent (buffer solution), k_B Boltzmann's constant, T temperature in Kelvin and b is the average axial charge spacing (along the helical axis for DNA, along the contour axis for more flexible polymers). Ma and Bloomfield (1995) developed an equation to describe the relation between fractional charge neutralization and electrophoretic mobility (the equation not shown). They showed the electrophoretic mobility of a polyion or polyelectrolyte is dependent on Debye length ($1/\kappa$) (i.e. the length of the ionic atmosphere surrounding the charged object). On the other hand, Debye length is a function of ionic strength according to equation 3, where, N_A is Avogadro's number.

$$\kappa^2 = \frac{8\pi N_A q^2}{1000\varepsilon_r k_B T} I \tag{3}$$

The ionic strength (I) is correlated to the ion concentration (c_i) and valence (Z_i) by the following equation:

$$I = \frac{1}{2}\sum c_i Z_i \qquad (4)$$

In general, from these equations (1-4) and others developed by Ma and Bloomfield (1995), it can be concluded that electrophoretic mobility of DNA molecules is dependent on salt concentration.

The effects of adsorbent ligand density and solvent or electrolyte ionic strength on the electrostatic interaction between an adsorbent and a charged molecule can be described by using the 'slab' model developed by Stahlberg (1991) for the electrostatic interaction of proteins during chromatography. This model was then modified and applied for different systems and under different conditions (Stahlberg et al., 1995; Stahlberg and Jonsson, 1996; Jonsson and Stahlberg, 1999 and Hallgren et al., 2000). Based on this model, the solution of the linearized Poisson-Boltzmann (P-B) equation for two oppositely charged planar surfaces (adsorbent and adsorbate) located with a distance of L from each other in the contact with an electrolyte solution (Figure 1) is used as a model to describe the dependency of electrostatic interaction on parameters such as ionic strength of solvent/electrolyte, charge densities and surface areas of adsorbate and adsorbent.

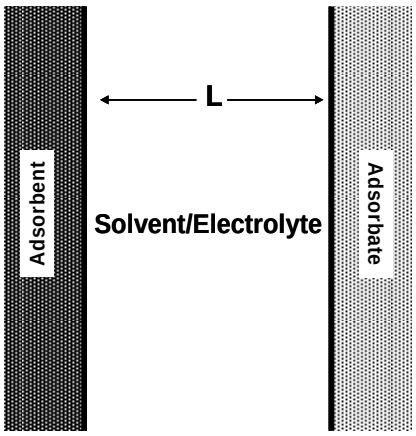

***Figure 1*: A schematic representation of the 'slab' model (Stahlberg et al., 1991).**

Teeters et al. (2004) used the slab model to study the effects of salt type and compaction agent on the adsorption and desorption of plasmid DNA to ion exchange membranes. However, this model could potentially be used in a similar way to elucidate the effects of salt concentration or ionic strength of the buffer and ligand density of the adsorbent on the adsorption of a DNA model system such as homogenized calf thymus to the EBA adsorbent Q HyperZ, and thus also to study the mechanisms of aggregation of adsorbent beads in an EBA system.

According to the 'slab' model, the free energy needed to bring an adsorbate close to an adsorbent with a distance of L between them can be determined by equation 5 (Stahlberg et al., 1991).

$$\frac{\Delta G_{(L)}}{A_{adsorbate}} = \frac{1}{\kappa \varepsilon_p \varepsilon_r} \left[\frac{(\sigma^2_{adsorbate} + \sigma^2_{adsorbent}).e^{-\kappa L} + 2\sigma_{adsorbate}\sigma_{adsorbent}}{e^{\kappa L} - e^{-\kappa L}} \right] \qquad (5)$$

Here, $\sigma_{adsorbate}$ and $\sigma_{adsorbent}$ are the charge densities of the adsorbent and adsorbate, respectively. $A_{adsorbate}$ is the adsorbate surface area or interaction area, κ is the inverse Debye length of the electrolyte solution, and ε_p and ε_r are the permeability of vacuum and the dielectric constant of the solvent, respectively. From close inspection of equation 5 it can be concluded that at a certain distance a minimum value of free energy will be attained, when the electrostatic attractive force between two oppositely charged surfaces is a maximum. It has been shown (Stahlberg and Jonsson, 1996) that the minimum free energy between two surfaces is dependent on the charge density of the planar surface having the lower value (σ*), interaction area or adsorbate surface area ($A_{adsorbate}$) and the inverse Debye length (κ) at a given temperature, according to equation 6.

$$\Delta G_{\min} = \frac{A_{adsorbate}(\sigma^*)^2}{\kappa \varepsilon_p \varepsilon_r} \qquad (6)$$

By taking into account the relation between κ and ionic strength (I) stated in equation 3, the minimum free energy can be correlated to the ionic strength of the buffer by:

$$\Delta G_{\min} \propto \frac{A_{adsorbate}\sigma^2_{adsorbate}}{\sqrt{I}} \qquad \text{when: } -\sigma_{adsorbate} < \sigma_{adsorbent} \tag{7a}$$

$$\Delta G_{\min} \propto \frac{A_{adsorbate}\sigma^2_{adsorbent}}{\sqrt{I}} \qquad \text{when: } -\sigma_{adsorbate} > \sigma_{adsorbent} \tag{7b}$$

On the other hand, the capacity factor (k) as the equilibrium ratio of adsorbate in the adsorbed and liquid phases in a chromatography column can be described by:

$$\ln k = -\frac{\Delta G_{\min}}{RT} + \ln \Phi \tag{8}$$

Here, Φ is the phase ratio of the column and is a function of the column dead volume, the characteristic width of the adsorption layer and the surface area of the stationary phase. Equation 8 can be simplified by eliminating lnΦ under the assumption that ionic strength, adsorbate surface and ligand density of the adsorbate have a very much greater effect on ΔG_{min} than on Φ (Stahlberg et al., 1991). Subsequently inserting equations 7a-b into the simplified form of equation 8, gives:

$$\ln k \propto \frac{A_{adsorbate}\sigma^2_{adsorbate}}{\sqrt{I}} \qquad \text{when: } -\sigma_{adsorbate} < \sigma_{adsorbent} \tag{9a}$$

$$\ln k \propto \frac{A_{adsorbate}\sigma^2_{adsorbent}}{\sqrt{I}} \qquad \text{when: } -\sigma_{adsorbate} > \sigma_{adsorbent} \tag{9b}$$

Based on equations 9a and 9b, there is a linear relationship between the logarithm of the capacity factor and the adsorbate surface, the charge density squared of either the adsorbate or adsorbent, and the reciprocal of the square root of ionic strength. As it was shown before, the latter is a function of salt concentration (equation 4).

Materials and Methods

Materials

Two stocks of prototype Q HyperZ adsorbents with lot numbers 210120/C105 (batch 1) and VC220801 (batch 2), respectively, were received as gifts from BioSepra, Ciphergen, France (Now part of Pall Europe Ltd.). The density and size distribution of both batches of support were 3.2 $g.cm^{-3}$ and 40-105 μm, respectively according to the manufacturer. Deoxyribonucleic acid (DNA) from calf thymus (type I: sodium salt 'highly polymerized') and bovine serum albumin (BSA) were purchased from Sigma-Aldrich. All other chemicals were also obtained from Sigma-Aldrich Company Ltd.

The calf thymus DNA feedstock was prepared by dissolution of sufficient DNA in 50 mM Tris-HCl pH 8 to yield a viscous 2 $mg.mL^{-1}$ solution. Following sonication on ice with an MSE soniprep 150 (MSE Scientific Instruments Ltd., Sussex, UK) and centrifugation at 20000×g at 4 ^{o}C for 15 minutes the sonicated DNA solution with an approximate concentration of 1.5 $mg.mL^{-1}$ was portioned into the sterile tubes and stored at -20^{o}C.

EBA setup

A 1-cm diameter EBA column (UpFront A/S, Copenhagen, Denmark) was used in all expanded bed experiments. The column contained a magnetic bar in the base for fluid distribution and was placed on a magnetic stirrer. The rotation rate of the magnet was 700 rpm in all experiments. A FPLC system (Amersham BioSciences (now part of GE Healthcare), Uppsala, Sweden) equipped with two pumps, UV monitor and conductivity meter was used.

Batch binding experiments with BSA and DNA

The adsorbents were first equilibrated in 50 mM Tris-HCl pH 8 containing the appropriate NaCl concentrations as mentioned in the text. In all batch binding and kinetics studies, 0.1 mL portions of the support were added to a series of 2 ml eppendorf style tubes. 1.5-mL aliquots of DNA solution (1.5 mg ml^{-1}) or bovine serum albumin (4 mg ml^{-1}) were then added and shaking on a vibromax shaker started. After the appropriate time, one of the tubes from the series was removed from the shaker, the adsorbent allowed to settle under gravity or centrifugation and the supernatant removed. The amount of DNA or protein was then determined in a Lambda 20 UV/VIS spectrophotometer (PerkinElmer Analytical Instruments, Shelton, CT, USA) at 260 or 280 nm, respectively, by relating to standard curves.

Expanded bed adsorption experiments

In all experiments the settled bed height of Q HyperZ adsorbents was 6.7±0.5 cm and the flow velocity was 350±20 $cm.h^{-1}$ giving 2-fold expansion of the bed. The bed was prepared by expansion with equilibration buffer composed of 50 mM Tris-HCl pH 8 supplemented with 0-0.75 M NaCl for 30 min (*ca.* 26 column volumes). The feedstock containing 50 mM Tris-HCl pH 8, and either 20-80 $\mu g.mL^{-1}$ homogenized calf thymus DNA (see results section) or 1 $mg.mL^{-1}$ BSA, and various concentrations of salt (0-0.75 M NaCl) was then loaded. The column outlet was monitored with a UV detector at 254 or 280 nm for DNA and BSA, respectively and fractions were collected. Loading was continued until at least 20% breakthrough was observed. The adsorbent was not washed or reused. The concentrations of DNA or BSA in the collected fractions were analysed offline at 260 or 280 nm, respectively, in a Lambda 20 UV/VIS spectrometer (PerkinElmer Analytical Instruments, Shelton, CT, USA) and related to standard curves. The concentrations of salt used in the

loading buffers were (M) 0, 0.05, 0.1, 0.15, 0.25, 0.35, 0.5 and 0.75, which corresponded to conductivities of ($mS.cm^{-1}$) 2.6, 7.5, 11.2, 16.2, 25.3, 32.8, 44.2 and 63.3, respectively.

Ionic capacity of the adsorbents

The ionic capacity of the adsorbents was determined using the same method used by Theodossiou and Thomas (2002), taken from Pitfield (1992). In summary, 0.5-2 mL of adsorbent was suspended in 50 mL of 2 M NaCl and incubated with mixing for 1.5 hours at room temperature to convert the ligands into the hydrochloride salt or quaternary alkyl ammonium chloride form. Then the adsorbents were washed three times on a glass sinter funnel with 50 mL aliquots of double distilled Milli-Q water. Washed supports were transferred to plastic 100 mL bottles containing 50 mL of 0.1 M NaOH and mixed at 150 rpm for 24 hours on an orbital shaker (Infors, Basel, Switzerland). In this step the chloride ions (Cl^-) from the supports were replaced by hydroxide ions (OH^-) ions (Roe, 1989). The released Cl^- concentration was measured by the colorimetric method described by Vogel (Vogel, 1989). In this method after taking 1 mL fractions from the liquid phase, samples, standards and blanks were each vigorously mixed on a Vortex-Genie 2 vibrax shaker (Scientific Industries, Bohemia, NY, USA) with 100 µL of 0.25 M ammonium iron (III) sulphate in 9 M HNO_3 and 100 µL of a saturated solution of mercury (II) thiocyanate in 96% ethanol in 1.5-mL plastic screw-capped vials. Thiocyanate ions are displaced from the mercury (II) thiocyanate by the Cl^- ions, and in the presence of ferric ions the highly coloured complex iron (III) thiocyanate forms. The intensity of the color is proportional to the original chloride ion concentration. After 10 minutes at room temperature, the absorbance of the liquid phase was measured by a Lambda 20 UV-Vis spectrophotometer (Perkin-Elmer Analytical Instruments, Shelton, CT, USA). The concentration of Cl^- was estimated from a standard

curve of chloride ion concentration in the range of 0.1-2 mM NaCl constructed by serial dilution of 10 mM NaCl (Milli-Q water served as both diluent and blank).

Support characterization

A Nikon Optiphot 2 microscope (Nikon, Melville, NY, USA) fitted with a Kappa CF-8/1 FMC monochrome video camera (Kappa Opto-electronics GmbH, Gleichen, Germany) in conjunction with Image-Pro® Plus software (version 4.1 for Windows™; Media Cybernetics, Silver Spring, MD, USA) was used to determine the size distribution of adsorbent beads. The diameter of between 700-900 adsorbent beads was measured by using the software after calibration with a micrometer equipped slide.

The bulk densities of the supports were determined by measuring the weight of a known settled volume of each support and particle densities then were calculated by assuming that the voidage of a settled bed is 0.4 (Theodossiou et al., 2002).

Results

Support characterization

The Q HyperZ support is a small and highly dense anion exchanger with a porous core made from zirconium oxide. The pores of the core are filled with a high charge-density hydrogel containing quaternary amine groups and synthesized through polymerization of methacryloylaminopropyl-trimethylammonium, as functionalized monomer and N,N' methyl bis methacrylamide (a bifunctional acrylic monomer), as cross-linker (Voute and Boschetti, 1999). The gel material and core combine to allow the adsorbent to be used in solutions with high conductivity (Voute and Boschetti, 1999). However when compared to other EBA

adsorbents including those containing quaternary amine groups only modest ionic capacities are measured (Table 1). Nevertheless, the batch and dynamic binding capacities for BSA are similar to those obtained with Streamline Q XL and UFC PEI. The dynamic binding capacities for DNA (measured by EBA later in this work) are very much higher than reported for the other EBA adsorbent types (Table 1). This is most likely due to a combination of the strong anion exchange ligand (quaternary amine groups), and small diameter of the beads (e.g. compared to Streamline QXL), which increases the external surface area for binding. Despite the small size of the Q HyperZ adsorbent, the high density (Table 1) necessitates the use of high flow rates (350 cm. h^{-1}) to give a 2-fold expansion of the bed (Figure 2).

Batch binding studies with DNA

When the kinetics of calf thymus DNA binding were examined in static binding experiments with both adsorbent batches, it was observed that almost half of the DNA offered was bound within the first 2 minutes (Figure 3), which is consistent with a scenario of rapid coverage of the outer surface of the adsorbent. Subsequently a plateau was apparent after ~10 minutes of binding for both adsorbent batches, after which binding came to equilibrium for batch 2. In contrast, batch 1 continued to bind DNA and equilibrium was not reached even after 60 minutes had elapsed. The result suggests that rearrangements of the DNA occurred allowing further binding on batch 1 but not batch 2. This will be discussed later.

When the effect of salt on DNA batch binding to the Q HyperZ adsorbent was studied, little change in capacity was seen even when up to 0.5 M NaCl was employed (Figure 4). However the capacity dropped markedly when salt was increased further to 0.75 M (Figure 4).

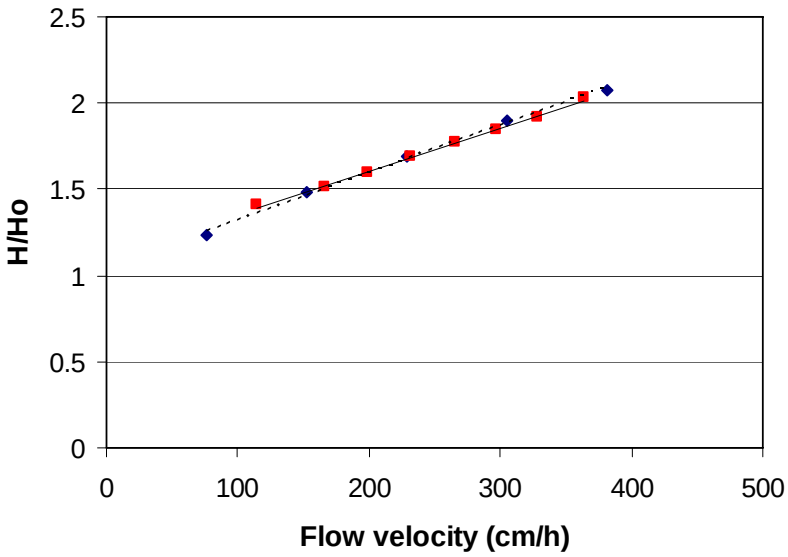

Figure 2: **Bed expansion for Q HyperZ beads in an EBA column showing the effect of increasing flow rate (of 50 mM Tris-HCl pH 8) on the ratio of the expanded bed height (H) to the settled bed height (Ho). Batch 1 (diamonds) and batch 2 (squares).**

Effect of salt on the binding of DNA during EBA

Breakthrough curves of DNA during binding to the two batches of Q HyperZ adsorbent in the EBA system are shown in Figures 5a and 5b and summarized in 5c. The results for batch 1 (Figure 5a) show that increasing the ionic strength of the feedstock by adding up to 0.25 M salt led to a doubling in the dynamic binding capacity at 10% breakthrough ($Q_{10\%}$) as compared to not adding salt. Further increases in NaCl reduced the value of $Q_{10\%}$ until immediate breakthrough was observed when the loading buffer contained 0.75 M NaCl (Figure 5a). Similar behaviour was observed for batch 2 (Figure 5b), except that the highest value of $Q_{10\%}$ (18.94 mg DNA.mL^{-1} gel) was obtained in the presence of 0.35 M NaCl, which is consistent with the higher ligand density of this adsorbent compared to that for batch 1. The breakthrough curves showed no leakage of DNA from the bed until the majority of the binding sites were occupied in the presence of salt up to 0.35 M and 0.50 M for batch 1

and 2 beads, respectively. Subsequently steep breakthrough was observed as more DNA was added. The results suggest that a strong interaction between the DNA and adsorbent occurred even at high ionic strength.

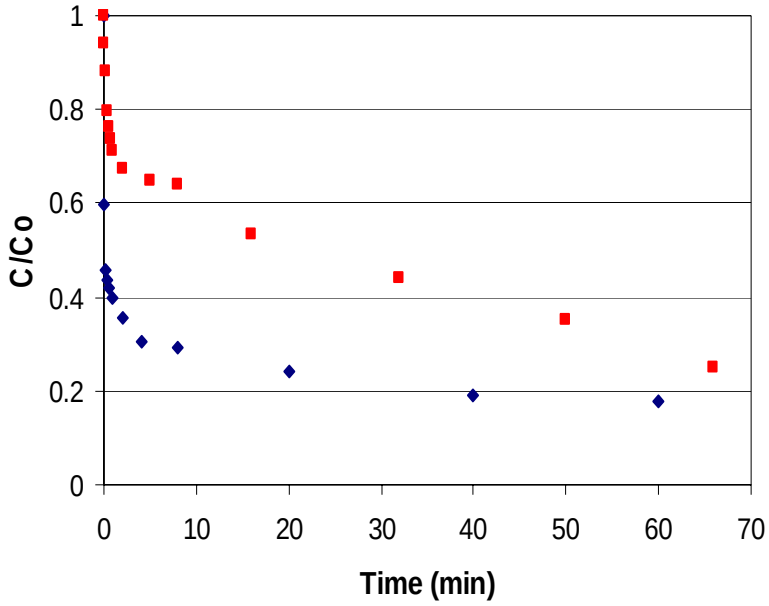

***Figure 3*: Kinetics of binding of homogenized calf thymus DNA to batches 1 (squares) and 2 (diamonds) Q HyperZ beads. DNA concentration of 1.5 mg.mL^{-1} was used. No salt was added to the buffer. The rapid unassisted sedimentation of adsorbent beads enabled short incubation times to be studied.**

***Table 1*: Properties of some EBA supports**

Reference	Adsorbent	Density ($g.cm^{-3}$)	Diameter range [mean] (µm)	Ionic capacity ($mmol\ Cl^{-}.mL^{-1}$)	Protein binding capacity ($mg.\ mL^{-1}$ gel)	DNA binding capacity ($mg.\ mL^{-1}$ gel)
Li et al. (2005)	Streamline Direct CST I	1.80	80-165 [135.0]	ND	>34[a]	ND
Theodossiou (2004) and Ferreira et al. (2000)	Streamline Q XL	1.15	70-260 [142.5]	0.230-0.330	>110[a]	2.5[a]
Theodossiou (2004)	Streamline DEAE	1.15	70-300 [142.7]	0.130-0.210	40-55[a]	0.2[b]
Theodossiou (2004)	UFC DEAE	1.38	100-300 [200]	0.050-0.100	70[a]	0.3[b]
Theodossiou (2004)	UFC PEI	1.52	110-300 [174.6]	0.180-0.200	90[a]	0.6[b]
Theodossiou (2004)	Prototype DEAE	3.70	20-40 [ND]	0.050	22[b]	2.7[b]
Theodossiou (2004)	Prototype PEI	3.70	20-40 [ND]	0.140	46[b]	5.6[b]
This work	Q HyperZ (Batch 1)	3.45[e] (3.2[f])	40-105 [70.6]	0.122	ND	12.6[c]
This work	Q HyperZ (Batch 2)	3.45[e] (3.2[f])	40-105 [73.3]	0.147	108[c] and 90[d]	14.7[c]

*ND: Not determined

[a]Capacities obtained in the dynamic binding mode

[b]Capacities obtained in the batch binding mode

[c]Batch binding capacity obtained by using 1.5 $mg.mL^{-1}$ homogenized calf thymus DNA or 4 $mg.mL^{-1}$ BSA in a 50 mM Tris-HCl pH 8 buffer

[d]Dynamic binding capacity obtained by using 1 $mg.mL^{-1}$ BSA in a 50 mM Tris-HCl pH 8 buffer in a 1-cm EBA column, fluid velocity: ~350 $cm.h^{-1}$

[e]Experimentally determined; [f]Reported by manufacturer

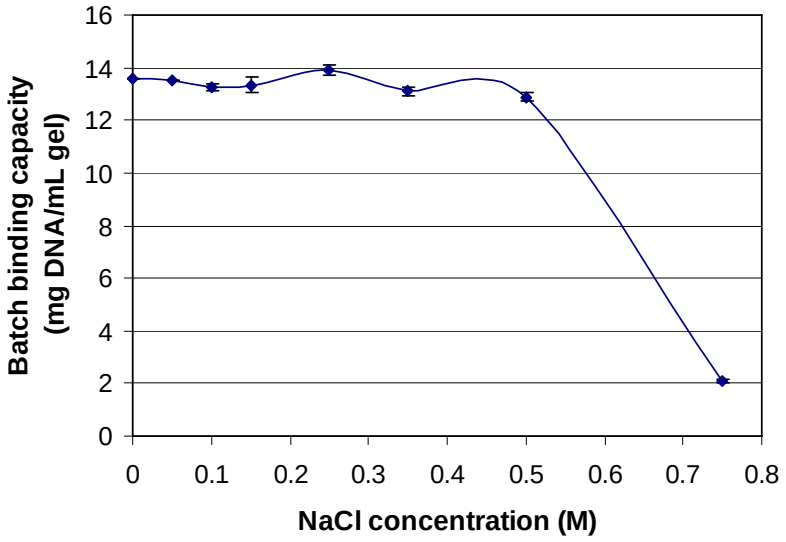

***Figure 4*: Effect of increasing ionic strength adjusted by adding salt on the binding of homogenized calf thymus DNA to the batch 2 Q HyperZ beads. DNA concentration of 1.5 mg.mL^{-1} was used.**

The heights of the expanded bed measured during loading of the DNA for the experiments in Figures 5a and 5b were measured and the average voidage in the bed at each time point determined. The results in Figures 6a and 6b show a distinctive pattern of reduction in bed voidage (i.e. contraction of the bed) as DNA is loaded to the column. In many cases a plateau or a minimum in bed voidage occurred after which the bed voidage increased as more DNA was loaded (Figures 6a and 6b). This plateau was reached after DNA corresponding to 38±6% of $Q_{10\%}$ or 40±7% of $Q_{10\%}$ for batch 1 and 2, respectively. Bed re-expansion was found to start on average after 45±13% and 56±17% of $Q_{10\%}$ was reached. No correlation could be seen between $Q_{10\%}$ and the extent of maximum bed contraction. Interestingly, no re-expansion of the EBA beds was seen at the highest salt concentrations used (i.e. 0.35 and 0.5 M), although bed contraction was not as severe under these conditions as when lower salt concentrations were used. Channelling was not observed in the presence of concentrations of ≥0.10 M salt, but was observed when no salt was added to the feed.

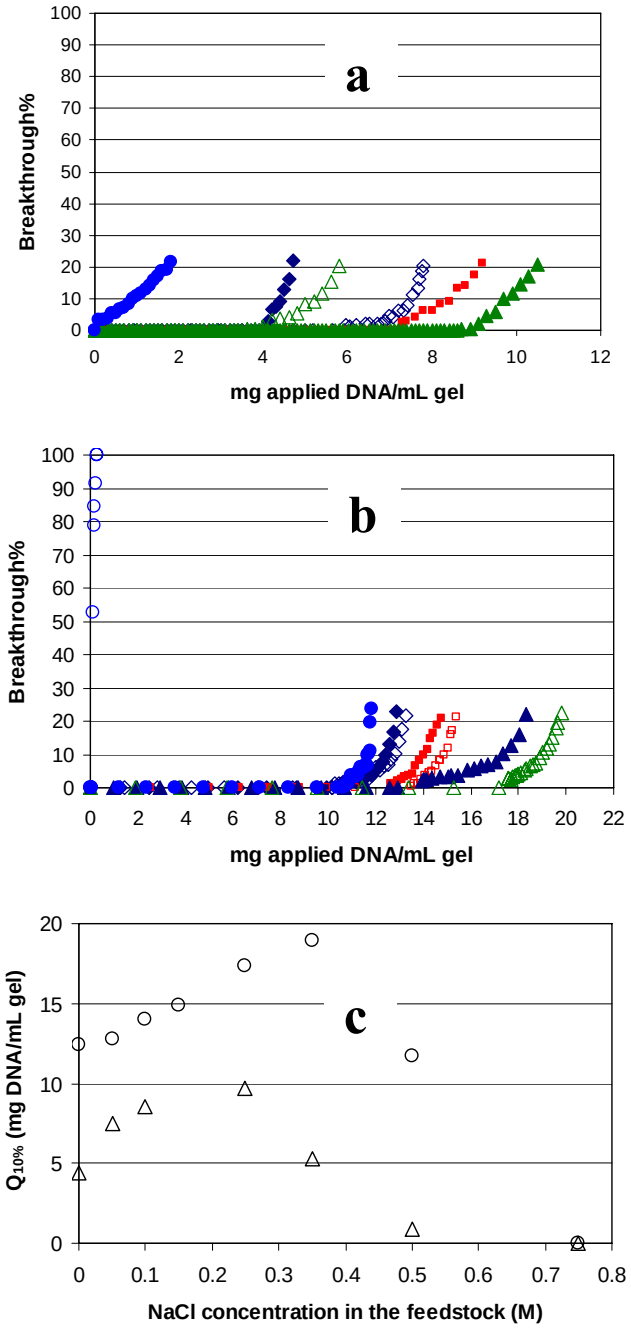

***Figure 5*: Influence of salt concentration during the expanded bed adsorption binding of homogenized calf thymus DNA to batches 1 (a) and 2 (b) Q HyperZ beads. Feedstock applied: 20 µg.mL^{-1} homogenized calf thymus DNA in 50 mM Tris-HCl pH 8 buffer containing: 0 M NaCl (closed diamonds), 0.05 M NaCl (open diamonds), 0.10 M NaCl (closed squares), 0.15 M NaCl (open squares), 0.25 M NaCl (closed triangles), 0.35 M NaCl (open triangles), 0.50 M NaCl (closed circles) and 0.75 M NaCl (open circles). The results are summarised in (c) for batch 1 (triangles) and batch 2 (circles).**

The extent of the reduction in bed voidage appears to be salt dependant as shown in Figure 7a when the data in Figures 6a and 6b is re-plotted. Figure 7a shows that the greatest reduction in bed voidage is not seen with zero added salt, but with 0.05 M NaCl for batch 1 and either 0.05 or 0.25 M for batch 2. At the highest salt concentration the least reduction in bed voidage is seen. Furthermore, when Figures 6a and 6b are examined further the data suggests that low salt concentration causes a greater reduction in voidage for a given amount of applied DNA than higher salt concentrations. When the initial slope (i.e. between 0 and 1.5 mg applied DNA.mL^{-1} gel) of the contraction curves in Figures 6a and 6b are plotted against salt concentration, steeper decline in voidage is also seen for low salt concentration (Figure 7b). In contrast, when the point of lowest voidage is plotted against the amount of DNA loaded at the point of lowest voidage, only a very weak correlation is observed (Figure 8c).

Effect of DNA concentration on EBA characteristics

In order to further examine the role of the amount of DNA loaded on EBA bed behaviour, three different concentrations of DNA were fed to the column. In this case, 0.15 M NaCl was included in the binding buffer, rather than for example 0.35 M, in order to ensure that the effects on bed contraction as well as its reversibility could be observed. No reversibility reversal of bed contraction was seen in Figures 6a and 6b, when 0.35 M salt was included in the feedstock. The results (Figures 9a, b) showed that lower values of $Q_{10\%}$ were obtained by increasing the DNA concentration in the feedstock; dynamic binding capacities of 14.91, 12.58, 11.35 and 10.59 mg applied DNA.mL^{-1} gel were obtained for DNA concentrations of 20, 40, 60 and 80 μg.mL^{-1}, respectively. However, bed contraction behaviour did not change significantly by applying different concentrations of DNA (Figure

9b). This also suggests that the rate of loading DNA does not affect the aggregation intensity which can be estimated from minimum contraction ($(\varepsilon/\varepsilon_i)_{min}$).

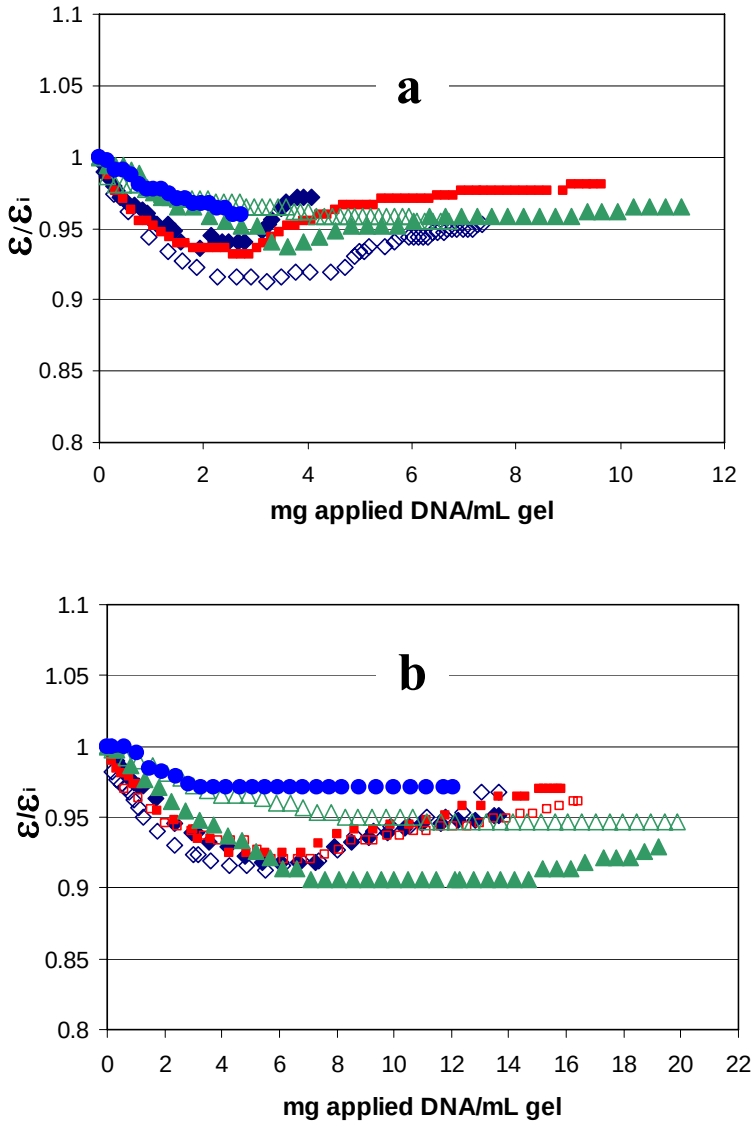

***Figure 6*: Influence of ionic strength (adjusted by adding salt) on the bed compression profiles during binding of homogenized calf thymus DNA to batches 1 (a) and 2 (b) Q HyperZ beads. Feedstock applied: 20 µg.mL^{-1} homogenized calf thymus DNA in 50 mM Tris-HCl pH 8 buffer containing: 0 M NaCl (closed diamonds), 0.05 M NaCl (open diamonds), 0.10 M NaCl (closed squares), 0.15 M NaCl (open squares), 0.25 M NaCl (closed triangles), 0.35 M NaCl (open triangles), 0.50 M NaCl (closed circles) and 0.75 M NaCl (open circles).**

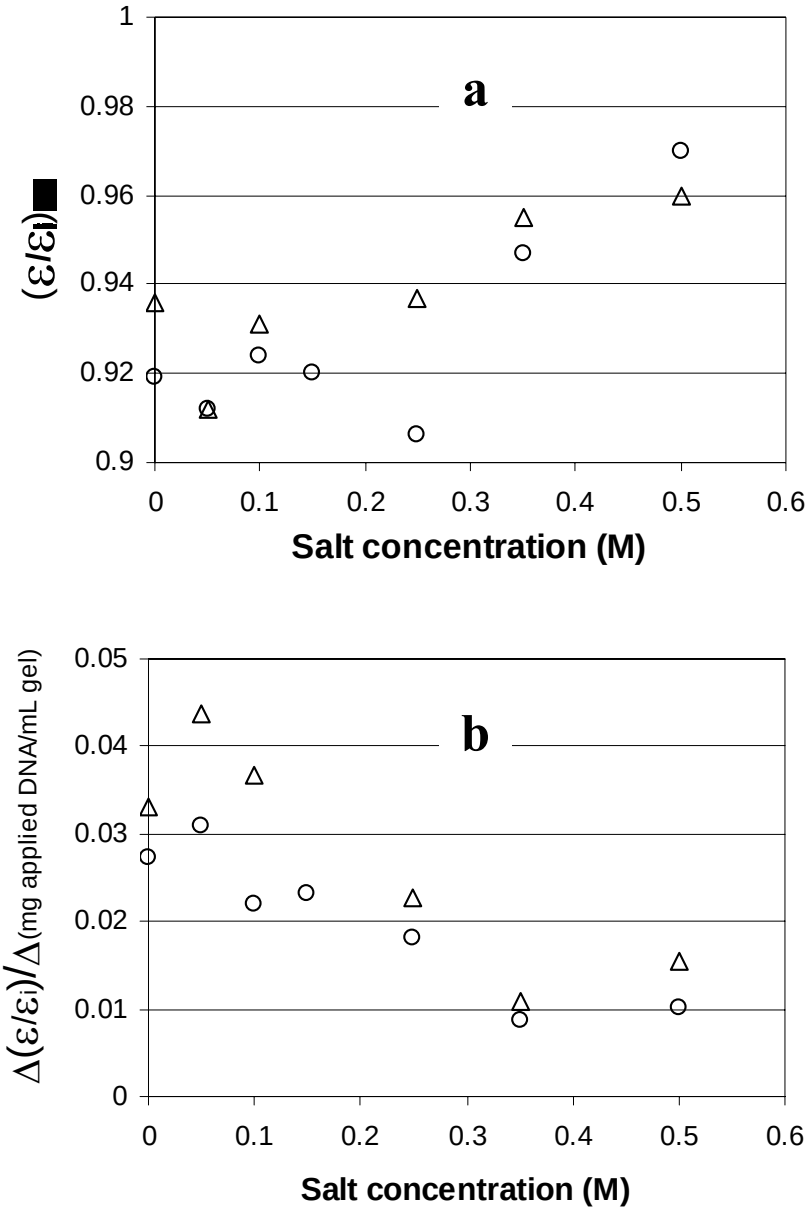

Figure 7. **Correlations between salt concentration and voidage derived from the data in figures 6a and b. (a): Effect of salt concentration on the minimum value of the voidage ratio ($(\varepsilon/\varepsilon_i)_{min}$). (b): Effect of salt concentration on the initial slope of the bed contraction (measured in the interval of 0-1.5 mg DNA applied.mL^{-1} gel). Batch 1 (triangles), batch 2 (circles).**

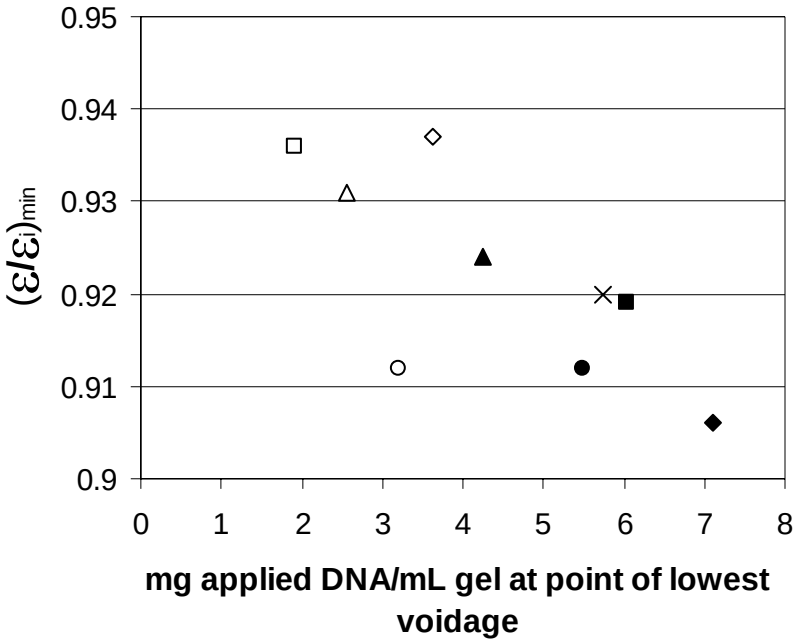

***Figure 8*. Correlation derived from the data in figures 6a and 6b between the amount of DNA applied when voidage is lowest, and the value of the voidage ratio at the point of lowest voidage ($(\varepsilon/\varepsilon_i)_{min}$). Batch 1: open symbols, batch 2: filled symbols. Legend: zero salt added (squares), 0.05 M salt added (circles), 0.1 M salt added (triangles), 0.15 M salt added (cross), 0.25M (diamonds).**

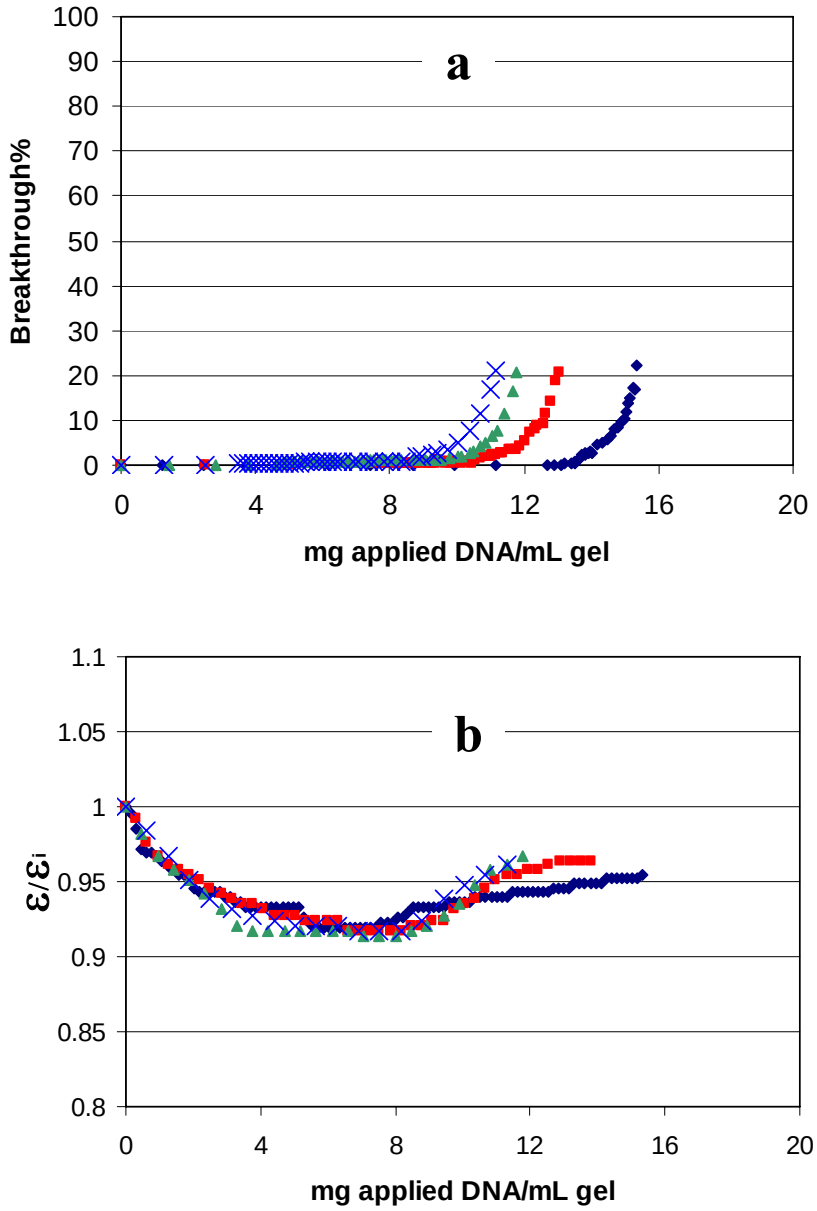

***Figure 9*: Influence of DNA concentration in the feedstock on (a) breakthrough curves and (b) bed compression profiles, during binding of homogenized calf thymus DNA to batch 2 Q HyperZ beads. Feedstock applied: 20 µg.mL^{-1} (diamonds), 40 µg.mL^{-1} (squares), 60 µg.mL^{-1} (triangles) and 80 µg.mL^{-1} (crosses) homogenized calf thymus DNA in 50 mM Tris-HCl pH 8 buffer containing 0.15 M NaCl.**

Effects of protein binding on EBA bed behaviour

The effects of a much smaller molecule than DNA were examined, namely the protein BSA which would be expected to be physically too small to cross-link and aggregate the adsorbents together. Classical protein breakthrough curves were obtained showing a very strong binding interaction between the protein and the adsorbent, followed by a sharp breakthrough as the free binding sites were exhausted (Figure 10a). This is also consistent with the finding of similar capacities measured statically and dynamically (Table 1). The dynamic BSA binding capacity obtained here (108 $mg.mL^{-1}$ gel) was very high and much more than that reported by Cabanne et al. (2004), >40 mg $BSA.mL^{-1}$ adsorbent. The details for which this BSA binding capacity was obtained were not mentioned by Cabanne et al. (2004). A reason for the high protein binding capacity of Q HyperZ beads compared to other types, is likely that protein uptake by these beads is governed by a so-called 'non-diffusive' mechanism (Dziennik et al., 2003 and Cabanne et al, 2004). Since, this adsorbent does not contain true pores. Furthermore, the combination of small size and high density permits high flow velocities (Figure 2) to be used without compromising binding capacity (Cabanne et al., 2004).

Interestingly, some bed contraction was observed in the absence of added salt, which was also reversible (Figure 10b). In contrast to the observations with DNA binding, the point of reversal corresponded with the point of protein breakthrough (Figures 10a and 10b). The observation of bed contraction is not believed to be due to cross-linking of the adsorbents, but rather due to binding of the protein to the surface of the adsorbent thus negating bead repulsion due to the charged Q ligands. As can be expected from the sharp breakthrough behaviour, the surface binding sites in the beads of the bottom of the column will be saturated first and those higher up the column will become occupied by protein as loading continues,

leading to continued bed contraction by charge neutralisation until breakthrough occurs. It was not possible to use zeta potential measurements to examine this hypothesis due to the large size and density of the Q HyperZ adsorbents.

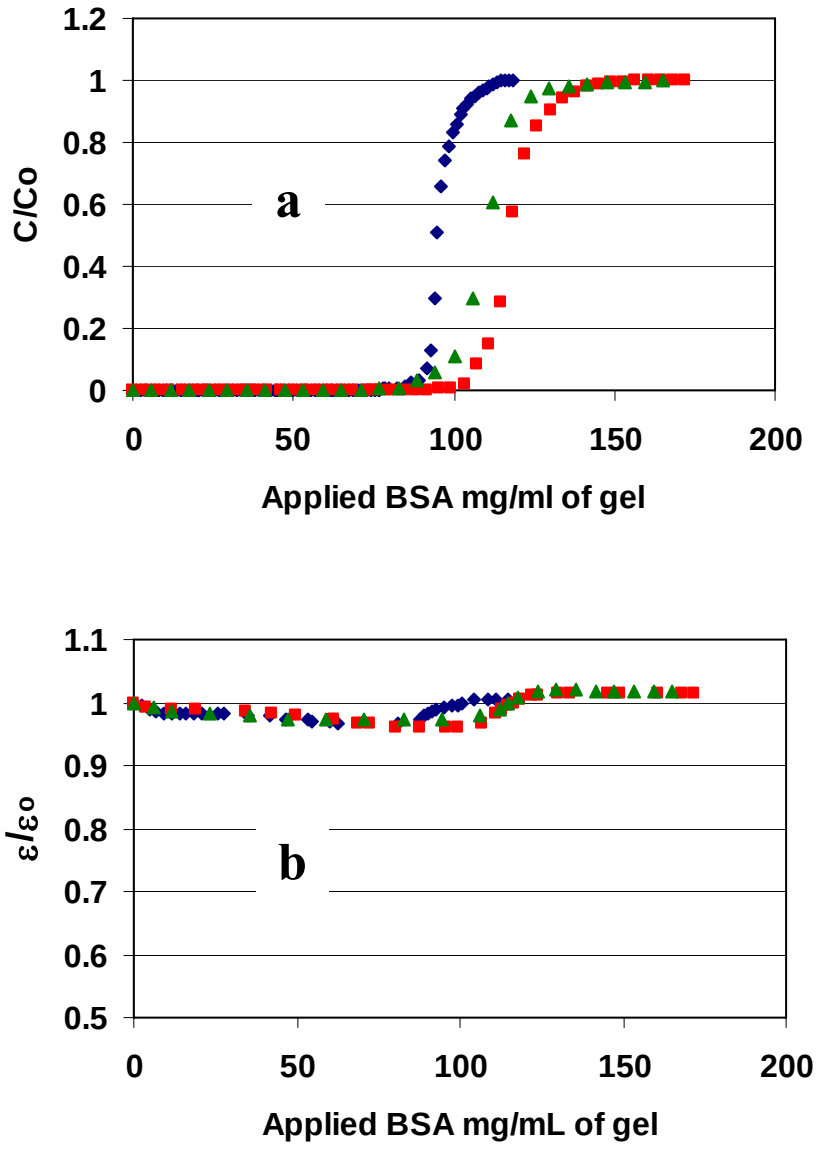

***Figure 10*. Expanded bed adsorption behaviour for the loading of BSA to Q HyperZ batch 2. Breakthrough curves (a) and ratio of voidage in the bed (b). The concentrations of protein loaded were: (diamonds) 1 g.L^{-1}, (squares) 3 g.L^{-1}, (triangles) 5 g.L^{-1}.**

Discussion

The results found in this work showed that increasing the concentration of added NaCl from 0 M up to 0.25-0.35 M led to more DNA binding during expanded bed adsorption and to increased bed contraction. This result is in contrast to what was reported by Theodossiou et al (2001) for much smaller agarose based polyethyleneimine derivatized anion exchangers. Furthermore, the results seem to contradict what is to be expected in general for anion exchangers upon increasing the ionic strength of a solution, including our own observations in the batch binding studies above. Thus the mechanisms behind the observations are discussed below.

In the batch binding experiments it was seen that the binding of DNA to batch 2 of the Q HyperZ beads occurred rapidly (Figure 3), implying that DNA molecules are adsorbed mostly on the surface of the beads. This is consistent with the conclusions of Ljunglof et al. (1999) using confocal microscopy to study DNA binding to chromatography adsorbents and was also concluded by Theodossiou et al. (2002). Ljunglof et al. (1999) showed that plasmid adsorbs only to the outer few microns, and that penetration deep into a chromatography adsorbent does not occur. Although in that work, plasmid DNA was used, which has a narrow size distribution. However, binding of calf thymus DNA to batch 1 of the Q HyperZ adsorbents studied in the current work (which had the lowest ligand density) showed evidence of a two stage binding phenomenon in which binding continued after the rapid first stage was completed (Figure 3). The homogenized calf thymus DNA which was used contains DNA molecules with a broad size range (0.5-10 kbp, data not shown). Thus one hypothesis could be that weaker binding due to the lower ligand density of the batch 1 compared to batch 2

adsorbents, allowed small DNA fragments to slowly penetrate partially into the gel after the rapid surface adsorption was complete, giving a two stage binding phenomenon.

Evidence for two-stage binding behaviour with trends almost identical to those seen in the current work has been observed for the adsorption of *Saccharomyces cerevisiae* cells to Streamline Q XL and Q HyperZ beads by Lin et al. (2001) and Vergnault et al. (2004), respectively. Given their size, cells can be expected to bind through multipoint attachments similarly to DNA. The two-step adsorption to Streamline Q XL took place in the presence of a moderate salt concentration (conductivity 12 $mS.cm^{-1}$), whereas a single-step adsorption occurred at lower salt concentrations where the binding interaction was stronger (Lin et al., 2001). Vergnault et al. (2004) also found that the two-step adsorption of cells to Q HyperZ occurred at moderate salt concentrations (150 mM NaCl). Both groups attributed the two-step binding to an adsorption of cells in a first layer via electrostatic interactions with the adsorbent followed by a second step of multi layer adsorption due to attractive interactions between free cells and previously adsorbed cells. The reasons for the effect of salt on causing one or two stage binding were not discussed. Penetration of the large *S. cerevisiae* cells into the adsorbents used by Lin et al. (2001) and Vergnault et al. (2004) is not possible, discounting the hypothesis raised above for the two-stage binding of calf thymus DNA. However, a closer look at the conditions used by Lin et al. (2001) and Vergnault et al. (2204) and their observations, suggests two likely hypotheses to describe the mechanism of the single-step and two-step adsorptions observed with different salt concentrations: (i) non-electrostatic interactions (e.g. hydrophobic interaction) between adsorbed cells and free cells are responsible for the second step of a two-step adsorption, which require a moderate salt concentration to reduce electrostatic repulsion between the cells giving rise to tighter packing or multilayer adsorption; (ii) slow rearrangements of the cells on the surface of the adsorbent

are possible, permitting further binding but only occur when the strong electrostatic interactions with the ligands have been reduced by the presence of salt.

The first hypothesis can not explain the two-step adsorption of DNA molecules seen in the current work, since in Figure 3 the binding was conducted in the absence of added salt, and the only difference between observing one or two-step binding was the ligand density of the adsorbents used. However, extension of the second hypothesis to include reduction of binding strength due to lower ligand density can explain the observations in the current work. It is proposed that the lower ligand density of batch 1 adsorbents compared to batch 2, leads to fewer sites for multipoint attachment and thus weaker binding of the DNA. Rearrangement of the molecules on the surface of these adsorbents is then permitted as exposure time is increased. These rearrangements may include movement of the long DNA strands lying on the surface to expose more ligands or could perhaps also include some penetration into the gel of very small DNA fragments, which can be expected to have sizes of less than 100 nm (Tyn and Gusek, 1990). Rearrangement of DNA molecules is proposed not to occur for the batch 2 beads because of the much greater number of multipoint attachments due to the higher ligand density, leading to stronger binding and consequently a lower dissociation constant for the highly charged DNA. Furthermore, the density of DNA fragments adsorbed on the surface of batch 2 beads would be expected to be much higher than on batch 1 (see Figure 3), and the resulting highly negatively charged surface would hinder the approach and penetration of small fragments into the gel.

In support of the hypothesis of adsorbate rearrangements proposed above, is the report of Johnson et al. (1994) who developed a mechanistic model to explain stepped isotherms for the adsorption of proteins to charged planar surfaces. Although Johnson did not examine the effect of ligand density, he predicted that when high concentrations of protein were used

during binding, or when ionic strength was increased, rapid binding occurred initially followed by a second stage of binding as longer times were used. Furthermore, as time progressed the pattern of protein binding was expected to change and a close-packed array of protein molecules was predicted on the surface rather than a widely-spaced array. It was concluded by Johnson et al. (1994) that when binding between the protein and the surface is sufficiently weak, the protein molecules are able to rearrange on the surface exposing more ligand and permitting further binding. The rearrangement is however slow and can thus be observed as a second binding stage. The above hypothesis of adsorbate rearrangements also explains the mechanism of two-step adsorption of *S. cerevisiae* to Streamline Q XL and Q HyperZ beads at moderate ionic strengths reported by Lin et al. (2001) and Vergnault et al. (2004), respectively. Thus, in general it is concluded here that the two-step adsorption of DNA to batch 1 beads was due to the weaker binding of the attached molecules and rearrangement of them given enough time, leading to access to more ligands for free DNA in solution.

The above arguments would suggest that reducing the interaction strength between batch 2 of the Q HyperZ adsorbents studied here, by small increases in the ionic strength of the solution used, would allow DNA rearrangements leading to two-stage binding and thus potentially to a higher capacity of the adsorbent at equilibrium. On the other hand, it is generally to be expected that increased ionic strength should lead to a reduction in overall binding capacity (see equation 9b above). When the data in Figure 4 is examined, it can be seen that there is essentially no change in adsorbent capacity at equilibrium as the salt concentration is increased to 0.5 M and this can be described by considering two counter-balancing effects. First, the ‘slab’ model of Ståhlberg et al. (1991) (see the theory section above) indicates that increasing the salt concentration will be expected to reduce the binding

capacity of the adsorbent due to increases in the ionic strength (I) leading to shielding of the charged ligands with counter ions (affecting both $A_{adsorbate}$ and I in the equations 9a and 9b, above). Second, the structure and configuration of the polyelectrolyte DNA are modified causing a decrease in the adsorbate surface area (see equation 1 above) and allowing more DNA to be packed onto the bead surface. In addition, increasing diffusion into the adsorbent is expected to be increased, based on results obtained by Ma and Bloomfield (1995) showing enhanced electrophoretic mobility of DNA molecules in the presence of salt, as discussed above. It is proposed that the two effects of salt have opposing influences on the adsorption of DNA molecules to Q HyperZ beads at moderate NaCl concentrations (up to 0.5 M NaCl) leading to the similar capacities observed in Figure 4. However at very high salt concentrations (i.e. > 0.5 M), charge shielding of both the adsorbent and the DNA reduces binding and capacity drops to zero in the presence of 0.75 M NaCl.

The effects of salt on DNA structure have been documented in the studies of Ma and Bloomfield (1995) and Murphy et al. (2003). Ma and Bloomfield (1995) showed that the electrophoretic mobility of DNA in agarose gels was increased in the presence of salt, suggesting that size had been decreased. Murphy et al. (2003) showed that plasmid DNA adsorption to anion-exchange chromatography beads (Q Sepharose Fast Flow) was increased by raising the salt concentrations of 100-600 mM in the presence of compaction agents (spermidine, spermine and $Co(NH_3)_6$), which was suggested to allow the smaller DNA molecules to pack more closely on the surface. This hypothesis was confirmed with that of Teeters et al. (2004) who examined the binding of plasmid DNA to anion-exchange membranes. In general, these workers concluded that even though electrostatic interactions decrease when the salt concentration and ionic strength are increased (i.e. having an adverse effect on adsorption, equation 9b), the decrease in size due to compaction of the DNA from

shielding by counter ions leads to DNA molecules can pack more closely on the surface and also have less repulsive forces towards approaching free DNA molecules. Also from the above, it is concluded that the reduction in size of the DNA in the presence of salt leads to increased diffusion of DNA molecules into the Q HyperZ bead. The reduced interaction with the adsorbent allows rearrangements to occur and thus potentially for closer packing. These effects are proposed to offset the general reduction in binding caused by salt, leading to the effect seen in Figure 4.

In light of the batch binding studies and the above discussion, it would be expected that dynamic binding capacities for DNA measured during EBA would be greater for Q HyperZ batch 2 than batch 1, but remain constant or drop when solutions containing increasing concentrations of added salt were loaded. Furthermore, it would be expected that bed contraction should be less severe when higher concentrations of salt were employed, since DNA binding and the strength of the interactions is expected to be reduced. The data in Figures 5a, 5b and 5c did indeed show that binding capacities were higher for batch 2 than batch 1 (confirmed by equation 9b), that batch 2 was more tolerant to high salt concentrations, and that in general bed contraction was less for batch 1 than batch 2 (Figure 7a). However, increasing the salt concentration in the feedstock to 0.25 M NaCl (for batch 1) or 0.35 M (for batch 2) led to an increase in the dynamic binding capacity which then decreased when the salt concentrations were increased (confirmed by equation 9b). This pattern of salt effects on DNA capacity was mirrored by observations of bed contraction, which was not steadily reduced as salt concentrations were increased. Rather, the results showed that for batch 1, bed contraction was greater when 0.05 M salt was used than when no salt was included. Increases in salt to 0.25 M lead to bed contraction to a similar extent as seen without having salt in the loading buffer, under which conditions the maximum capacity was obtained. Subsequently

less bed contraction was seen and capacity decreased further only when the salt concentration was raised above 0.25 M (Figure 7a). A similar trend was seen for batch 2 adsorbents, except the maximum capacity was observed with 0.35 M salt. Interestingly, the initial slope of the bed contraction profiles (in the presence of 0.25 M or 0.35 M salt) was less than in the absence of added salt in all cases except for when 0.05 M salt was employed (Figure 7b).

The above would suggest that there is a link between the extent of bed contraction and dynamic capacity, however no conclusive correlation could be found in the current work (Figures 8 and 9). Furthermore, no direct relationship between bed contraction and parameters such as DNA binding capacity, adsorbent ligand density and size of the beads was found by Theodossiou and Thomas (2002). The reasons for the lack of correlations were concluded by those workers to be due to the wide differences in the beads tested, preventing a systematic analysis. However from the current results (Figure 7a) it can be concluded that the extent of DNA binding and bed contraction is dependent in part on the interplay between salt concentration and ligand density of the adsorbent, as discussed above. However, the reasons for the effect of salt on dynamic DNA binding by the Q HyperZ adsorbents during EBA requires consideration of new parameters, namely those in relation to bed hydrodynamics.

In the current work, channelling in the EBA bed during DNA loading was only observed when no salt and 0.05 M was added. At salt concentration 0.1 M and above that, no channelling was seen, even though bed contraction was observed (Figure 7a). An absence of channelling in an EBA bed is a prerequisite for optimal performance, since the bed is properly fluidized and all adsorbents are exposed to the feedstock. Thus reduction of channelling as salt concentration was increased implies that more of the adsorbents were in contact with the DNA in the feed, leading to greater DNA binding. At a certain point (i.e. at 0.25 M and 0.35 M for batch 1 and 2 of Q HyperZ, respectively) the salt concentration became so great that

DNA binding was hindered due to charge shielding which outweighed the benefits on bed hydrodynamics. Close examination of the results of Theodossiou et al. (2000) shows evidence of a similar phenomenon. Using PEI-linked 20-40 μm diameter adsorbents it was observed in one experiment that adding 0.5 M NaCl to sonicated calf thymus DNA in 50 mM Tris-HCl buffer (pH 8) led to reduced aggregation of the adsorbents in comparison to if no salt was added. Breakdown of the bed was inhibited and thus the hydrodynamics were improved, which allowed more DNA to be loaded, giving a higher dynamic capacity in the presence of salt (Theodossiou et al., 2000).

Theodossiou et al. (2001) reported a different effect of salt on dynamic calf thymus DNA binding capacity during EBA than observed in the current work. In that work, Theodossiou et al. (2001) found using both DEAE-linked and PEI-linked 20-40 μm diameter adsorbents with DNA in 0.8 M potassium phosphate buffer that a steady decline in capacity and in bed contraction occurred as the concentrations of NaCl were increased up to 1.0 M. However, the conductivity of the DNA containing solutions (59 $mS.cm^{-1}$ for a 0.8 M potassium acetate buffer without added salt) were very high and similar to that of the DNA solutions in 50 mM Tris-HCl buffer with the highest concentration of salt used (0.75 M) used in the current work (63 $mS.cm^{-1}$). Under such conditions the dynamic binding capacity was 0 (Figure 5b) and bed contraction was non existent during the short duration of the experiment in the current work. The fact that Theodossiou et al. (2001) reported significant binding capacities, is most likely due to the very small adsorbents used (20-40 μm) in comparison to those in the current work. It could thus be expected that had those workers used the same buffer systems as in the current work, that similar trends may have been observed, i.e. that dynamic binding capacity for DNA increased as salt concentration was increased up to a certain point.

In the current work, the highest dynamic binding capacity during EBA (18.9 $mg.mL^{-1}$ for batch 2 with 0.35 M NaCl) was considerably higher than that seen in the batch binding studies (~13.2 $mg.mL^{-1}$; Figure 4), even though a much lower DNA concentration (20 $\mu g\ ml^{-1}$) was used in EBA than batch binding (1.5 $mg.mL^{-1}$). This is postulated to be due to the possibility for more ordered packing of DNA during EBA due to the low concentration used and the gradual addition of fresh DNA in the presence of salt which permitted re-arrangements of the molecules bound as discussed above. At very high DNA concentrations, such as those used during batch binding, it is supposed that a rapid blanket covering took place, which hindered further re-arrangements. Further support for this contention is seen when the data in Figure 9 is examined. Increasing the DNA concentration to 80 $\mu g.mL^{-1}$ during loading led to a $Q_{10\%}$ of 10.5 $mg.mL^{-1}$ (Figure 9a).

Further support for the arguments rose above that DNA re-arrangements occur over time (which are affected by the strength of binding) leading to increased adsorption to the beads was the observation that bed contraction was partly reversible. When the results in Figures 6a and 6b are examined, it can be seen that batch 1 recovers to a higher voidage than batch 2 at all salt concentrations (in the range 0-0.25 M), except at 0.05 M where the reverse is seen. Greater reversal of batch 1 than batch 2 implies that adsorbent aggregate break up (i.e. reversibility of bed contraction) is also a function of ligand density at low salt concentrations (<0.35 M NaCl). At moderate salt concentrations of 0.35 M NaCl and above, bed contraction was reduced but was also irreversible. These results suggest that some aggregates are stable even in the presence of high salt concentrations. This is speculated to be due to very stable binding of long calf thymus DNA strands due to multipoint attachments.

Theodossiou and Thomas (2002) attributed a mechanism similar to flocculation in colloid systems to explain reversible bead aggregation leading to reversible bed contraction.

Briefly, using this mechanism it is thought that before starting DNA loading, adsorbent beads with similar charges (positively charged) repel each other. Adsorption of DNA molecules on the surface causes the net charge on the bead surface to approach zero which leads to getting beads closer. DNA molecule chains bound on one bead will then be able to cross-link neighbour beads to each other. This is very similar to the phenomenon called bridging flocculation (Franks, 2005). Continued accumulation of DNA molecules on the surface is proposed to lead to a change in the net charge on the surface of cross-linked beads which become negatively charged, causing a repulsion force (electrical double layer (Theodossiou and Thomas, 2002 and Franks, 2005)) between the beads.

Changes of the net charge on the surface of particles can be quantified by measuring electrophoretic mobility and from that zeta potential of particles. Lin et al. (2003) and Hubbuch et al. (2006) studied the effect of different parameters (e.g. pH and conductivity) on zeta potential of adsorbent beads and particulates present in bio-feedstocks. Then they quantified the electrostatic interaction between particulates present in bio-feedstocks and adsorbent beads under different conditions. Hubbuch et al. (2006) introduced a strategy to control unwanted interaction between particulates based on zeta potential measurements. In order to study the mechanism of reversible bead aggregation by DNA, the zeta potential of Q HyperZ adsorbent beads which had been loaded with different amounts of DNA were examined. However, no conclusive results were obtained due to the high values of the standard deviation measured. This was because conventional equipment for determining the zeta potential cannot measure particles with sizes of more than 10 μm, and in particular not those having high densities.

Examination of the literature revealed that a very similar phenomenon (reversible aggregation and its relationship with surface net charge and zeta potential) has been observed

for plasmid DNA-cationic liposome complexes used for gene transfection (Birchall et al., 1999; Ishiwata et al., 2000 and Sakurai, et al., 2000). Characterization of DNA-cationic liposome mixtures showed that by adding plasmid DNA molecules to cationic liposome particles, the zeta potential of the liposome particles decreased from a positive value while aggregate size increased (Figure 11). At a certain amount of DNA loaded the zeta potential of the complexes reached zero at which aggregates have their maximum size. Loading more plasmid DNA resulted in a decrease in the zeta potential to negative values which implies the surface net charge is negative, which leads to the aggregates breaking up. A schematic illustration of this phenomenon summarizing the results of Birchall et al. (1999), Ishiwata et al. (2000) and Sakurai et al. (2000) has been constructed and is shown in the Figure 11. It is proposed in the current work that similar behaviour occurs between Q HyperZ beads (positively charged) and their interaction with DNA molecules.

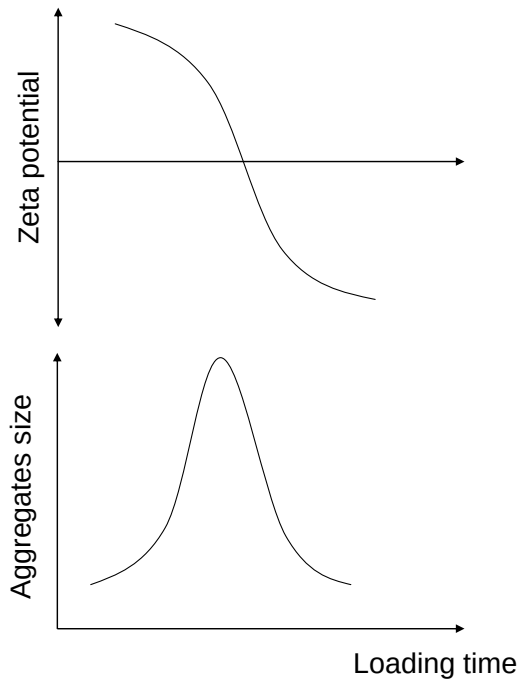

***Figure 11*: A schematic illustration of reversible aggregation of beads/particles due to changes on the zeta potential/surface net charge during DNA binding.**

Conclusions

The Q HyperZ adsorbents examined here have high DNA binding capacities, which are increased rather than reduced as the feedstock is conditioned by adding NaCl up to a concentration that is dependant on the adsorbents ligand density. Thus high concentrations of NaCl (> 0.35 M) are needed to reduce bead aggregation and bed contraction. The reasons for the unexpected effect of NaCl on DNA binding are concluded to be due to the interplay of effects on the DNA molecules and adsorbent, which mediate changes to the bed hydrodynamics. The presence of NaCl increases ionic strength and causes DNA compaction by shielding the many negative charges present, as well as shielding those of the adsorbent's charged ligands. These effects permit closer packing of DNA on the adsorbent surface due to the smaller sizes of the molecules and reduced repulsion between the negatively charged strands, allow DNA rearrangements on the surface, as well as increasing the mobility of small fragments permitting their penetration into the adsorbents. The increased ionic strength arising from adding NaCl weakens bead cross-linking and aggregation in the EBA column, which improves bed hydrodynamics by reducing channelling and leading to better contact of the DNA feed with the adsorbents, and thus to greater binding. When a certain salt concentration is exceeded, which is dependant on the adsorbents ligand density, charge shielding leading to reduced DNA binding becomes the dominating effect and capacity for DNA falls. It is therefore concluded that attempting to improve the EBA performance of Q HyperZ by adding NaCl to condition crude feedstocks containing DNA is likely to result in worse behaviour unless excessive amounts of salt are added. Under such conditions protein binding capacity is likely to be compromised. Other alternatives such as new adsorbent

designs are needed to fully exploit the potential of EBA for processing crude feeds containing DNA and particulates in solution.

Acknowledgments

Iranian ministry of science, research and technology supported this work by granting a PhD scholarship to Ayyoob Arpanaei.

References

1. Anspach, F.B.; Curbelo, D.; Hartmann, R.; Grake, G. and Deckwer, W.; **1999; Expanded-bed chromatography in primary protein purification**; *Journal of Chromatography A*, 865, 129-144.
2. Birchall, J.C.; Kellaway, I.W. and Mills S.N.; 1999; **Physico-chemical characterization and transfection efficiency of lipid-based gene delivery complexes**; *International Journal of Pharmaceutics*, 183, 195-207.
3. Bloomfield, V.A.; 1998; DNA condensation by multivalent cations**; *Biopolymers*, 44(3), 269-282.**
4. Cabanne, C.; Noubhani, A.M.; Dieryck, W.; Hocquellet, A. and Santarelli, X.; 2004; **Evaluation of three expanded bed adsorption anion exchange matrices with the aid of recombinant green fluorescent protein overexpressed in *Escherichia coli***; *Journal of Chromatography B*, 808, 91-97.
5. Cherny, D.I. and Jovin, T.M.; 2001; **Electron and scanning force microscopy studies of alterations in supercoiled DNA tertiary structure**; *Journal of Molecular Biology*, 313, 295-307.
6. Dainiak, M.B.; Galaev, I.Y. and Mattiasson, B.; 2002a; **Direct Capture of Product from Fermentation Broth Using a Cell-Repelling Ion Exchanger**; *Journal of Chromatography A,* 942, 123-131.
7. Dainiak, M.B.; Galaev, I.Y. and Mattiasson, B.; 2002b; Polyelectrolyte**-Coated Ion Exchangers for Cell-Resistant Expanded Bed Adsorption**; *Biotechnology Progress,* 18, 815-820.
8. Draeger, N.M. and Chase, H.A.; 1991; **Liquid Fluidised Bed Adsorption of Protein in the Presence of Cells**; *Bioseparation, 2*, 67-80.
9. Dziennik, S.R.; Belcher, E.B.; Barker, G.A., DeBergalis, M.J.; Fernandez, S.E. and Lenhoff, A.M.; 2003; **Nondiffusive mechanisms enhance protein uptake rates in ion exchange particles**; *Proceedings of the National Academy of Sciences of the United States of America (PNAS)*, 100(2), 420-425.
10. Feuser, J.; Walter, J.; Kula, M.R. and Thömmes, J.; 1999a; **Cell/Adsorbent interactions in expanded bed adsorption of proteins**; *Bioseparation*, 8, 99-109.
11. Feuser, J; Halfar, M.; Lutkemeyer, D.; Ameskamp, N.; Kula, M.R. and Thömmes, J.; 1999b; **Interaction of mammalian cell culture broth with adsorbents in expanded bed adsorption of monoclonal antibodies**; *Process Biochemistry*, 34, 159-165.
12. Franks, G.; 2005; **Innovation applications of controlled particle interactions**; *Transactions of IChemE, Part A, Chemical Engineering Research and Design*, 83(A7), 937-9345.
13. Galaev, I; Hatti-Kaul, R. and Mattiasson, B.; 2002; **Method for the separation of bioproducts**; *World patent*, WO02/102490.

14. Hallgren, E.; Kalman, F.; Farnan, D.; Horvath, C. and Ståhlberg, J.; 2000; **Protein retention in ion-exchange chromatography: effect of net charge and charge distribution**; *Journal of Chromatography A*, 877, 13-24.
15. Hansson, M.; Stahl, S.; Hjorth, R.; Uhlen, M. and Moks, T.; 1994; **Single-Step Recovery of a Secreted recombinant Protein by Expanded Bed Adsorption**; *Bio/Technology,* 12, 285-288.
16. Hjorth, R.; Leijon, P; Barnfield Frej, A.K. and Jagersten, C.; 1998; **Expanded Bed Adsorption Chromatography**; In: Subramanian, G. (ed.), *Bioseparation and Bioprocessing*, Vol. 8, Wiley-VCH Verlag GmbH, Weinheim, Germany, Pages: 199-226.
17. Hubbuch, J.J.; Brixius, P.J.; Lin, D.Q.; Mollerup, I. and Kula, M.R.; 2006; **The influence of homogenisation conditions on biomass-adsorbent interactions during ion-exchange expanded bed adsorption**; *Biotechnology and Bioengineering*, 94(3), 543-553.
18. Hunt, N.G. and Hearst, J.E.; 1991; **Elastic model of DNA supercoiling in the infinite-length limit**; *Journal of Chemical Physics*, 95(12), 9329-9336.
19. Ishiwata, H.; Suzuki, N.; Ando, S.; Kikuchi, H. and Kitagawa, T.; 2000; **Characteristics and biodistribution of cationic liposomes and their DNA complexes**; *Journal of Controlled Release*, 69, 139-148.
20. Johnson, C.A.; Wu, P. and Lenhoff, A.M.; 1994**; Electrostatic and van der Waals contributions to protein adsorption: 2. Modeling of ordered arrays**; *Langmuir*, 10, 3705-3713.
21. **Jonsson, B. and Ståhlberg, J.; 1999; The electrostatic interaction between a charged sphere and an oppositely charged planar surface and its application to protein adsorption; *Colloids and Surfaces B: Biointerfaces*, 14, 67-75.**
22. Kaczmarski, K. and Bellot, J.C.; 2004; **Theoretical investigation of axial and local particle size distribution on expanded bed adsorption process**; *Biotechnology Progress,* 20, 786-792.
23. Lin, D.Q.; Fernandez-Lahore, H.M.; Kula, M.R. and Thömmes, J.; 2001; **Minimising biomass/adsorbent interactions in expanded bed adsorption processes: a methodological design approach**; *Bioseparation*, 10(1-3), 7-19.
24. Lin, D.Q.; Kula, M.R.; Liten, A. and Thömmes, J.; 2003a; **Stability of expanded beds during the application of crude feedstock**; *Biotechnology and Bioengineering*, 81(1), 21-26.

25. Lin, D.Q.; Brixius, P.; Hubbuch, J.; Thömmes, J. and Kula, M.R.; 2003b; B**iomass/adsorbent electrostatic interactions in expanded bed adsorption: a zeta potential study**; *Biotechnology and Bioengineering,* 83(2), 149-157.
26. Lin. D.Q.; Thömmes, J.; Kula, M.R. and Hubbuch, J.; 2004; **The Influence of Biomass on the Hydrodynamic Behaviour and Stability of Expanded Beds**; *Biotechnology and Bioengineering*, 87(3), 337-346.
27. Ljunglof, A.; Bergvall, P; Bhibkhabhai, R. and Hjorth, I.; 1999; **Direct visualization of plasmid DNA in individual chromatography adsorbent particles by confocal scanning laser microscopy**; *Journal of Chromatography A*, 844, 129-135.
28. Ma, C. and Bloomfield, V.A.; 1994; **Gel electrophoresis measurement of counterion condensation on DNA**; *Biopolymers*, 35, 211-216.
29. Manning, G.S.; 1978; **The molecular theory of polyelectrolyte solutions with applications to the electrostatic properties of polynucleotides**; *Quarterly Reviews of Biophysics II*, 2, 179-246.
30. Murphy, J.C.; Fox, G.E. and Willson, R.C.; 2003; **Enhancement of anion-exchange chromatography of DNA using compaction agents**; *Journal of Chromatography A*, 984, 215-221.
31. Pitfield, I.D.; 1992; **Perfluorocarbon chromatographic supports**; *PhD Thesis*, University of Cambridge, Cambridge, UK.
32. Rito-Palomares, M.; 2004; **Novel bioengineering strategies for the development of processes for the recovery of proteins**; *Chemical and Biochemical Engineering Quarterly*, 18(3), 279-284.
33. Roe, S.; 1989; **Separation based on structures**; In: Harris ELV and Angal S (eds.), *Protein purification methods: a practical approach*, IRL Press, Oxford, UK, Pages: 200-222.
34. Rybenkov, V.V.; Vologodskii, A.V. and Cozzarelli, N.R.; 1997a; **The effect of ionic conditions on DNA helical repeat, effective diameter and free energy of supercoiling**; *Nucleic Acids Research*, 25(7), 1412-1418.
35. Rybenkov, V.V.; Vologodskii, A.V. and Cozzarelli, N.R.; 1997b; **The effect of ionic conditions on the conformations of supercoiled DNA. I. Sedimentation analysis**; *Journal of Molecular Biology*, 267, 299-311.
36. Sakurai, F.; Inoue, R.; Nishino, Y.; Okuda, A.; Matsumoto, O.; Taga, T.; Yamashita, F.; Takakura, Y. and Hashida, M.; **Effect of DNA/liposome mixing ratio on the physicochemical characteristics, cellular uptake and intracellular trafficking of plasmid DNA/cationic liposome complexes and subsequent gene expression**; *Journal of Controlled Release*, 66, 255-269.

37. Schlick, T.; Li, B. and Olson, W.K.; 1994; **The influence of salt on the structure and energetics of supercoiled DNA;** *Biophysical Journal*, 67, 2146-2166.
38. Senthuran, A.; Senthuran, V.; Hatti-Kaul, R. and Mattiasson, B.; 2004; **Lactate Production in an integrated process configuration: reducing cell adsorption by shielding of adsorbent**; *Applied Microbiology and Biotechnology,* 65, 658-663.
39. Ståhlberg, J. and Jonsson, B.; 1996; **Influence of charge regulation in the electrostatic interaction chromatography of proteins**; *Analytical Chemistry*, 68(9), 1536-1544.
40. Ståhlberg, J.; Appelgren, U. and Jonsson, B.; 1995; **Electrostatic interactions between a charged sphere and charged planar surface in an electrolyte solution**; Jou*rnal of Colloid and Interface Science*, 176, 397-409.
41. Ståhlberg, J.; Jonsson, B. and Horvath, C.; 1991; **Theory for electrostatic interaction chromatography of proteins**; *Analytical Chemistry*, 63, 1867-1874.
42. Stigter, D. and Dill, K.A.; 1993; **Theory for second virial coefficients of short DNA**; *The Journal of Physical Chemistry*, 97(49), 12995-12997.
43. Stigter, D.; 1977**; Interactions of highly charged colloidal cylinders with applications to double-stranded**; *Biopolymers*, 16, 1435-1448.
44. Teeters, M.A.; Thatcher, W.R. and Lightfoot, E.N.; 2004; **Adsorption and desorption behaviour of plasmid DNA on ion-exchange membranes-Effect of salt valence and compaction agents**; *Journal of Chromatography A*, 1036, 73-78.
45. Theodossiou, I. and Thomas, O.R.T.; 2002; **DNA-induced inter-particle cross-linking during expanded bed adsorption chromatography: impact on future support design**; *Journal of Chromatography A*, 971, 73-86.
46. Theodossiou, I.; Elsner, H.D.; Thomas, O.R.T. and Hobley T.J.; 2002; **Fluidisation and dispersion behaviour of small high density pellicular expanded bed adsorbents**; *Journal of Chromatography A*, 964, 77-89.
47. Theodossiou, I.; Olander, M.A.; Soendergaard, M. and Thomas, O.R.T.; 2000; **New expanded bed adsorbents for the recovery of DNA**; *Biotechnology Letters*, 22(24), 1929-1933.
48. Theodossiou, I.; Soendergaard, M. and Thomas, O.R.T.; 2001; **Design of expanded bed supports for the recovery of plasmid DNA by anion exchange adsorption**; *Bioseparation*, 10(3), 31-44.

49. Thömmes, J.; 1997; **Fluidized Bed Adsorption as a Primary Recovery Step in Protein Purification**; *Advances in Biochemical Engineering /Biotechnology*, 58, 185-230.
50. Thömmes, J.; Weiher, M.; Karau, A. and Kula M.R.; 1995; **Hydrodynamics and performance in fluidized bed adsorption**; *Biotechnology and Bioengineering*, 48, 367-374.
51. Tyn, M.T. and Gusek, T.W.; 1990; **Prediction of diffusion coefficients of proteins**; *Biotechnology and Bioengineering*, 35(4), 327-338.
52. Vergnault, H.; Mercier-Bonin and Willemot, R.M.; 2004; **Physicochemical parameters involved in the interaction of *Saccharomyces cerevisiae* cells with ion-exchange adsorbents in expanded bed chromatography**; *Biotechnology Progress*, 20, 1534-1542.
53. Viloria-Cols, M.E.; Hatti-Kaul, R. and Mattiasson, B.; 2004; **Agarose-Coated Anion Exchanger Prevents Cell-Adsorbent Interactions**; *Journal of Chromatography A*, 1043(2), 195-200.
54. Vogel, A.I.; 1989; ***Vogel's textbook of chemistry and physics***; 5th edition, CRC Press, Inc. Boca Raton, Florida, USA.
55. Voute, N. and Boschetti, E.; 1999; **Highly dense beaded sorbents suitable for fluidized bed applications**; *Bioseparation*, 8, 115-120.
56. Voute, N.; Bataille, D.; Girot, P. and Boschetti, E.; 1999; **Characterization of very dense mineral oxide-gel composites for fluidized-bed adsorption of biomolecules**; *Bioseparation*, 8, 121-129.
57. Yun, J.; Lin, D.Q. and Yao, S.J.; 2005; **Predictive modeling of protein adsorption along the bed height by taking into account the axial non-uniform liquid dispersion and particle classification in expanded beds**; *Journal of Chromatography A*, 1095(1-2), 16-26.

4 Surface plasma modification: a means of preparing expanded bed adsorption beads with reduced surface binding

Arpanaei, Ayyoob[1]; *Hobley, Timothy John[1]; Thomas, Owen R.J.[2,1]; **Winther-Jensen, Bjørn[3]; ***Kingshott, Peter[3]; West, Keld[3]

[1]Center for Microbial Biotechnology, Building 223, BioCentrum-DTU, Technical University of Denmark, 2800-Kgs. Lyngby, Denmark

[2]Department of Chemical Engineering, University of Birmingham, Edgbaston, B15 2TT, UK

[3]The Danish Polymer Centre, Risø National Laboratory, DK-4000, Denmark

*Author for correspondence: Timothy J. Hobley, Center for Microbial Biotechnology, BioCentrum-DTU, Technical University of Denmark, Building 223, Søltofts Plads, DK-2800-Kgs. Lyngby, Denmark (Tel: +45 4525 2706, Fax: +45 4588 4148; E-mail: th@biocentrum.dtu.dk)

**Present address: Department of Material Engineering, Monash University, Clayton, 3800-Victoria, Australia

***Present address: iNANO, Faculty of Science, Building 1521, Ny Munkegade, The University of Århus, 8000-Århus C, Denmark

Abstract

Low temperature glow discharge plasma was used to prepare multifunctional beads with non-adsorptive surfaces for expanded bed adsorption chromatography. Q HyperZ beads, were employed and a nano-scale thin hydrophilic neutral layer was constructed on the surface by plasma etching and oxidation or coating with plasma-polymerized layers. Light microscopy, electron scanning microscopy and X-ray photoelectron spectroscopy revealed that plasma treatment did not have any destructive effect on the surface morphology or the structure of the beads. Batch binding tests with bovine serum albumin (BSA) and homogenized calf thymus DNA showed that the beads obtained by plasma etching and oxidation of the surface or by coating with plasma-polymerized vinyl acetate had better performance than those coated with plasma-polymerized vinyl pyrrolidinone or safrole. Examination of the binding kinetics during the first few minutes of reaction showed that the adsorption of homogenized calf thymus DNA and plasmid DNA by the treated beads was affected much more than BSA binding as compared to untreated ones. Expanded bed adsorption (EBA) tests were conducted in a 1-cm diameter EBA column and the dynamic DNA binding capacities of plasma-treated adsorbent beads at 10% breakthrough (1.29 and 2.45 mg applied DNA.mL gel^{-1} for surface-etched and plasma-polymerized vinyl acetate coated adsorbent beads, respectively) were much less than for untreated ones (6.92 mg applied DNA.mL gel^{-1}). Contraction of the bed during DNA loading was also reduced markedly by using the treated beads. The plasma-treated adsorbents had no significant change in BSA binding capacity during EBA as compared to that for untreated adsorbents and in both cases, the dynamic binding capacities were ~34 mg BSA.mL gel^{-1} at 10% breakthrough. These results suggest that plasma treatment can be used as an efficient method for the preparation of EBA beads with non-adsorptive surfaces.

***Keywords*:** Plasma surface modification, Chromatography, Non-adsorptive surface, Adsorbent cross-linking, Surface etching and oxidation, Graft polymerization

Introduction

In general, downstream processing accounts for a major part of the total production costs for biological products, especially biopharmaceuticals. Moreover, a significant part of the costs for biopharmaceutical production arises from the chromatography steps which are frequently used in such processes (Gupta and Mattiasson, 1994). Integrating or combining different steps in downstream processing of bioproducts can potentially lead to higher yields as well as lower capital and operating costs (Schuger and Hubbuch, 2005). In the early 1990s expanded bed adsorption (EBA) was developed to achieve such an objective (Draeger and Chase, 1991). EBA is a type of stabilized fluidized bed chromatography that was originally conceived to be compatible with crude bio-feedstocks containing a mixture of insoluble and soluble biological molecules e.g. proteins, genomic DNA fragments, RNA molecules and cell debris, (Draeger and Chase, 1991; Thömmes, 1997; and Anspach et al., 1999). The original inventors hoped that EBA would be a generic solution for combining solid-liquid separation and primary product capture, since in theory, crude substances (particulates) can pass through the fluidised bed without causing blockage (Draeger and Chase, 1991; Thömmes, 1997; Hjorth et al., 1998; and Anspach et al., 1999). Subsequently a number of reports showed that all or part of the clarification, concentration and initial purification steps for a biological product can be combined and integrated into one single unit operation by using this system (Hansson et al., 1994; Chang et al., 1995; Strætkvern et al., 1999; Fahrner et al., 1999; Ezequiel et al., 1999; Beck et al., 1999; Clemmitt and Chase, 2000; Ohashi et al., 2002; Gonzalez et al., 2003; Brixius et al., 2005; Jin et al., 2005; Chang et al., 2006; and Jahic et al., 2006). Despite commercialization of the technology by Pharmacia (now GE Healthcare), the technology was quickly found to have a critical problem, namely that for the vast majority of

process streams, the hydrodynamic properties of EBA were fatally compromised. This condition arose either from column distributor blockage or cross-linking of the fluidized adsorbent beads by crude substances (particulates) in the feed (Feuser et al., 1999a and 1999b; Lin et al., 2003a and 2004). A solution to distributor blockage has recently been proposed (Hubbuch et al., 2002) and commercialized.

Bead cross-linking in EBA is most severe with anion-exchangers and led to the working hypothesis that negatively charged cells, large debris or DNA strands were able to attach to more than one adsorbent bead (Thömmes, 1997 and Theodossiou et al., 2001 and 2002). A mechanism for cross-linking was hypothesized similar to flocculation (Theodossiou and Thomas, 2002), after developing new prototype pellicular adsorbents of small size (Olander et al., 2000 and Theodossiou et al., 2000 and 2001). These new adsorbents were designed for the purification of plasmid DNA. However, results showed that aggregation of the adsorbent beads inhibits the ability of EBA to purify plasmid DNA. In order to relieve the problem of bead cross-linking in EBA systems, a pragmatic approach was taken where methods were proposed to search for broth conditions (i.e. pH and conductivity) under which interaction of the crude substances (particulates) with the adsorbent beads were minimized (Lin et al., 2001). Another proposed approach was simply to break all particulates, debris or DNA into such small pieces that they could not bind to more than one bead (Lin et al., 2003b and Hubbuch et al., 2006). These solutions were only partially successful since they did not address the root of the problem, which was proposed to be that the outer surface of the adsorbents were populated with active sites, which bound both the product of interest and crude material causing cross-linking and thus breakdown of the hydrodynamic properties essential for EBA. Furthermore, applying the above broth conditioning approaches usually led to loss of capacity of the adsorbents or of compromised chromatographic properties.

In light of the above it can be seen that in order to inhibit binding of particulates to EBA bead surfaces and also prevent cross-linking of the adsorbents, ligands exposed on the surface must be either eliminated or covered, without hindering access to, or damaging the ligands within the adsorbent beads, which bind the protein of interest. Three strategies have recently been applied to prepare non-adsorptive surface beads for chromatography or EBA: i) coating or shielding adsorbent beads by polyelectrolytes (Dainiak et al., 2002a and 2002b); ii) coating or shielding adsorbent beads with a layer of an inert (non-ionic) polymer (Viloria-Cols et al., 2004; and Senthuran et al., 2004); and iii) using adsorbent beads which have been constructed in such a way that no ligands exist in their outer layers (2-3 μm deep) (lid particles) (Kepka et al., 2004; and Gustavsson et al., 2004). These approaches attempt to combine two functionalities in one: namely adsorption of proteins and size exclusion of large particulates. By using such an approach the selectivity of the adsorptive method is increased. This allows the EBA system to exploit its potential and to act as a multifunctional system. Nevertheless, the above approaches to design of new EBA beads seem to be problematic. Shielding adsorbent beads with an electrolyte polymer could lead to unspecific adsorption, because electrolytes are charged. Furthermore, the reusability of such shielded beads is questionable. Coating adsorbents with a layer of agarose or other gel-forming polymers (i.e. the second approach above) is problematic since any inert layer must be ultra thin in order not to decrease mass transfer (molecular diffusion) of protein into the particle interior where the ligands for binding are situated. Intra-particle mass transfer has been shown as the main parameter affecting dynamic capacity of an EBA support (Kaczmarski and Bellot, 2004 and Yun et al., 2005). The coating layers obtained by using the second strategy have been too thick (with a diameter of a few microns) and it is expected they ca not meet this condition. This has limited the application of such coated adsorbent beads only to the processes in which

very small molecules (e.g. organic acids) are target molecules (Galaev et al., 2002). The same problem of mass transfer limitations can be predicted for the 'lid' beads since controlling the chemical methods used, which involve either selective ligand elimination from the surface, or removing functional groups prior to ligand coupling is extremely difficult. Over-reaction is likely to be difficult to avoid, leading to a deep layer around the adsorbent devoid of ligand and thus a long diffusion path length before the product reaches the ligands for binding. The conclusion therefore is that the ligand devoid layer must be on the nano-scale. Furthermore, the method used to generate the layer should be generic for different types of EBA or chromatography adsorbent beads and allow a wide range of surface modifications. Plasma irradiation technology would seem to have potential to meet these requirements.

Plasma treatment is one of the methods (including plasma, corona discharge, photo activation (UV), laser, ion beam, electron beam and gamma radiation) which have widely been used for a variety of surface modifications (Liston et al., 1993; Fisher, 2002; and Chu et al., 2002). Plasma is defined as a partially or wholly ionized medium consisting of electrons, ions and possibly neutrals and photons, which also meets additional criteria (see e.g. Fisher, 2002). To conduct a surface modification by plasma, a glow discharge is created in an evacuated vessel refilled by a low pressure gas, since increasing the pressure leads to increased temperature. Then radio frequency (RF), microwave (MW), alternating current (AC), or direct current (DC) is used to energize the gas. Surfaces in contact with plasma will be bombarded by energetic species (e.g. ions, electrons, radicals), which transfer energy to the surface causing chemical and physical reactions. For example, during an oxygen plasma treatment, the exposed surface is oxidized and atoms and chemical groups existing on the surface will be replaced by hydroxyl and carbonyl groups (Hollahan and Carlson, 1970; Yamamoto et al., 1984; Boenig, 1988 and Inagaki et al., 1991). Removing molecular or

atomic layers on the surface can also be conducted by using plasma etching (Schram et al., 1987). The main advantages of plasma treatment of surfaces are: i) low temperature reactions, ii) changes occur to the chemical structure of the surface in a shallow nano-scale layer with no change to the bulk properties, iii) a very wide range of surface modifications are possible, and iv) low amounts of toxic by-products are formed during the treatment (Schram et al., 1987).

Plasma technology has been widely used for coating surfaces to make them resistant to bioadhesion and thus anti-biofouling for a variety of very different applications (Ulbricht and Belfort, 1995; Kingshott and Griesser, 1999; McArthur et al., 2000; and Kingshott et al., 2002). This has been performed by both surface coating by graft polymerization or polymer deposition in the presence of plasma with or without concurrent surface activation by oxygen, nitrogen or ammonia via plasma treatment. Changing the characteristics of the surface of different moieties including particles in order to convert a hydrophobic surface to a hydrophilic one or vice versa is another application of plasma technology. For example, argon and oxygen plasma have been used to improve the surface characteristics of silica gel beads for adsorption of water vapor (Tao et al., 2004). The main reason for this improvement has been attributed to the surface oxidation, the introduction of polar groups (e.g. hydroxyl groups) and increase of surface roughness (Lai et al., 1996).

Plasma technology has also been used in the fabrication of restricted access media and materials for analytical chromatography supports and packings. These packing materials consist of two parts; (i) an internal active region for binding of metabolites which is not accessible for macromolecules like proteins and (ii) an inert outer layer or barrier. By using columns packed by restricted access media, there is no need to use an off-line pretreatment of biological sample to remove proteins and macromolecules that adhere to the packing materials causing fouling (Souverain et al., 2004). For construction of such packings, plasma

is generally used to activate the surface, which is then coated by grafting a polymer which has negligible nonspecific adsorption of macromolecules. For example, octadecylsilylated silica gel beads were treated by oxygen plasma to produce silanol groups on the beads surface. Then, the silanol groups were chemically silylated to give restricted access media (Sudo et al., 1998).

In this paper, we have investigated whether plasma can be used to create a new generation of restricted access EBA beads with ultra-thin ligand devoid layers. As a model system we have chosen to apply plasma treatment to the commercial strong anion exchanger Q HyperZ, which has a robust ceramic skeleton and polymer filling with quaternary amine groups (Voute and Boschetti, 1999; Vergnault et al., 2004 and Cabanne et al., 2004).

Materials and methods

Materials

The anion exchange EBA adsorbent Q HyperZ was obtained from BioSepra (now PALL). All chemicals including calf thymus DNA, bovine serum albumin, safrole, vinyl pyrrolidinone and vinyl acetate were purchased from Sigma-Aldrich and were of analytical grade.

Plasma reactor

A home-made reactor was used and the experimental set up is shown in Figure 1. The plasma condition was created in a horizontal chamber made from Pyrex (40 mm × 250 mm) and a copper/nylon paper was coated on the outside to act as one electrode. A stainless steel

bar was used as the second electrode and was centered in the middle of plasma chamber (Figure 1). The plasma chamber was rotated at a rate of 10-30 rpm during the treatment to ensure complete exposure of the surface of the beads to the plasma. An electrical field was created within the chamber by using a 20 KHz AC generator powered by a standard 0-240V vario transformer.

Plasma treatment

Surface etching and oxidation

In this procedure ligands are removed from the surface when oxygen atoms become excited and lead to formation of hydroxyl and carbonyl groups on the surface of the beads. The rotating plasma reactor shown in Figure 1 was used and 5-8 grams of Q HyperZ beads were added within the plasma chamber. The air inside the chamber was removed using a vacuum pump to reduce the pressure to below 10 Pa. Reduced pressure within the chamber, is needed for a low temperature/pressure glow discharge plasma treatment and has the side effect of vaporizing the water within the beads. The pressure inside the plasma chamber was then increased by opening the oxidation gas (e.g. air or oxygen or water) valve (valve 2) and the pressure adjusted to the desired value (e.g. 10 Pa). Reactor rotation was started with a low rate (e.g. 10-30 rpm), the electrodes were connected and plasma was sustained by applying an electric potential of 220 volts (corresponding to 35.8 $W.L^{-1}$ power applied per volume) and a frequency of 20 MHz. A visible radiation showed that plasma was being generated. After treatment for 2-3 h, the tumbling was stopped, power turned off, electrodes disconnected and gas evacuation was ceased. Valve 2 was opened to allow the pressure to rise to atmospheric pressure. Then, the chamber was opened and the treated beads were taken out. Equipment in contact with reactive materials was cleaned before the next batch was treated. Beads were

washed with water, 0.1 M NaOH, 0.1 M HCl, 20% v/v ethanol solutions and again with water. Then, they were immersed in 50 mM Tris-HCl buffer pH 8 overnight before use.

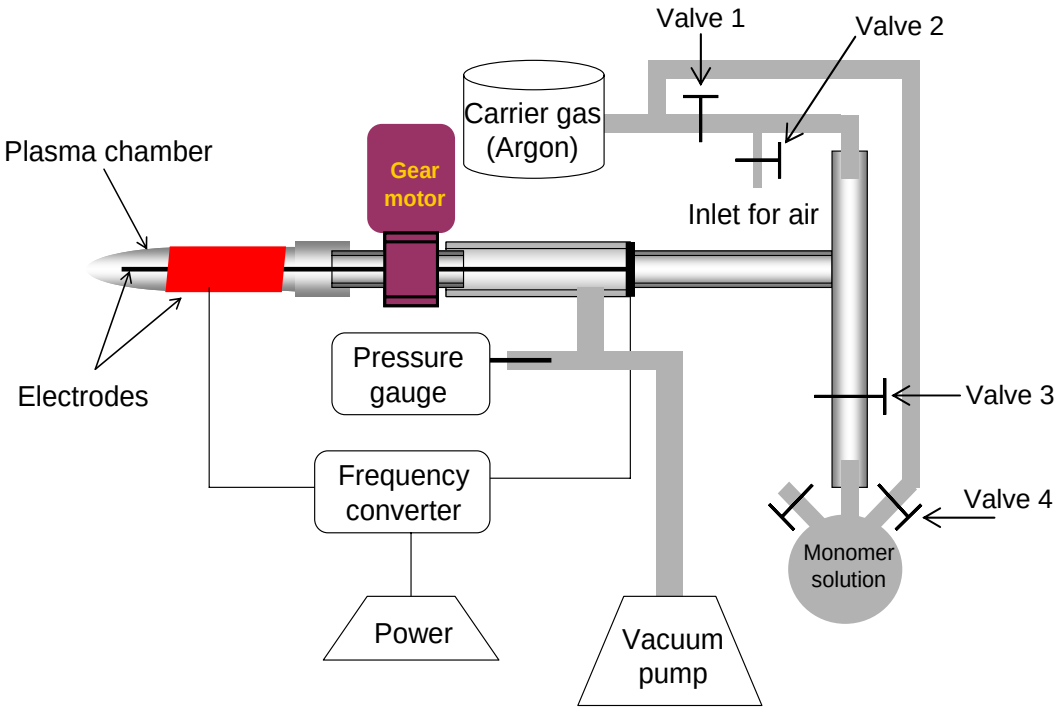

***Figure 1*: Schematic diagram of the experimental apparatus used for plasma treatment of Q HyperZ beads.**

Coating beads by surface graft polymerization

The procedure was initially the same as described above, namely that the rotating plasma reactor shown in Figure 1 was used and 5-8 grams of Q HyperZ beads were added within the plasma chamber. The air inside the chamber was removed using a vacuum pump to reduce the pressure to below 10 Pa. However, in this treatment, the solution containing monomer as well as a carrier gas reservoirs were connected to the plasma chamber. After lowering the pressure to a value slightly less than that desired (e.g. 10 Pa), valves 4 and 1 (Figure 1) were opened to evacuate gas within all connecting lines. Once the pressure started decreasing, valve 3 was opened completely. When the pressure once again started decreasing,

valve 3 was closed to avoid losing the active compound (i.e. the monomer to be used during coating). Then, the carrier gas (argon) was started to flow into the active compound reservoir. In the next step, valve 3 was opened very slowly to achieve the desired pressure (e.g. 15-20 Pa) and flow rate of carrier gas (5 $mL.min^{-1}$) in the reactor. Reactor rotation was started and then power was connected at the voltages mentioned in the text. Once treatment was finished, the carrier gas flow was first stopped and then valve 4 and 3 were closed. The beads were collected and washed as described above. The monomers, vinyl pyrrolidinone, vinyl acetate and safrole (Figure 2) were used and the treatment time varied from 0.5, 1, 2 or 3 hours depending on the monomer type.

Vinyl pyrrolidinone:

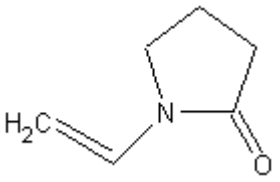

Vinyl acetate: **$CH_3COOCH=CH_2$**

Safrole:

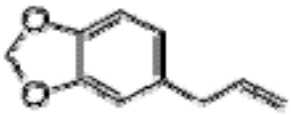

***Figure 2*: Chemical structures of the monomers used for graft polymerization with plasma.**

Testing plasma-treated beads

Study of the structure and surface of the beads

Light microscopy (LM) of the beads was performed with a Nikon Optiphot microscope (Nikon, Melville, NY, USA) fitted with a Kappa CF-8/1 FMC monochrome video camera (Kappa Opto-electronics GmbH, Gleichen, Germany) and digitized images and average size measurements were produced with the aid of Image-Pro® Plus software (version 4.1 for Windows™; Media Cybernetics, Silver Spring, MD, USA).

The surface topography of the beads was monitored with scanning electron microscopy (SEM; DSM-960, Zeiss). Before the SEM imaging, the samples were coated with a thin layer of palladium/gold to minimize the charging effect and increase the image contrast. The elemental composition of the surface was studied by x-ray photo electron spectroscopy (XPS). XPS was performed using a SPECS Sage 100 instrument (Specs, Berlin, Germany) using a non-monochromatic MgK_a X-ray source at a power of 275 Watts (11 keV and 25 mA). The pressure in the chamber was always below 1 x 10^{-7} mbar. The elements were identified and quantified from survey spectra, acquired at 100 eV pass energy in the range from 0 to 1100 eV. The samples were mounted on the holder using by use of double-side sticky tape. XPS data was used for the evaluation of the surface changes after a plasma treatment and in particular to determine if plasma treatment has been able to coat or eliminate active groups (ligands), e.g. quaternary amine groups from the surface.

Preparation of DNA feedstocks for batch binding tests

Calf thymus DNA was dissolved slowly overnight in 50 mM Tris-HCl, pH 8, to give a 2 $mg.mL^{-1}$ solution and then sonicated on ice with an MSE soniprep 150 (MSE Scientific Instruments Ltd., Sussex, UK). Then, the solution was centrifuged at 20000×g in the SS-34 rotor of a SORVAL RC5C laboratory centrifuge for 30 minutes at 4 ^{o}C. The sonicated DNA (0.5-10 kbp) in the supernatant was portioned into sterile tubes and stored at -20 ^{o}C.

In order to prepare stock solutions of pUG6 (4.009 kbp plasmid), *Escherichia coli* DH5á cells containing pUG6 (Guldener et al., 1996) was grown in Luria Bertani (LB) medium (Tryptone 10 $mg.mL^{-1}$, Yeast extract $mg.mL^{-1}$ and NaCl 10 $mg.mL^{-1}$) containing 100 $\mu g.mL^{-1}$ ampicillin in a 5-L batch fermentor. The biomass was harvested after ~20 hours when the dry weight had reached ~10 $mg.mL^{-1}$ by centrifugation for 30 min at 4 ^{o}C at 10000×g in the SLA 3000 rotor of a SORVAL RC5C centrifuge. The cell paste was then washed by

resuspension in 50 mM Tris-HCl pH 8 buffer before recentrifuging at 10000×g. The cell paste was stored at -20 ^{o}C. A QIAGEN kit (QIAGEN Sciences, Maryland, USA) was used for the purification of the plasmid using the protocol described by the manufacturers.

Protein and DNA batch binding tests

The capacity of the plasma treated Q HyperZ adsorbent beads was tested in batch binding studies using bovine serum albumin (BSA) and homogenized calf thymus DNA. Untreated or plasma-treated Q HyperZ beads (0.1 mL) were equilibrated in 50 mM Tris-HCl pH8 buffer then incubated in 4 mL BSA solution (4 mg.mL^{-1}) or 1.5 mL DNA solution (1.5 mg.mL^{-1}) prepared in equilibration buffer. Either 2 or 30 minutes was used for binding, with shaking on an orbital shaker (Infors, Basel, Switzerland). The beads were then settled by a short (30 s) centrifugation at 2000×g in a microfuge (Biofuge *pico*, HAEREUS Instruments, Osterode, Germany), the supernatant collected and analysed at 280 or 260 nm in a Lambda 20 UV-Vis spectrophotometer (Perkin-Elmer Analytical Instrument, Shelton, CT, USA) for BSA and DNA, respectively.

The kinetics of adsorption of the plasmid pUG6, sonicated calf thymus DNA and BSA to the plasma-treated and untreated adsorbent beads were studied batch wise as described above, with the following exceptions. For each time point in all tests, 0.1 mL of adsorbent beads was used and the initial concentrations of BSA (5 mL), plasmid DNA (2.5 mL) and homogenized calf thymus DNA (2.5 mL) solutions were 3.2, 0.7 and 1 mg.mL^{-1}, respectively.

Evaluation of the plasma-treated beads performance in an EBA system

A 1-cm diameter EBA column (UpFront Chromatography A/S, Copenhagen, Denmark) with ~5 cm settled bed height, i.e. ~4 mL Q HyperZ adsorbent was used. The expanded bed column was connected to a FPLC system equipped with a peristaltic pump, flow through UV detector (260 or 280 nm) and fraction collector (Pharmacia Biotech,

Uppsala, Sweden). The column was equilibrated with > 50 column volumes (CV) of 50 mM Tris-HCl pH 8 buffer containing 100 mM NaCl. The feedstock was loaded at a superficial flow velocity of 350±20 $cm.h^{-1}$ or 308±10 $cm.h^{-1}$ which gave two fold expansion of the bed for untreated and plasma-treated beads, respectively. During loading the bed height was recorded and fractions were collected, which were analysed at 280 or 260 nm in a Lambda 20 UV-Vis spectrophotometer (Perkin-Elmer Analytical Instrument, Shelton, CT, USA) for BSA and DNA, respectively. Washing and elution of the bed was not examined and the beads were not reused. The feedstock was 1 $mg.mL^{-1}$ BSA or 0.06 $mg.mL^{-1}$ DNA (either homogenized calf thymus or plasmid) solution in 50 mM Tris-HCl, pH 8 buffer containing 100 mM NaCl (conductivity ~11 $mS.cm^{-1}$).

The voidage (ε) corresponding to the expanded bed height (H) at each time point was calculated by using following equation (Anspach et al., 1999):

$$\frac{H}{H_0} = \frac{1-\varepsilon_0}{1-\varepsilon} \qquad (1)$$

Here, H_0 and ε_0 are the height and voidage of the settled bed, respectively. A value of 0.4 was assumed for ε_0. The ratio between voidage at each time to the initial voidage (before starting loading feed) ($\varepsilon/\varepsilon_i$) was used to study the bed contraction profile.

Results and discussion

Strategies applied for plasma treatment

The commercial EBA adsorbent Q HyperZ was chosen for this work as it has a rigid ceramic skeleton that can be expected to maintain the shape and protect the ligand containing gel inside from potential abrasion in the plasma reactor, and the effects of dehydration in the

low pressure atmosphere used. Two strategies were employed to provide a multifunctional adsorbent devoid of ligands on the surface (Figure 3). Plasma technology was used to either: (i) shave off only those ligands located on the surface of the adsorbent beads (surface etching and oxidation), or (ii) to cover the ligands by coating adsorbent beads with a nano-scale polymer layer (surface graft polymerization). The monomer type and treatment time were chosen based on our previous experience and some preliminary tests (data not shown). The plasma treatments used and the beads obtained in each case are summarized in Table 1.

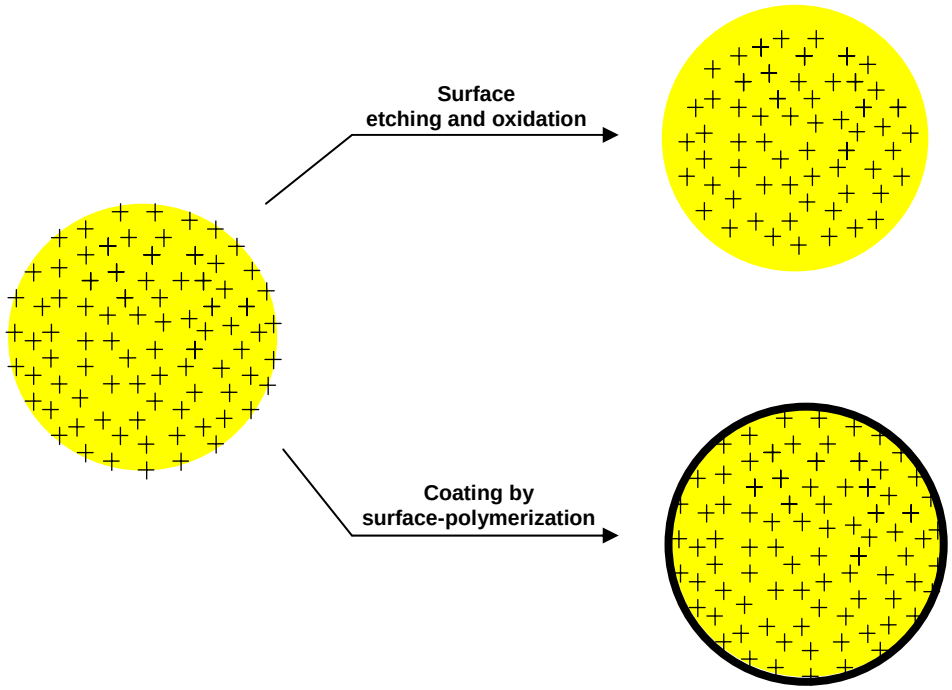

***Figure 3*: Strategies applied for plasma surface modification of adsorbent beads. Here '+' represents the quaternary amine ligand distributed on the surface and throughout the adsorbent.**

***Table 1*: Conditions used in the plasma treatment of Q HyperZ adsorbents.**

Bead name	Type of treatment	Monomer	Treatment time (hour)	Voltage (v)	Power per volume ($W.L^{-1}$)	Pressure (Pa)
Et220-2	Etching and oxidation by air plasma	-	2	220	35.8	10
Et220-3	Etching and oxidation by air plasma	-	3	220	35.8	10
VP100	Coating by plasma polymerization	Vinyl pyrrolidinone	1	100	7.4	15-20
VP140	Coating by plasma polymerization	Vinyl pyrrolidinone	1	140	9	15-20
VA170-2	Coating by plasma polymerization	Vinyl acetate	2	170	16.5	15-20
VA170-3	Coating by plasma polymerization	Vinyl acetate	3	170	16.5	15-20
SA130	Coating by plasma polymerization	Safrole	0.5	130	8.2	15-20

Characterization of plasma treated beads

Physical structure

Light microscopy images showed no difference between untreated beads (Figure 4a), surface-etched beads (Et220-3) (Figure 4b) and surface-coated beads (VA170-3) (Figure 4c). The diameters of at least 800 beads of each type were measured using light microscopy and the average diameters were 73.3, 72.2 and 73.2 micron for the untreated, surface-etched (Et220-3) and surface-coated (VA170-3) beads, respectively. Furthermore, there was no

evidence of fines or broken beads seen. The results imply that plasma treatment is a mild process and does not affect the size or shape of the beads. SEM images of untreated, Et220-3 and VA170-3 beads are shown in Figure 5 and no differences between the adsorbents can be discerned.

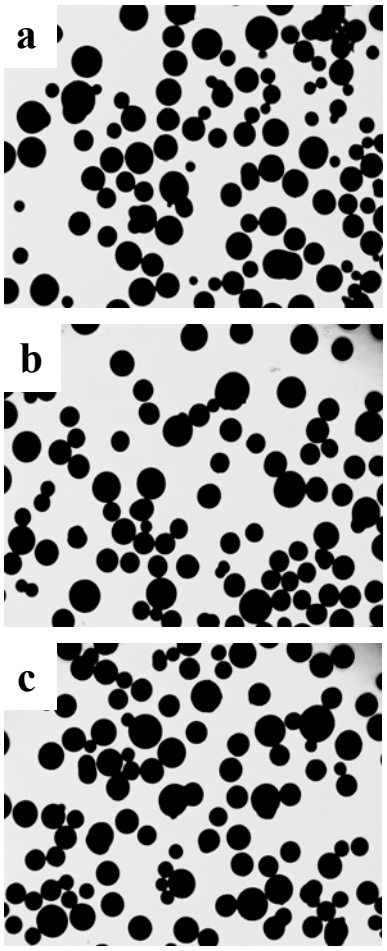

***Figure 4*: Light microscopy images of unmodified (a), surface-etched (b) and surface-coated (c) Q HyperZ beads.**

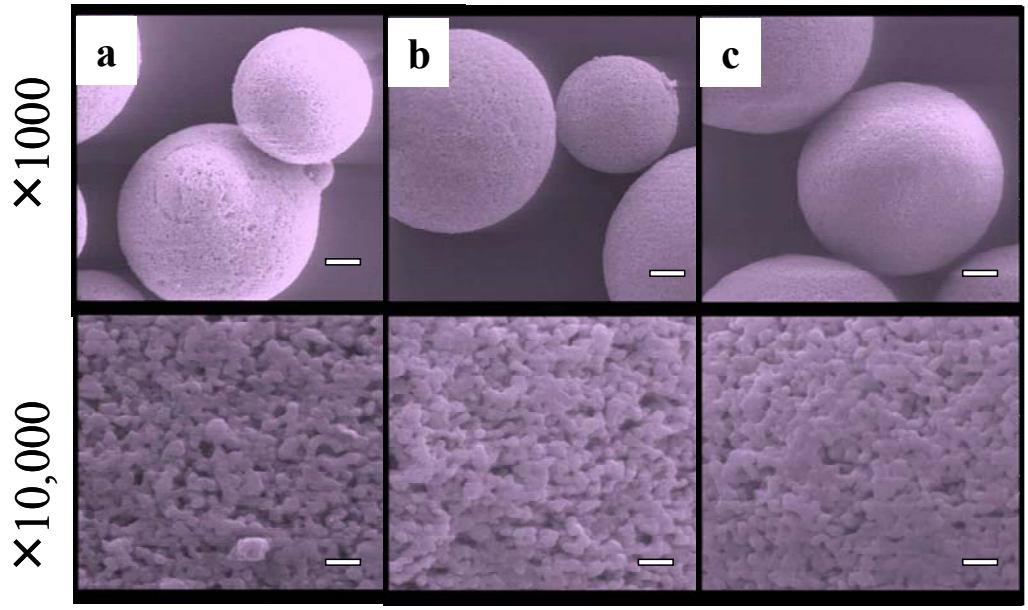

***Figure 5*: SEM images of unmodified (a), surface-etched (b) and surface-coated (c) Q HyperZ beads, with magnification of 1000 (top) and 10000 (bottom). The bar represents a size of 10 µm (top) or 1 µm (bottom).**

Elemental analysis of the adsorbent surface by XPS

The Q HyperZ bead is a composite material consisting of a porous core made from yttrium-stabilized zirconium oxide filled and coated with a gel material synthesized through polymerization of methacryloylaminopropyl-trimethylammonium, as functionalized monomer and N,N' methyl bis methacrylamide (a bifunctional acrylic monomer), as cross-linker (Voute and Boschetti, 1999). A successful plasma treatment can be expected to lead to a change in the elemental composition of the surface, which was analyzed by using x-ray photo electron spectroscopy (XPS) and the results are shown in Table 2. After ligand shaving by air/oxygen plasma etching (beads Et220-2 and Et220-3) it was found that the amount of nitrogen on the surface decreased to an undetectable level (Table 2). This implies that the quaternary amine ligands were efficiently removed by the treatment. The percentage of oxygen increased for these beads (Et220-2 and Et220-3) due to oxidation of the surface, a result that is in agreement

with what was observed by Kim et al. (1998) through their investigation on the effect of the oxygen plasma treatment on SiO_2 aerogel film. Changing the treatment time from 2 hours to 3 hours did not affect the surface composition significantly (Table 2).

***Table 2*: Data obtained from XPS analysis of the surface of untreated and plasma-treated beads.**

Bead name	Carbon%	Oxygen%	Nitrogen%	Zirconium %	Yttrium%
Untreated	45.9	33.3	5.1	14.1	1.5
Et220-2	20.2	58.3	ND*	17.9	3.6
Et220-3	30.3	50.1	ND*	17.0	2.5
VP100	63.6	20.9	10.0	4.9	0.6
VP140	70.3	17.0	11.6	1.0	ND*
VA170-2	58.6	30.4	5.7	4.6	0.7
VA170-3	64.3	28.8	3.2	2.4	0.3
SA130	74.4	22.2	1.3	1.7	0.4

***ND: Not detected**

Treatment of the beads with plasma and the all of the different monomers led to a large increase in the percentage of carbon and a decrease in zirconium on the beads (Table 2) indicating that coating of the surface had occurred. The SA130 beads had less surface nitrogen than the VA170 types suggesting more efficient coating with safrole occurred than vinyl acetate. The VP100 and VP140 beads had an increased percentage of nitrogen on the surface compared to the untreated types, however this result does not provide direct evidence that the quaternary amine ligands have been covered due to this fact that vinyl pyrrolidinone contains nitrogen, but does suggest that a modification to the surface has occurred. Increasing the voltage/power during treatment led to better coating as shown by a decrease in the

percentages of zirconium and yttrium on the surface of VP140 beads compared to VP100. Moreover, the XPS data for zirconium and yttrium suggest that the VP140 beads have been coated more efficiently than beads coated by vinyl acetate (VA170) and safrole (SA130). Increasing the treatment time from 2 to 3 hours also led to a more efficient coating treatment as shown by the change in the percentages of carbon, nitrogen, zirconium and yttrium for the VA170-2 compared to VA170-3 beads.

Binding characteristics of plasma modified beads

The results presented above show that the outer structure of the adsorbents has not been damaged by the treatments, and that there has been a change in the surface chemistry, indicating that new groups containing oxygen (e.g. hydroxyl and carbonyl) for surface-etched beads or polymers for surface-coated beads have been attached. Studies to characterize the protein and DNA binding properties of the adsorbents under the conditions to be used in EBA were thus examined. In all cases the beads were equilibrated in binding buffer (50 mM Tris-HCl pH 8) over night. It was observed that the adsorbents treated by safrole agglomerated in the buffer solution suggesting a hydrophobic interaction between the beads. This is consistent with the hydrophobic nature of the polymer layer formed using the safrole monomer (Figure 2), however aggregation is not a suitable trait for an EBA adsorbent. In contrast, none of the other beads (Table 1) were observed to self-agglomerate in solution.

To examine the effects of the different treatments on protein and DNA binding, the different modified EBA beads were reacted with BSA or calf thymus DNA and the supernatants collected and analysed. The results in Figure 6 show that the Et220-3 beads had the most promising performance, with the largest reduction in DNA binding after 2 or 30 minutes as compared to the other bead types. Furthermore the reduction in BSA binding for the Et220-3 was less than that observed for the VA170-3 and the SA-130 types. Excluding the

SA130 beads, which had an unwanted propensity for aggregation, the VA170 adsorbents showed the next best reduction in capacity for DNA binding.

The results above suggest that the Et220-3 and VA170-3 adsorbents had the most potential for yielding a high capacity protein binding adsorbent with reduced DNA induced cross-linking. Thus these adsorbents were used in further studies to examine the kinetics of protein and DNA binding. When the calf thymus DNA binding kinetics were examined, the results in Figure 7 showed that equilibrium was essentially reached after ca. 15 minutes (Figure 7a) for all three bead types, but that the capacity (Figure 7b) and the kinetics were lower for the Et220-3 than the VA170-3 and both were lower than the unmodified beads. In particular Figure 7b shows that there was a large amount of DNA (2 $mg.mL^{-1}$ beads) bound to the unmodified adsorbents within 30 s which was not seen for the Et220-3 type. When binding of plasmid DNA to the three bead types was examined (Figures 7c and 7d), a similar pattern was observed to that for calf thymus DNA (Figure 7a and 7b). However in this case although a very large amount of DNA (~2.5 $mg.mL^{-1}$ beads) was bound to the unmodified adsorbents within 30 s, only a small amount of further adsorption occurred (Figure 7a and 7b) compared to that seen with calf thymus DNA. Much less plasmid binding occurred to the VA170-3 and Et220-3 adsorbents within 30 s than to the unmodified type, however binding continued until 30-45 minutes had elapsed when equilibrium was reached. Nevertheless, the plasmid binding capacities at equilibrium were less than half of those for calf thymus DNA.

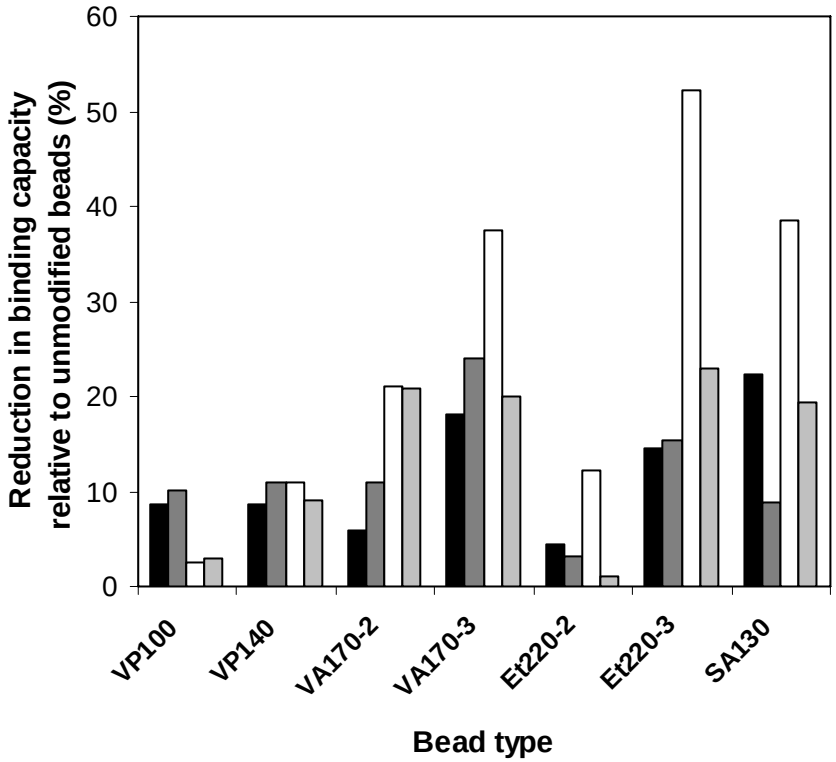

***Figure 6*: Reduction in binding capacity for surface-coated and surface-etched beads expressed as a percentage of the capacity of untreated Q hyper Z adsorbents. Batch biding tests with BSA for 2 (black bar) and 30 (dark grey bar) minutes, and homogenized calf thymus DNA for 2 (white bar) or 30 (light grey bar) minutes.**

Kinetics of protein, homogenized calf thymus DNA and plasmid DNA adsorption

The results suggest that binding of sonicated calf thymus DNA to the Et220-3 (surface-etched) adsorbents is much slower than that of plasmid DNA (Figures 7a and 7b). This could be due to the non-uniformity of size of the pieces of calf thymus DNA formed during the sonication procedure. Sonicated calf thymus DNA contains a smear of fragments with a molecular size range of ~0.5-10 kbp when analysed by agarose gel electrophoresis (results not shown). In contrast the plasmid DNA is a discrete size of ~4 kbp. It is thus speculated that large molecules of plasmid or calf thymus DNA have no accessibility to the ligands located inside the adsorbent gel and thus only interact with the outer surface. However

very small DNA molecules produced during sonication might possibly diffuse slowly to a small extent into the pores, accounting for the extended time to reach equilibration as seen in Figure 7b as compared to Figure 7d.

When the time course of BSA binding was examined the results for the modified adsorbents were the same as for the unmodified types after the first 30 s, at which time ~27 mg BSA.mL^{-1} beads had bound (Figure 7e and 7f). For the unmodified types, equilibrium (70 mg.mL^{-1}) was reached after 10 minutes, whereas for both the modified adsorbents binding continued for at least 60 minutes, at which time the capacity for the VA170-3 and Et220-3 was ~80 and 90%, respectively, of that for the unmodified beads.

The data at each time point in Figures 7b, 7d and 7f was used to calculate the reduction in binding capacity of calf thymus DNA, plasmid DNA and BSA for each of the modified beads as a percentage of the capacity of the unmodified ones at the corresponding time point. The results in Figures 8a and 8b for VA170-3 and Et220-3, respectively, show that in the beginning of the binding reaction (e.g. after 30 s) there is almost no difference in BSA binding capacity for the modified beads compared to the unmodified types (see open and closed triangles), however at the same time point there is an extremely large reduction in binding capacity for calf thymus and plasmid DNA for both modified adsorbents, but with the best performance seen for the Et220-3 (Figure 8b). As the binding reactions progressed, the differences between the modified and unmodified adsorbents were reduced. At all time points the Et220-3 had a greater reduction in binding capacity for calf thymus or plasmid DNA than for BSA binding (Figure 8b), however for the VA170-3 the reduction in BSA binding capacity after 5 minutes was greater than for the calf thymus DNA (Figure 8a).

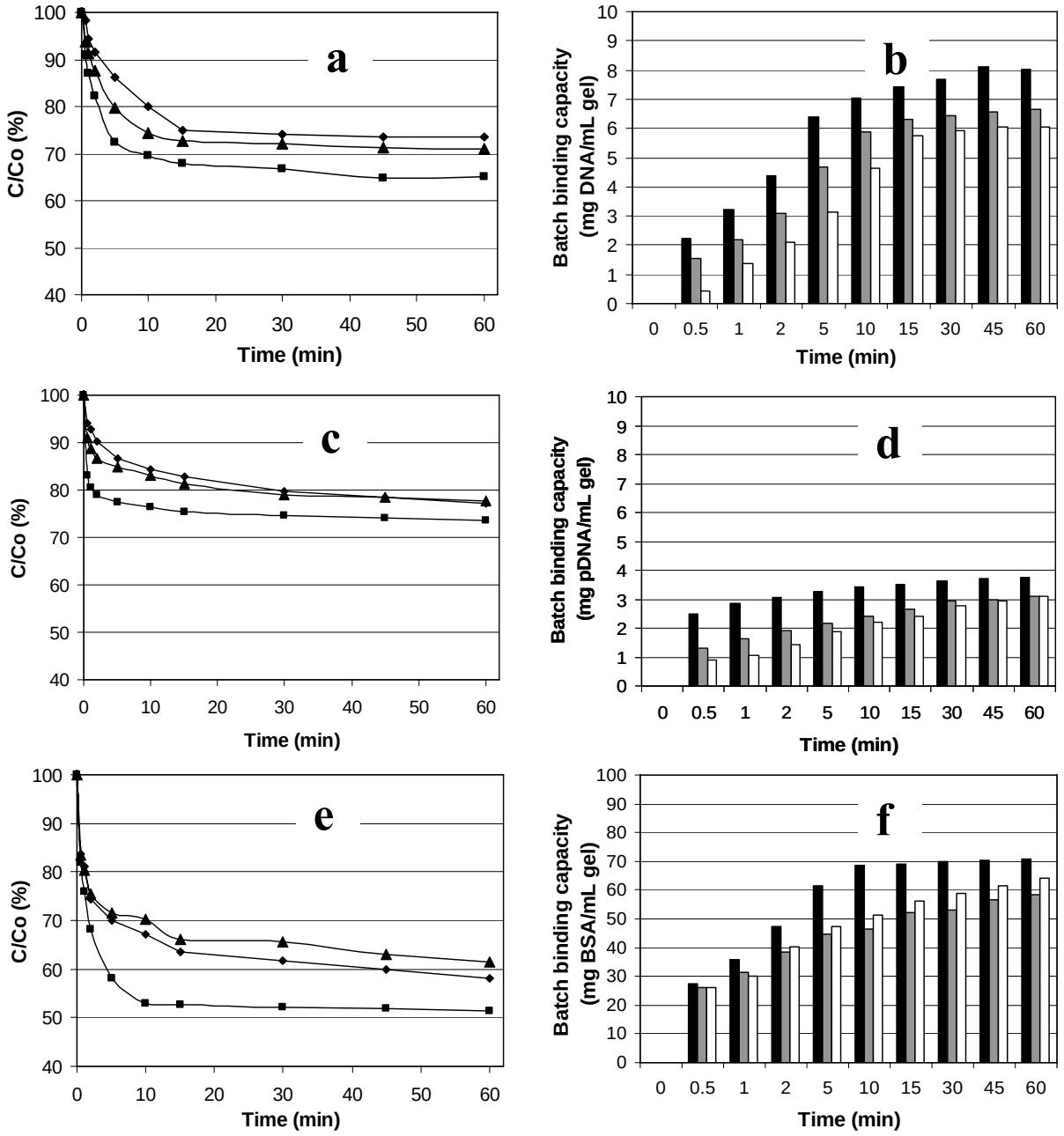

***Figure 7*: Comparison of the kinetics of DNA and protein binding to modified and unmodified Q hyper Z adsorbents in batch reactions with homogenized calf thymus DNA (a and b), plasmid pUG6 (c and d) and BSA (e and f). Legend: unmodified adsorbents (squares, black), surface-coated (VA170-3) (triangles, grey) and surface-etched (Et220-3) (diamonds, white).**

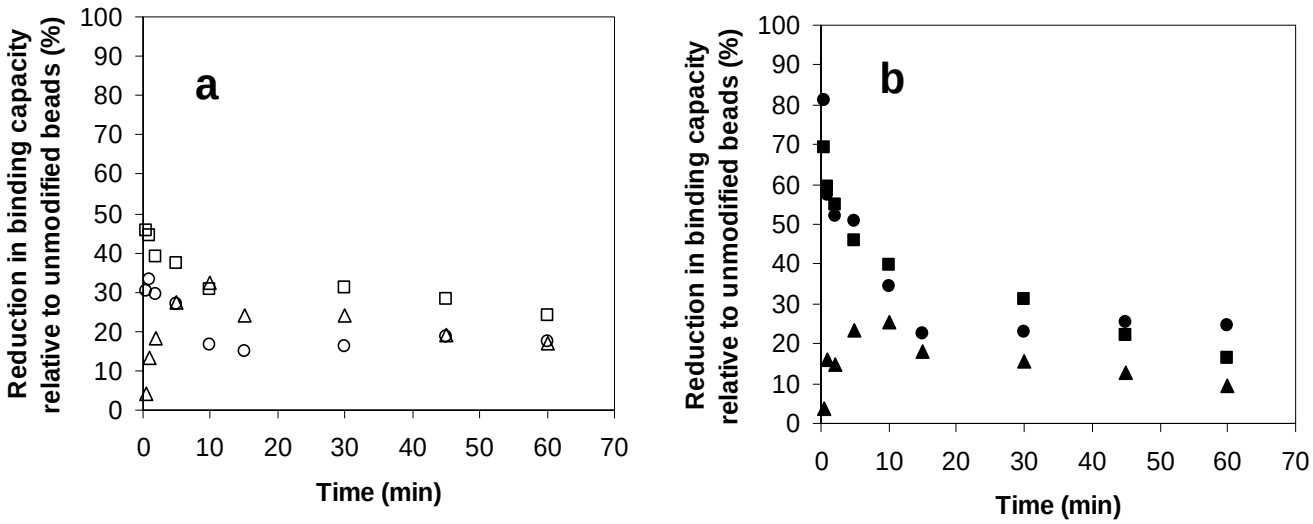

Figure 8. **Comparison of the reduction in binding capacity of calf thymus DNA (circles), plasmid DNA (squares) and BSA (triangles) to (A) VA170-3 or (B) Et220-3 adsorbents compared to the unmodified adsorbents. The data in Figures 7 B, D and E was used for generation of the results. At each time point for the particular plasma modified adsorbent, the reduction in binding capacity for DNA or protein was calculated as a percentage of the DNA or protein capacity measured at that time point for the unmodified adsorbents.**

In general the results from this part of the study suggest that the Et220-3 has better performance than the VA170-3 with respect to minimizing DNA binding whilst having the least impact on BSA binding. Nevertheless the results from both adsorbent types suggest that the plasma modification has successfully generated adsorbents with lower accessibility and binding of large molecules (i.e. DNA molecules) to the quaternary amine ligands in the adsorbent than that for protein (i.e. BSA). The results suggest that removing the surface ligands by etching is more successful than covering them via graft polymerization. In addition the results for BSA binding suggest that accessibility to the ligands located in the gel material within the pores of the etched adsorbent bead (Et220-3) is better than that of the surface-coated one (VA170-3). Nevertheless, it is difficult to predict the performance of the modified adsorbents in an EBA system in which the residence time in a small column may only be in

the order of e.g. ~5 minutes, but in which loading may take in the order of hours e.g. 1-2 hours.

Evaluation of the plasma-treated beads performance in an EBA system

The dynamic binding characteristics of the plasma modified beads were examined using EBA. The results in Figure 9a suggest that there was no significant difference in the BSA binding capacity of the Et220-3 and PV170-3 adsorbents as compared to the unmodified beads. The dynamic BSA binding capacity averaged for the three bead types examined was 33.7±1.01 $mg.mL^{-1}$ of gel at 10% breakthrough. In contrast, a very large reduction in the dynamic binding capacity of calf thymus DNA to the modified adsorbents was seen (Figure 9b). The lowest capacity (1.29 mg applied $DNA.mL^{-1}$ gel) was observed for the surface-etched support (Et220-3) as compared to 6.92 mg applied $DNA.mL^{-1}$ gel for the unmodified support. A similar but less dramatic pattern was observed when the capacity for plasmid DNA was studied (Figure 9c). The Et220-3 beads had the lowest dynamic binding capacity for plasmid of 0.76 $mg.mL^{-1}$ gel compared to that for the unmodified beads (1.5 $mg.mL^{-1}$ gel). The results are consistent with what was observed in the batch binding studies in which the Et220-3 adsorbents were found to have the greatest reductions in DNA binding and least effects on BSA capacity (Figures 8a and 8b).

The expanded bed contraction profiles measured during the EBA experiments are shown in Figures 10a and 10c. It is observed that there is no significant difference between bed contraction for unmodified and plasma-treated adsorbent beads (Et220-3 and VA170-3) during loading of BSA (Figure 10a). However, bed contraction is more severe for the unmodified support compared to that for plasma treated supports (Et220-3 and VA-170) when a feedstock containing homogenized calf thymus DNA is loaded (10b). The results are consistent with the dynamic binding capacities shown above in which calf thymus DNA

binding was dramatically reduced for the plasma modified beads. However, there was little difference in bed contraction during the loading of plasmid DNA (Figure 10c), which may be due to the much lower binding capacity for plasmid DNA of the unmodified adsorbents compared to that for calf thymus DNA (compare Figures 9b and 9c).

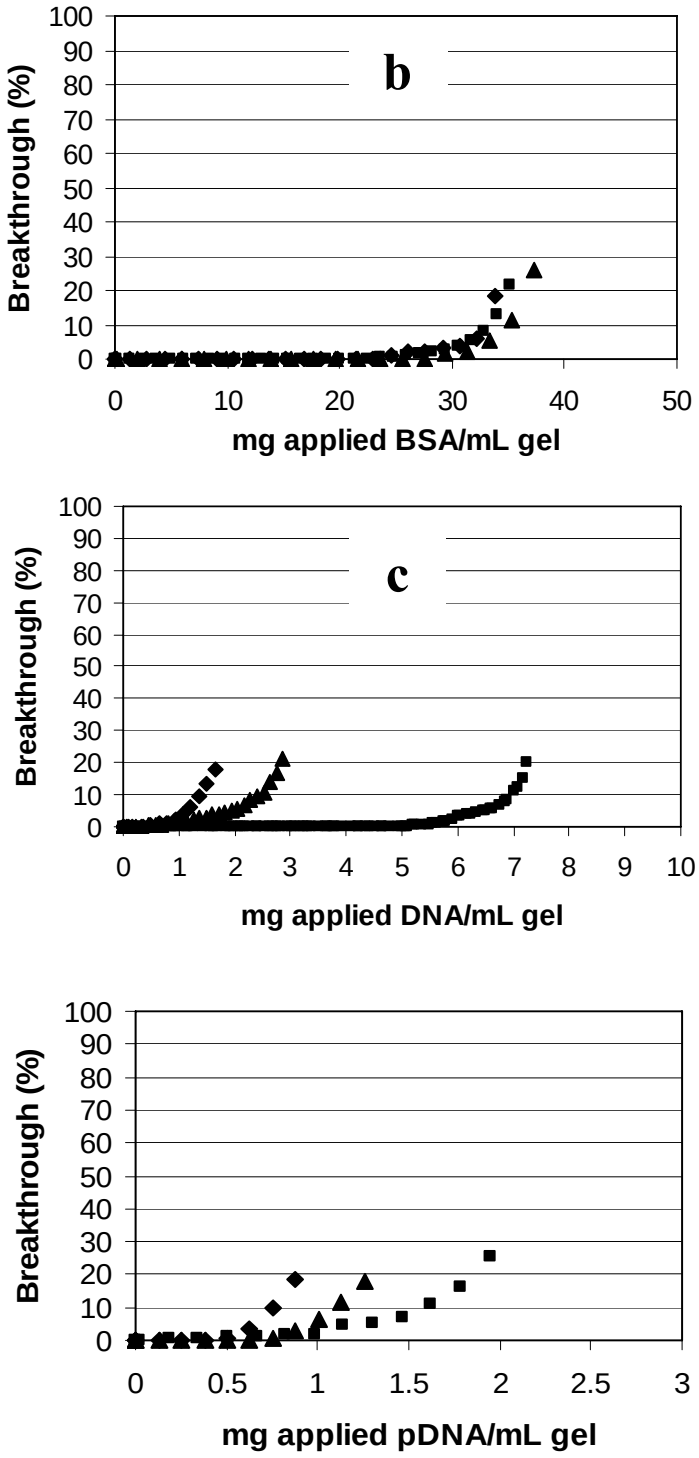

***Figure 9*: Breakthrough curves in EBA for a) BSA, b) homogenized calf thymus DNA and c) plasmid DNA. DNA and BSA concentrations in the feeds were 0.06 mg.mL^{-1} and 1 mg.mL^{-1}, respectively, in 50 mM Tris-HCl pH 8 buffer containing 100 mM NaCl. Unmodified Q HyperZ (squares), ET220-3 (diamonds), VA170-3 (triangles).**

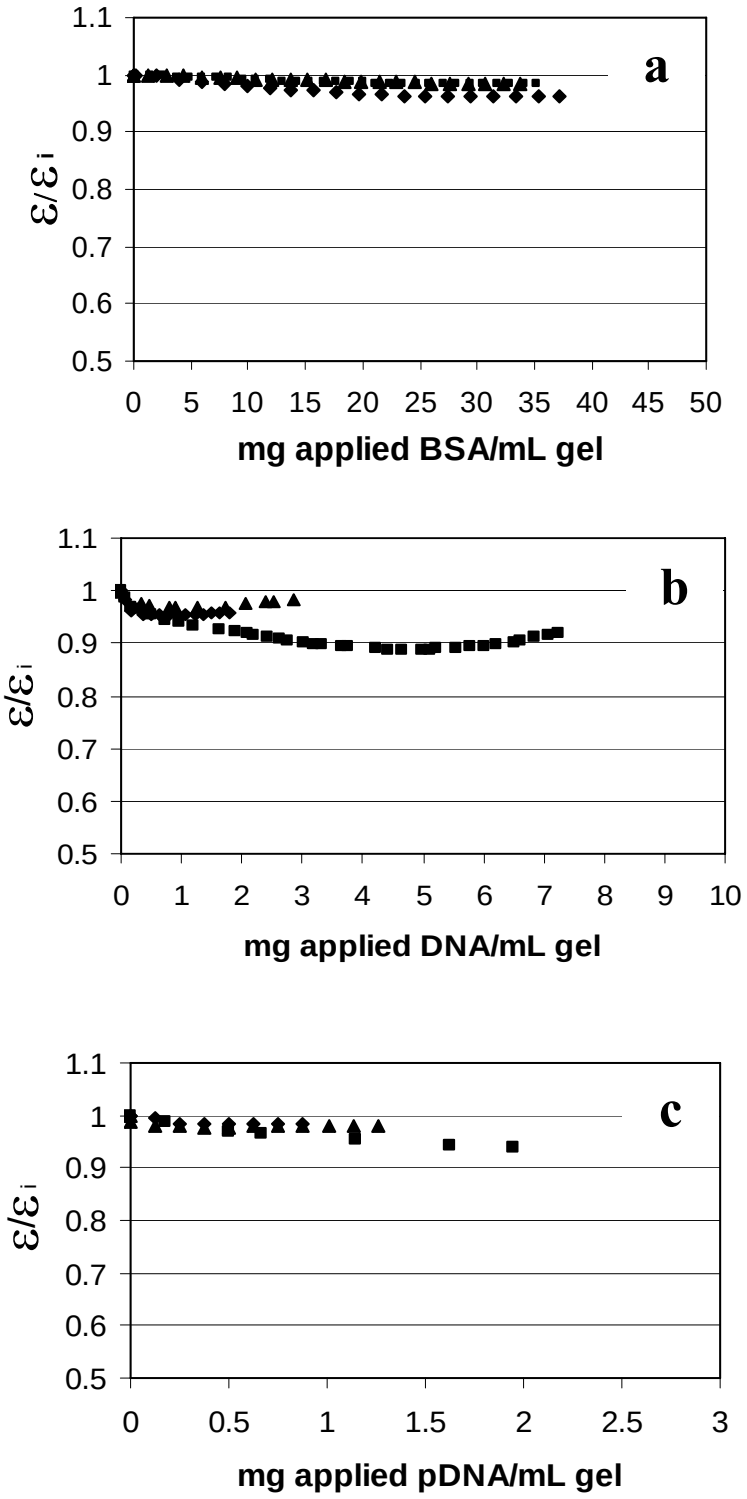

***Figure 10*: Bed compression profiles in EBA for a) BSA, b) homogenized calf thymus DNA and c) plasmid DNA. DNA and BSA concentrations in the feeds were 0.06 mg.mL^{-1} and 1 mg.mL^{-1}, respectively, in 50 mM Tris-HCl pH 8 buffer containing 100 mM NaCl. Unmodified Q HyperZ (squares), Et220-3 (diamonds), VA170-3 (triangles).**

General discussion

The results found here demonstrate that shaving the surface of Q HyperZ adsorbents using plasma oxidation is an effective means of producing beads with dramatically reduced dynamic DNA binding capacity and reduced bed contraction in the presence of DNA, but with no effect on BSA binding. It can therefore be expected that such adsorbents would reduce adsorbent cross-linking by crude materials such as genomic DNA, cell wall debris or whole cells during the capture of proteins from real crude feedstocks. Since the procedures developed here have been applied to commercially available adsorbents, it can be expected that application of the plasma technology to rapidly generating large amounts of adsorbents should be a straightforward matter. No complicated re-design or engineering of the beads and manufacturing process is required. Plasma treatment is already conducted at large scale (reactor volume ≈ 120 L), for example for the preparation of dispersible polyolefin powders (diameter 20-120 μm) by oxygen plasma treatment of non-dispersible ones (Babacz, R.J., 1993 and Wertheimer et al., 1996), and would thus be an add on to the already established EBA bead manufacturing process. Although we have used a rigid zirconia based bead, the gentle nature of the plasma treatment may prove applicable to more conventional hydrogel EBA matrices such as those based on agarose.

A myriad of variations of the plasma treatments reported here can be foreseen for generation of new types of EBA adsorbents. For example, the etching and oxidation of the surface used here should be applicable to a different strategy for making non-adsorptive surface adsorbent beads using a variation of the two-step procedure of Burton and Harding (1997). In the first step chemical groups existing on the bead exterior and pore surfaces are replaced by reactive groups (activation step). In the final step ligands are coupled to the

reactive sites created in the previous step (fuctionalization step). Surface etching and oxidation by plasma could potentially also be applied for deactivation of the exterior surface of beads which have already been activated, prior to a later fuctionalization step. In that strategy, fuctionalization would only occur on activated sites which are situated within the bead and not on the surface. Plasma graft polymerization was not as effective as surface etching and oxidation in the current study, however graft polymerization may have potential for being used in different strategies for preparing chromatography beads with non-adsorptive surfaces as well as with coatings of new generations of 'smart' polymers with multiple and different functionalities. For example, beads could potentially be coated with thermo-, pH-, or photo-sensitive polymers through a graft polymerization treatment. Plasma treated beads would also likely prove useful for the separation of biological products by conventional preparative packed bed chromatography, mixed tank adsorption, fluidized bed adsorption or have other applications in bioprocessing.

Conclusions

Low temperature plasma discharge treatment was found to be an effective means of conducting nano-scale surface modifications to expanded bed adsorption beads. Ligands could be shaved off the surface of the adsorbents via plasma etching and oxidation or coated with a very thin polymer layer by graft polymerization. The treatment was gentle and no physical damage occurred to the adsorbents. Such treatment on Q HyperZ beads resulted in adsorbents with reduced binding sites on the surface and thus reduced dynamic binding of large DNA molecules and reduced adsorbent aggregation during loading. Plasma treatment had little effect on bovine serum albumin mass transfer to the interior of the beads and ligand

attachment, leading to high protein binding capacities. Optimization of plasma treatment parameters has not been conducted and should be investigated to achieve a robust method for large scale preparation of EBA supports with non-adsorptive surfaces.

Acknowledgments

The authors would like to thank Lene Hubert for running the XPS instrument. Iranian ministry of science, research and technology supported this work by granting a PhD scholarship to Ayyoob Arpanaei.

References

1. Anspach, F.B.; Curbelo, D.; Hartmann, R.; Garke, G. and Deckwer, W.D.; 1999; **Expanded-bed chromatography in primary protein purification**; *Journal of Chromatography A, 865,* 129-144.
2. Babacz, R.J.; 1993; **Continuous plasma activated species treatment process for particulate**; *US Patent*, US5234723.
3. Beck, J.T.; Williamson, B. and Tipton, B.; 1999; **Direct coupling of expanded bed adsorption with a downstream purification step**; *Bioseparation*, 8, 201-207.
4. Boenig, H.V.; 1988; ***Fundamentals of plasma chemistry and technology***, Technomic Pub., Lancaster.
5. Brixius, P.; Mollerup, I.; Elvang Jensen, O.; Halfar, M.; Thömmes, J. and Kula, M.R.; 2005; **Expanded bed adsorption as a primary recovery step for the isolation of the insulin precursor MI3 process development and scale up**; *Biotechnology and Bioengineering*, 93(1), 14-20.
6. Burton, S. C. and Harding, D.R.K.; 1997; **Bifunctional etherification of a bead cellulose for ligand attachment with allyl bromide and allyl glycidyl ether**; *Journal of Chromatography A*, 775, 29-38.
7. Cabanne, C.; Noubhani, A.M.; Dieryck, A.; Hocquellet, W. and Santarelli, X.; 2004; **Evaluation of three expanded bed adsorption anion exchange matrices with the aid of recombinant enhanced green fluorescent protein overexpressed in *Escherichia coli***; *Journal of Chromatography B*, 808, 91-97.
8. Chang, Y.K.; McCreath, E.G. and Chase, H.A.; 1995; **Development of an expanded bed technique for an affinity purification of G6PDH from unclarified yeast cell homogenates**; *Biotechnology and Bioengineering*, 48, 355-366.
9. Chang, Y.K.; Hong, J.T.; Haung R.-Z. and Lin, S.Y.; 2006; **Direct capture of factor IX from unclarified human plasma by IMEBAC**; *Biochemical Engineering Journal*, 29, 12-22.
10. Chu, P.K.; Chen, J.Y.; Wang, L.P. and Huang, N.; 2002; **Plasma-surface modification of biomaterials**; *Materials Science and Engineering R*, 36, 143-206.
11. Clemmitt, R.H. and Chase, H.A.; 2000; **Facilitated downstream processing of a histidine-tagged protein from unclarified *E.coli* homogenates using immobilized**

metal affinity expanded-bed adsorption; *Biotechnology and Bioengineering*, 67(2), 206-216.

12. Dainiak, M.B.; Galaev, I.Y. and Mattiasson, B.; 2002a; **Polyelectrolyte-coated ion exchangers for cell-resistant expanded bed adsorption**; *Biotechnology Progress,* 18, 815-820.
13. Dainiak, M.B.; Galaev, I.Y. and Mattiasson, B.; 2002b; **Direct capture of product from fermentation broth using a cell-repelling ion exchanger**; *Journal of Chromatography A,* 942, 123-131.
14. Draeger, N.M. and Chase, H.A.; 1991; **Liquid fluidized bed adsorption of protein in the presence of cells**; *Bioseparation, 2*, 67-80.
15. Ezequiel de Oliveira, J.; Soares, C.R.J.; Peroni, C.N.; Gimbo, E.; Camargo, I.M.C.; Morganti, L.; Bellini, M.H.; Affonso, R.; Arkaten, R.R.; Bartolini, P.; Teresa, M. and Ribela, C.P.; 1999; **High-yield purification of biosynthesis human growth hormone secreted in *Escherichia coli* periplasmic space**; *Journal of Chromatography A*, 852, 441-450.
16. Fahrner, R.L.; Blank, G.S. and Zapata, G.A.; 1999; **Expanded bed protein A affinity chromatography of a recombinant humanized monoclonal antibody: process development, operation, and comparison with a packed bed method**; *Journal of Biotechnology*, 75, 273-280.
17. Feuser, J.; Walter, J.; Kula, M.R. and Thömmes, J.; 1999a; **Cell/adsorbent interactions in expanded bed adsorption of proteins**; *Bioseparation*, 8, 99-109.
18. Feuser, J; Halfar, M.; Lutkemeyer, D.; Ameskamp, N.; Kula, M.R.; Thömmes, J.; 1999b; **Interaction of mammalian cell culture broth with adsorbents in expanded bed adsorption of monoclonal antibodies**; *Process Biochemistry*, 34, 159-165.
19. Fisher, E.R.; 2002; **On the interplay between plasma ions, radicals and surfaces: who dominates the interaction**; *Plasma Sources Sciences and Technology*, 11(2), 175-182.
20. Galaev, I; Hatti-Kaul, R. and Mattiasson, B.; 2002; **Method for the separation of bioproducts**; *World patent*, WO02/102490.
21. Gonzalez, Y.; Ibarra, N.; Gomez, H.; Gonzalez, M.; Dorta, L.; Padilla, S. and Valdes, R.; 2003; **Expanded Bed Adsorption Processing of Mammalian Cell Culture Fluid: Comparison with Packed bed Affinity Chromatography**; *Journal of Chromatography B*, 784, 183-187.

22. Guldener, U.; Heck, S.; Fielder, T.; Beinhauer, J. and Hegemann, J.H.; 1996; **A new efficient gene disruption cassette for repeated use in budding yeast**; *Nucleic acids research*, 24(13), 2519-2524.
23. Gupta, M.N. and Mattiasson, B.; 1994; **Novel technologies in downstream processing**; *Chemistry and Industry*, 17, 673-675.
24. Gustavsson, P.E.; Lemmens, R.; Nyhammar, T.; Busson, P. and Larsson, P.O.; 2004; **Purification of plasmid DNA with a new type of anion-exchange beads having a non-charged surface**; *Journal of Chromatography A,* 1038(1-2), 131-140.
25. Hansson, M.; Stahl, S.; Hjorth, R.; Uhlen, M. and Moks, T.; 1994; **Single-step recovery of a secreted recombinant protein by expanded bed adsorption**; *Bio/Technology,* 12, 285-288.
26. Hjorth, R.; Leijon, P; Barnfield Frej, A.K. and Jagersten, C.; 1998; **Expanded bed adsorption chromatography**; In: Subramanian, G. (ed.), *Bioseparation and Bioprocessing*, Vol. 8, pp. 199-226, Wiley-VCH Verlag GmbH, Weinheim, Germany.
27. Hollahan, J.R. and Carlson, G.L.; 1970; **Hydroxylation of polymethylsiloxane surfaces by oxidizing plasmas**; *Journal of Applied Polymer Science*, 14, 2499-2508.
28. Hubbuch, J.J.; Brixius, P.J.; Lin, D.Q.; Mollerup, I. and Kula M.R.; 2006; **The influence of homogenisation conditions on biomass-adsorbent interactions during ion-exchange expanded bed adsorption**; *Biotechnology and Bioengineering*, 94(3), 543-553.
29. Hubbuch, J.J.; Heebøll-Nielsen, A.; Hobley, T.J. and Thomas, O.R.T.; 2002; **A new fluid distribution system for scale-flexible expanded bed adsorption**; *Biotechnology and Bioengineering*, 78, 35-43.
30. Inagaki, N.; Tasaka, S. and Horikawa, Y.; 1991; **Durable, hydrophilic surface modification of polypropylene films by plasma graft polymerization of glycidyl methacrylate**; *Polymer Bulletin*, 26, 283-289.
31. Jahic, M.; Knoblechner, J.; Charoenrat, Th.; Enfors, S.O. and Veide, A.; 2006; **Interfacing *Pichia pastoris* cultivation with expanded bed adsorption**; *Biotechnology and Bioengineering*, 93(6), 1040-1049.
32. Jin, T.; Guan, Y.X.; Yao, Sh.-J.; Lin, D.Q. and Cho, M.G.; 2005; **On-column refolding of recombinant human interferon-ã inclusion bodies by expanded bed adsorption chromatography**; *Biotechnology and Bioengineering*, 93(4), 755-760.

33. Kaczmarski, K. and Bellot, J.C.; 2004; **Theoretical investigation of axial and local particle size distribution on expanded bed adsorption process**; *Biotechnology Progress,* 20, 786-792.
34. Kepka, C.; Lemmens, R.; Vasi, J.; Nyhammar, T.; Gustavsson, P.E.; 2004; **Integrated process for purification of plasmid DNA using aqueous two-phase systems combined with membrane filtration and lid bead chromatography**; *Journal of Chromatography A,* 1057(1-2), 115-124.
35. Kim, H.R.; Park, H.H.; Hyun, S.H. and Yeom, G.Y.; 1998; **Effect of O_2 plasma treatment on the properties of SiO_2 aerogel film**; *Thin Solid Films*, 332(1-2), 444-448.
36. Kingshott, P. and Griesser, H.J.; 1999; **Surfaces that resist bioadhesion**; *Current Opinion in Solid State and Materials Science*, 4, 403-412.
37. Kingshott, P.; Thissen, H. and Griesser, H.J.; 2002; **Effects of cloud-point grafting, chain length, and density of PEG layers on competitive adsorption of ocular proteins**; *Biomaterials*, 23, 2043-2056.
38. Lai. J.Y.; Lin, Y.Y.; Denq, Y.L.; Shyu, S.S. and Chen, J.K.; 1996; **Surface modification of silicone rubber by gas plasma treatment**; *Journal of Adhesion Science and Technology*, 10, 231-242.
39. Lin, D.Q.; Fernandez-Lahore, H.M.; Kula, M.R.; Thömmes, J.; 2001; **Minimising biomass/adsorbent interactions in expanded bed adsorption processes: a methodological design approach**; *Bioseparation*, 10(1-3), 7-19.
40. Lin, D.Q.; Kula, M.R.; Liten, A. and Thömmes, J.; 2003a; **Stability of expanded beds during the application of crude feedstock**; *Biotechnology and Bioengineering*, 81(1), 21-26.
41. Lin, D.Q.; Brixius, P.; Hubbuch, J.; Thömmes, J. and Kula, M.-R.; 2003b; **Biomass/adsorbent electrostatic interactions in expanded bed adsorption: a zeta potential study**; *Biotechnology and Bioengineering,* 83(2), 149-157.
42. Lin. D.Q.; Thömmes, J.; Kula, M.R.; Hubbuch, J.; 2004; **The influence of biomass on the hydrodynamic behaviour and stability of expanded beds**; *Biotechnology and Bioengineering*, 87(3), 337-346.
43. Liston, E.M.; Martinu, L. and Wertheimer, M.R.; 1993; **Plasma surface modification of polymers for improved adhesion: a critical revie**w; *Journal of Adhesion Science and Technology*, 37, 1091-1127.

44. McArthur, S.L.; McLean, K.M.; Kingshott, P.; St John, H.A.W.; Chatelier, R.C. and Griesser, H.J.; 2000; **Effect of polysaccharide structure on protein adsorption**; *Colloids and Surfaces B: Biointerfaces*, 17, 37-48.
45. Ohashi, R.; Otero, J.M.; Chwistek, A.; Yamato, I. and Hamel, J.F.P.; 2002; **On-line purification of monoclonal antibodies using an integrated stirred-tank reactor/expanded-bed adsorption system**; *Biotechnology Progress*, 18, 1292-1300.
46. Olander, M.; Lihme, A.; Hobley, T.J.; Simon, M.; Theodossiou, I. and Thomas, O.R.T.; 2000; **Fluidized bed purification of bio-macromolecules such as plasmid DNA, chromosomal DNA, RNA, viral DNA, bacterial and viruses**; International patent application WO00/57982.
47. Schram, D.C.; Bisschops, Th.H.J.; Kroesen, G.M.W. and de Hoog, F.J.; 1987; **Plasma surface modification and plasma chemistry**; *Plasma Physics and Controlled Fusion*, 29(10A), 1353-1364.
48. Schuger, K. and Hubbuch, J.; 2005; **Integrated bioprocesses**; *Current Opinion in Microbiology*, 8, 294-300.
49. Senthuran, A.; Senthuran, V.; Hatti-Kaul, R. and Mattiasson, B.; 2004; **Lactate production in an integrated process configuration: reducing cell adsorption by shielding of adsorbent**; *Applied Microbiology and Biotechnology, 65,* 658-663.
50. Souverain, S.; Rudaz, S. and Veuthey, J.L.; 2004; **Restricted access materials and large particle supports for on-line sample preparation: an attractive approach for biological fluids analysis**; *Journal of Chromatography B*, 801, 141-156.
51. Strætkvern, K.O.; Schwarz, J.G.; Wiesenborn, D.P.; Zafirakos, E. and Lihme, A.; 1999; **Expanded bed adsorption for recovery of patatin from crude potato juice**; *Bioseparation*, 7, 333-345.
52. Sudo, Y.; Miyagawa, R. and Takahata, Y.; 1998; **Method for the preparation of restricted access media by low-temperature plasma treatment**; *Journal of Chromatography B*, 705, 55-62.
53. Tao, W.H.; Chang, K.S.; Chung, T.W. and Chang, Y.N.; 2004; **Surface properties and adsorption breakthrough curves of plasma-treated silica gels**; *Chemical Engineering Communications*, 191, 682-693.

54. Theodossiou I. and Thomas, O.R.T.; 2002; **DNA-Induced inter-particle cross-linking during expanded bed adsorption chromatography: Impact on future support design**; *Journal of Chromatography A*, 971, 73-86.
55. Theodossiou, I.; Olander, M.A.; Soendergaard, M. and Thomas, O.R.T.; 2000; **New expanded bed adsorbents for the recovery of DNA**; *Biotechnology Letters*, 22(24), 1929-1933.
56. Theodossiou, I.; Soendergaard, M. and Thomas, O.R.T.; 2001; **Design of expanded bed supports for the recovery of plasmid DNA by anion exchange adsorption**; *Bioseparation*, 10(3), 31-44.
57. Thömmes, J.; 1997; **Fluidized bed adsorption as a primary recovery step in protein purification**; *Advances in Biochemical Engineering /Biotechnology*, 58, 185-230.
58. Ulbricht, M. and Belfort, G.; **Surface modification of ultrafiltration membranes by low temperature plasma. I. Treatment of polyacrylonitrile**; *Journal of Applied Polymer Sciences*, 1995, 56, 325-343.
59. Vergnault, H.; Mercier-Bonin, M. and Willemot, R.M.; 2004; **Physicochemical parameters involved in the interaction of *Saccharomyces cerevisiae* with ion-exchange adsorbents in expanded bed chromatography**; *Biotechnology Progress*, 20, 1534-1542.
60. Viloria-Cols, M.E.; Hatti-Kaul, R. and Mattiasson, B.; 2004; **Agarose-coated anion exchanger prevents cell-adsorbent interactions**; *Journal of Chromatography A*, 1043(2), 195-200.
61. Voute, N. and Boschetti, E.; 1999; **Highly dense beaded sorbents suitable for fluidized bed applications**; *Bioseparation*, 8, 115-120.
62. Wertheimer, M.R.; Thomas, H.R.; Perri, M.J.; Klemberg-Sapieha, J.E. and Martinu, L; 1996; **Plasmas and polymers: From laboratories to large scale commercialization**; *Pure & Applied Chemistry*, 68(5), 1047-1053.
63. Yamamoto, Y.; Oka, S. and Hayashi, K.; 1984; **Oxygen-plasma treatment of packing materials for gas chromatography. The incorporation of oxygen into the hydrocarbon liquid phase and the formation of cross-linked products on the support surface**; *Bulletin of Chemical Society of Japan*, 57(12), 3450-3453.
64. Yun, J.; Lin, D.Q. and Yao, S.J.; 2005; **Predictive modeling of protein adsorption along the bed height by taking into account the axial non-uniform liquid dispersion**

and particle classification in expanded beds; *Journal of Chromatography A*, 1095(1-2), 16-26.

5 Concluding remarks

The robustness and performance of unit operations applied in downstream processing of biological products are crucial given the high demands placed on cost minimization and productivity maximization. To date, the serious problems found during the application of EBA systems, including fouling of the fluid distribution system and aggregation of adsorbent beads by crude materials in biological feedstocks have limited the commercial applications of this promising method to only a few cases. Fouling of fluid distribution systems appears to have been overcome following the development of rotating or oscillating fluid distributors and the current work (chapter 2) demonstrates the significant advantages of these distributors over the alternative locally stirred design popularized in the literature. However, the work conducted here (chapter 2) also raises questions as to whether significant improvements can not still be made. In particular, the effect of different design parameters including distributor geometry and dimensions, and fluid outlet hole patterns on the quality of the flow introduced, and its relation to scalability must still be investigated, both with model and real feeds (Chapter 2).

If the moderate numbers of theoretical plates (N≈30) obtained by the current rotating fluid distribution systems can be significantly increased, EBA may evolve from a capture step delivering clarified, concentrated and partially purified process streams, to a unit operation with much greater resolving power during elution. Thus not only more highly concentrated, but also more highly purified process streams would be possible, leading to lower numbers of subsequent unit operations needed to deliver the necessary purity of a biological product. Furthermore, increased numbers of theoretical plates could be expected to also lead to other

benefits such as lower consumption of elution buffer. It is thus predicted, and expected, that redesign of rotating fluid distributors with focus not only on capture, but also on elution performance will be seen in the future.

Regardless of the role of fluid distribution systems in EBA columns, the important problem which has drastically reduced the robustness and quality of EBA systems is aggregation of the adsorbents with large molecules existing in crude biological feedstocks (Chapters 3 and 4). EBA is supposed to be compatible with crude feedstocks in order to integrate the different functions needed in the first parts of downstream processing of biological products (i.e. direct capture), including clarification, concentration and preliminary purification. However, aggregation of adsorbent beads necessitates applying a clarification step before EBA, which consequently increases costs and negates the advantages of EBA. Study of the mechanisms of adsorbent bead aggregation by macromolecules either when they are products, e.g. plasmids, or when they are contaminants, e.g. genomic DNA, cell debris and intact cells, results in better understanding of this phenomenon and possibly more efficient ways by which these unwanted interactions can be minimized (Chapter 3). Ligand density and type, adsorbent size, buffer composition, and bead surface architecture must be considered as crucial parameters in such studies (Chapter 3). However, to minimize the interaction between macromolecule contaminants or particulates and adsorbent beads, it seems the best way is to physically hamper these interactions.

Coating adsorbents with hydrogels, e.g. agarose or polyelectrolytes leads to new problems such as decreasing the capacity due to increased mass transfer limitations or unspecific binding, respectively. Thus, the creation of a hydrophilic, neutral, ultra-thin layer on EBA adsorbent surfaces using low temperature plasma (Chapter 4) could become the method of choice in the future. The method is scaleable and can be applied as an ‘add on’ to

existing manufacturing procedures for commercial adsorbents. Such treatment not only reduces bead aggregation, but also may lead to greater purity during elution, thus reducing the need for further unit operations in the later parts of the downstream processing train. The promising results obtained in Chapter 4 are the first reported and considerable further work is required to demonstrate the applicability of the adsorbents produced. Studies in crude feeds are needed and extension of the treatment to other types of EBA beads which are not based on a rigid zirconia skeleton should be conducted. Further applications can also be foreseen for plasma surface modification, for example for the preparation of multifunctional beads used for packed bed chromatography as well as other types of adsorptive methods. The ability to simply introduce different functionalities to the surface without changing the adsorbent interior is highly attractive.